INDUCED SEISMICITY IN CARBON AND EMERY COUNTIES, UTAH

A Thesis

presented to

the Faculty of the Graduate School

at the University of Missouri-Columbia

In Partial Fulfillment

of the Requirements for the Degree

Master of Sciences

---

by

MEGAN R. M. BROWN

Dr. Mian Liu, Thesis Supervisor

MAY 2015

The undersigned, appointed by the dean of the Graduate School, have examined the thesis entitled

INDUCED SEISMICITY IN CARBON

AND EMERY COUNTIES, UTAH

presented by Megan R. M. Brown,

a candidate for the degree of Master of Sciences,

and hereby certify that, in their opinion, it is worthy of acceptance.

Professor Mian Liu

Professor Martin Appold

Professor Baolin Deng

Professor Eric Sandvol

ACKNOWLEDGEMENTS

Firstly, I would like to thank my thesis supervisor, Dr. Mian Liu, for his help and support with both my classwork and my research. In addition, I thank my thesis committee for giving their time and energy toward my thesis. I would also like to acknowledge the Geology Department and the Graduate School for funding my time at University of Missouri. I also need to acknowledge the Walter D. Keller Scholarship Fund and Dr. M. Ray Thomasson and Merrill Shields, who fund the Thomasson Fellowship. In addition, I would like to acknowledge the donors of the Houston Geological Society, Calvert Memorial Scholarship fund. I also wish to thank Jiyang Ye for all his help with GMT and MATLAB. Finally, I need to thank my family and friends who supported me during my time at University of Missouri.

TABLE OF CONTENTS

LIST OF FIGURES

LIST OF TABLES

ABSTRACT

Utah is one of the top producers of oil and natural gas in the United States. Over the past 18 years, more than 4.2 billion gallons of wastewater from the petroleum industry have been injected into the Navajo Sandstone, Kayenta Formation, and Wingate Sandstone in two areas in Carbon and Emery County, Utah, where seismicity has increased during the same period. In this study, I investigated whether or not wastewater injection is related to the increased seismicity.

Previous studies have attributed all of the seismicity in central Utah to coal mining activity. I found that water injection might be a more important cause. In the coal mining area, seismicity rate increased significantly 1-5 years following the commencement of wastewater injection. The increased seismicity consists almost entirely of earthquakes with magnitudes of less than 3, and is localized in areas seismically active prior to the injection. I have established the spatiotemporal correlations between the coal mining activities, the wastewater injection, and the increased seismicity. I used simple groundwater models to estimate the change in pore pressure and evaluate the observed time gap between the start of injection and the onset of the increased seismicity in the areas surrounding the injection wells. To ascertain that the increased seismicity is not fluctuation of background seismicity, I analyzed the magnitude-frequency relation of these earthquakes and found a clear increase in the b-value following the wastewater injection. I conclude that the marked increase of seismicity rate in central Utah is induced by both mining activity and wastewater injection, which raised pore pressure along pre-existing faults.

Chapter 1: Introduction

Induced seismicity is a phenomenon that has been recognized for decades and has recently become the focus of more intense study. Increased production of hydrocarbons across the country has caused the occurrence of induced seismicity to become a mainstream topic of concern and debate. Induced seismicity occurs in many forms including mining induced seismicity, reservoir induced seismicity, and injection induced seismicity. Injection induced seismicity is linked with the higher magnitudes events, mainly due to larger volumes of injection correlating with larger magnitude induced seismicity [*McGarr*, 2014].

Currently, the U.S. Environmental Protection Agency's (EPA) Underground Injection Control (UIC) program governs all injection wells, including Class II injection wells. Class II injection wells are wells used to inject non-hazardous waste fluids that are byproducts of oil and natural gas production or storage or fluids used for enhanced recovery of oil or natural gas. Injection wells that inject hydrocarbons for storage are also classified as Class II wells. Often, state agencies administer the UIC program for the EPA. The main goal of the UIC regulations is to prevent the contamination of usable aquifers [*Ellsworth*, 2013]. In this way, well integrity and the maximum injection pressure are the main monitoring concerns. Seismic activity is not part of the regulations, either in the placement or in the monitoring of the injection wells. There are no current regulations for the placement of injection wells in terms of proximity to active seismic zones or critical facilities like hospitals or nuclear power plants [*Horton*, 2012]. In addition, the lack of seismic safety regulations allows for a lower quantity of reported

injection volume and pressure data and the timeliness of reporting to be much slower than it should be to be helpful for seismic monitoring [*Ellsworth*, 2013].

Many previous injection induced seismicity studies use Davis and Frohlich's [1993] criteria to determine the validity of injection wells inducing the seismicity. Questions in the criteria include: 1.) Are these events the first known earthquakes of this character in the region; 2.) Is there a clear correlation between injection and seismicity; and 3.) Are epicenters near wells (within 5 kilometers), among others [*Davis and Frohlich*, 1993]. While this is definitely criteria for some injection induced seismicity, this criteria can bias studies. The first question limits the areas of study to largely seismically inactive regions. In addition, in areas with limited prior seismicity, the seismic networks will not be as extensive as seismically active areas. The earthquakes that instigate investigation will often be felt earthquakes, and therefore, they likely will be magnitude 3 or larger. The criteria can also limit the extent of the study to only seismicity close to the wells, while more recent studies have shown induced seismicity can reach up to more than 20 kilometers (km) from the injection wells [*Keranen et al.*, 2014; *King et al.*, 2014]. Smaller magnitude induced seismicity, as well as events that occur further from the injection wells, must be examined in order to characterize and understand injection induced seismicity.

My research focuses on induced seismicity in Utah, which has a history of seismicity. I examine four areas in Utah that have active injection wells [Figure 1], either wastewater disposal or water injection for enhanced recovery. I focus the majority of my research on one area, labeled Area 3 [Figure 1], which has numerous wastewater injection wells and an active underground coal mining area. Seismicity in the region has

long been inferred to be mining induced, due to the strong correlation with the active coal mining in the region and the very shallow focal depths [*Pechmann et al.*, 2008]. The magnitudes of the seismicity are mostly less than magnitude 3. Area 3 also has numerous UIC Class II wastewater disposal wells. Thirty-three designated wastewater disposal wells are located within Area 3; twenty-seven of which inject into the Navajo aquifer [UIC public record well files]. Five of the wells inject into aquifers other than the Navajo aquifer and one well was never utilized and is now abandoned. The injected fluid is mostly produced water from nearby methane coal beds [UIC public record well files].

Between 2000 and 2010, the seismicity rate in Area 3 increased significantly. Due to the spatial and temporal correlation between the wastewater injection and seismicity, I suspect the increased seismicity in Area 3 is not entirely due to mining activity, but instead is enhanced by injection induced seismicity, caused by pore pressure increase along pre-existing faults. To test this hypothesis, I analyze temporal and spatial correlations between seismicity, coal mining activity, and wastewater disposal well injection volumes. In addition, I created basic groundwater models, based on published parameters for the main injection aquifer, to determine if there is the possibility of pore pressure increase to the extent needed to trigger seismicity. I also conducted evaluations of temporal and spatial variations of b-values to test the hypothesis.

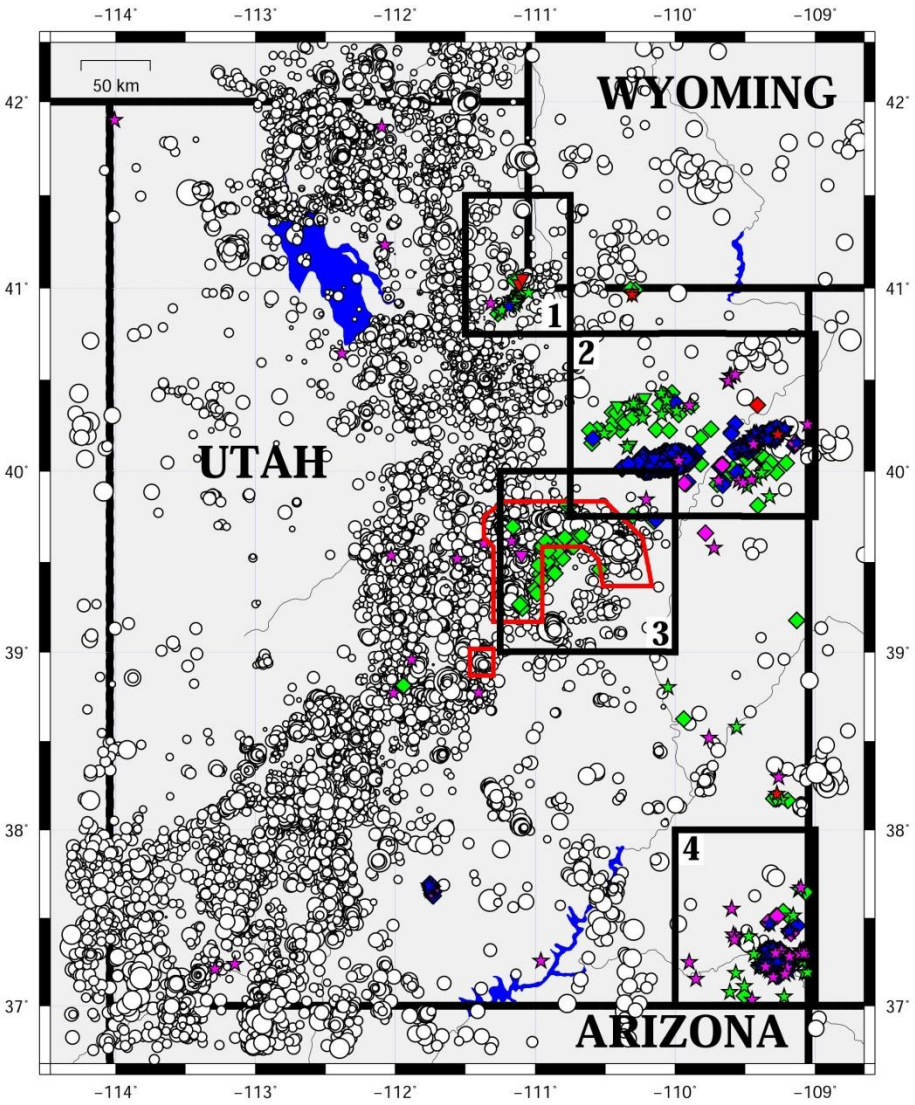

Figure 1: The seismicity of Utah since 1981. Red polygons outline coal mining areas adapted from [*Arabasz and Pechmann*, 2001] and black rectangles outline Areas 1 – 4.

Chapter 2: Background

2.1 Induced Seismicity

2.1.1 Injection Induced Seismicity

Injection induced seismicity has been studied for decades. One of the most notable cases was the Denver earthquakes in the 1960s associated with the Rocky Mountain Arsenal, Colorado injection project [*Healy et al.*, 1968]. Several types of injection have been shown to induce seismicity: injection associated with geothermal energy; hydraulic fracturing associated with unconventional oil and gas extraction; injection for enhanced oil and gas recovery; and, wastewater disposal wells often associated with energy extraction [*National Research Council of the National Academies*, 2013].

Injection induced seismicity occurs when the injection volume modifies the stress and/or pore pressure [*Ellsworth*, 2013]. This can happen as a result of gravitational loading based on the volume/mass change created by the injection volume or as a result of pore-pressure diffusion [*Ellsworth*, 2013]. A volume/mass change can induce seismicity without a hydrologic connection between the injected volume and the faults on which the seismicity occurs, while pore-pressure diffusion induced earthquakes do require hydrologic connectivity between the injected volume and effected faults [*Ellsworth*, 2013].

Earthquakes induced by pore-pressure diffusion occur when the increase pore-pressure decreases the normal stress on a fault plane to cause it to slip. Failure of the fault is often expressed by the equation: $\tau_{crit} = \mu(\sigma_n - P) + \tau_o$, where τ_{crit} is the

critical shear stress, μ is the coefficient of friction, σ_n is the applied normal stress, τ_o is the cohesion strength, and P is the pore pressure. When pore pressure increases, the shear stress needed to produce slip along the fault decreases.

A strong positive correlation is observed between the cumulative volume of injection and the maximum magnitude of the injection induced earthquake [*McGarr*, 2014]. Enhanced recovery and geothermal injection wells are often part of processes that involve injection and extraction creating an almost net zero injection volume; wastewater disposal wells inject much larger volumes than enhanced recovery and geothermal injection wells without any extraction, which generates a higher risk for induced seismicity [*Ellsworth*, 2013; *National Research Council of the National Academies*, 2013]. Sumy et al. [2014] suggest that it may be possible for wastewater injection induced seismicity to trigger larger magnitude earthquakes on adjacent or nearby larger faults. The M5.7 earthquake in Prague, Oklahoma may have been one such triggered earthquake [*Sumy et al.*, 2014].

2.1.2 Mining Induced Seismicity

Mining operations have long been correlated with seismicity; mining induced seismicity (MIS) has been reported worldwide in underground mining operations and other underground projects [*Li et al.*, 2007]. MIS is an all-encompassing term for rockbursts (often referred to as coal bumps), fracture initiation and propagation, and movement along pre-existing fracture planes, which result from the redistribution of stress that results from mass removal of large volumes of rock at depth [*Li et al.*, 2007]. MIS can also refer to the fault slip that occurs as a result of the interaction of local tectonic stresses and the mining-induced stresses, near and around the mine area [*Li et*

al., 2007]. MIS is often characterized by bimodal magnitude-frequency distributions due to two different modes of seismicity: 1.) friction-dominated slip events associated with geologic features; and, 2.) fracture-dominated events associated with fracturing in the areas of high stress concentrations ahead of the longwall mining operation [*Gibowicz,* 2009].

2.2 Utah Geology

2.2.1 Tectonic Setting

The geologic history of Utah in general is a complex history of periods of sedimentation, orogenic activity, igneous activity, and large-scale extension and uplift. Central Utah is particularly interesting as it forms a hinge line (the Wasatch line) that marks the boundary between Cambrian stable shelf area in eastern Utah and the more rapidly subsiding miogeoclinal area of western Utah [*Hintz and Kowallis,* 2009]. The area consisted of thick miogeoclinal strata to the west and thin shelf-margin sedimentary rocks to the east throughout the late Precambrian and the Paleozoic until the Late Jurassic [*Neuhauser,* 1988]. In addition, the hinge line marks the transition from the Basin and Range Province, a large-scale extensional region to the west, and the Colorado Plateau, a region of large uplift with limited deformation to the east [*Wannamaker et al.*, 2001]. The transition zone [Figure 2] is about 600 km long and 125 km wide [*Neuhauser,* 1988].

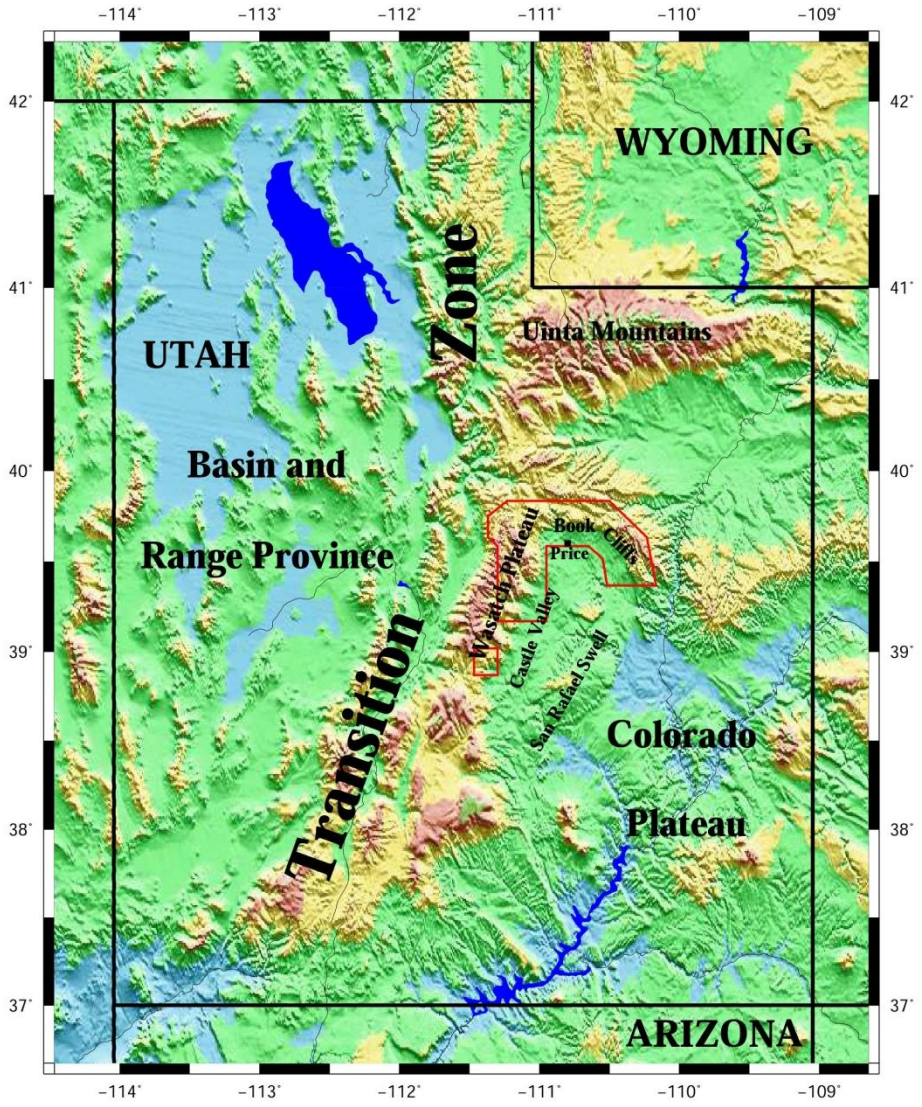

Figure 2: The key features of Utah. Red polygons outline coal mining areas [adapted from *Arabasz and Pechmann*, 2001].

My study area lies to the east of the transition zone within the Colorado Plateau. This area was affected by the Laramide Orogeny in the Early Cenozoic. The Laramide orogeny is marked by thick-skinned deformation [*Jordán et al.*, 1983] in the western United States, and it caused upwarps and downwarps in eastern Utah [*Hintz and Kowallis*, 2009]. This thick-skinned deformation of gentle, broad-wavelength monoclinal uplifts in the Colorado Plateau, [Figure 2] such as the Uinta Mountains and San Rafael

swell, are associated with shallow (to near horizontal) subduction of the Farallon plate [*Wannamaker et al.*, 2001]. The monoclinal drape folds, like the San Rafael swell, are associated with near-vertical, uplifted basement blocks along reactivated Precambrian basement faults [*Neuhauser*, 1988; *Zuluaga et al.*, 2014].

The northeast-trending, asymmetric San Rafael swell [Figure 2] is an approximately 115 km long elongated upwarp, with a maximum width of approximately 50 km across forming a domelike structure [*Witkind*, 1988; *Witkind et al.*, 2006]. The swell is flanked on the west and east sides by northeast and northwest trending valleys, respectively [*Witkind*, 1988]. Castle Valley is located to the west while an unnamed valley is located to the east. The Book Cliffs run on the east and north of the swell and the cliffs on the west side of the swell form the east flank of the Wasatch Plateau [*Witkind et al.*, 2006]. Figure 2 shows the locations of key features. Coal mining is plentiful in the region, as thick coal beds in the Late Cretaceous Blackhawk Formation crop out along the cliffs in this area [*Witkind et al.*, 2006]. A broad band of northwesterly to west trending, and moderate to high angle, normal faults occurs from the east side of the swell, Book Cliffs, across the swell to Castle Valley on the western side of the swell [*Witkind*, 1988].

The San Rafael swell is actually part of a much larger structural unit, the San Rafael anticline, which is a doubly plunging anticline that trends northeast [*Witkind*, 1988]. Witkind [1988] explains that the physiographic unit (the swell) and the structural unit (the anticline) are often viewed as one feature based on the concurring location when they are actually wholly different, with the anticline extending far beyond the swell and strongly influencing the surrounding rocks. Near the northern end of the San Rafael

swell, the northeast trending axis of the San Rafael anticline bifurcates to form two north-trending anticlinal axes [*Witkind,* 1988].

While the bifurcation has little effect on the overall structure of the swell, the western main axis trends almost due north toward the Book Cliffs and the eastern axis trends about N25°E. The units on the west flank of the swell gently dip 2° to 6° westward and the units on the eastern flank steeply dip 45° to 85° eastward [*Witkind*, 1988]. Overall, the asymmetry of the swell creates a large monocline structure [*Witkind*, 1988]. Based on the ages of folded and deformed strata, it is believed that the San Rafael swell formed some time during the early Tertiary, with possible continued growth during the middle Tertiary, and was stable by the late Tertiary [*Witkind,* 1988].

Zuluaga et al. [2014] explain the San Rafael swell formation as reverse reactivation of high-angle normal faults in the Precambrian basement. They interpret the San Rafael swell as either a forced fold or a fault propagation fold. If the swell is a fault propagation fold, it is likely associated with a blind fault of either pure thrust-slip or reverse-slip kinematics, as is seen in other more eroded uplifts within the Colorado Plateau [*Zuluaga et al.*, 2014 and references therein]. Hintz and Kowallis [2009] explain erosion of the upwarps fills subsiding basins directly adjacent to the uplift, a discreet difference in sedimentation style from the Sevier orogeny.

The flat-topped, northeast trending, Wasatch Plateau [Figure 2] that runs to the west of the San Rafael swell is approximately 130 km long and 40 km wide [*Witkind et al.*, 2006]. The Wasatch plateau reaches elevations of approximately 10,000 feet (3,050 meters). The Wasatch monocline makes up the west flank of the Wasatch Plateau in a continuous westward-facing downwarp. High-angle, north and northeast-trending normal

faults cut the Wasatch Plateau and are often paired, forming narrow elongated grabens like the Joes Valley graben [*Witkind et al.*, 2006]. The faults are extremely straight and traceable for extended distances as single breaks or very narrow fault zones. Many of the faults are not visible on the surface as a result of burial beneath mass-wasting deposits. The north and northeast trending faults do not extend into the San Rafael swell area, which instead appears to be dominated by west and northwest-trending faults [*Witkind et al.*, 2006].

2.2.2 Stratigraphy

The Triassic and Jurassic sedimentary sequence in Utah accumulated in a gently subsiding basin [*Hintz and Kowallis*, 2009]. The deposition of the Upper Jurassic to Lower Cretaceous sequences are related to change in accommodation produced by the eastward migrating foreland-basin system and regional sea-level influences [*Currie*, 1997]. The early Triassic to mid-Jurassic time was characterized by marine incursions with at times very shallow, nearly landlocked seas [*Hintz and Kowallis*, 2009].

Triassic deposits include marine and tidal flat sediments as well as continental clastics with reworked volcanic ash. Hintz and Kowallis [2009] explain that the sediments are thinner on the craton in eastern Utah and thicker on the miogeocline that is west of the hinge line. The Early Jurassic sedimentary sequence is characterized by eolian and fluviatile deposits including the famous Navajo Sandstone thought to be formed from possibly the largest eolian dune field ever [*Hintz and Kowallis*, 2009]; these deposits are also thicker to the west of the hinge line. The mid-Jurassic sedimentary sequence consists of deposits from a shallow seaway that extended from Canada southward into Utah; evaporites are abundant indicating marginal marine conditions. By

the Late Jurassic, the seaway had retreated and deposits indicating a variety of environments such as wetlands, lakes, flood plains, and riparian systems were present. Some of this sequence is known for abundant dinosaur bones [*Hintz and Kowallis*, 2009].

Triassic Units

The Middle and Lower Triassic Moenkopi Formation [Figure 3] ranges in total thickness from 115 to 285 meters (m) and consists of three main parts: the Upper part, Sinbad Limestone Member, and the Lower part [*Witkind*, 1988]. The formation as a whole is often a deep reddish brown, but in the San Rafael swell area it has been bleached to a pale greenish gray, a possible result of reducing effects of petroleum or natural gas as it migrated into the anticline [*Witkind*, 1988]. The Upper part of the Moenkopi Formation is altered greenish-gray, very fine-grained sandstone and shaly siltstone and ranges in thickness from 60 to 185 m [*Witkind*, 1988]. The Sinbad Limestone Member is a yellowish-gray to light brown crystalline to locally oolitic limestone. The thickness ranges from 12 to 45 m. The Lower part of the Moenkopi Formation is a greenish-gray to yellowish brown, quartzose sandstone, shaly siltstone and interbedded mudstone with thicknesses ranging from 45 to 60 m [*Witkind*, 1988]. In some areas, the Lower part of the Moenkopi Formation is named the Black Dragon Member [*Hintz and Kowallis*, 2009].

The Upper Triassic Chinle Formation [Figure 3] is divided into three members: the Church Rock Member, Moss Back Member, and Temple Mountain Member [*Witkind*, 1988]. The Church Rock Member is a fluvial deposit consisting of reddish-brown to dark-brown, thin- to medium-bedded sandstone and shaly siltstone and ranges in thickness from 45 to 55 m. The Moss Back Member is a light-gray to gray, thin- to

medium-bedded crossbedded sandstone, conglomeratic sandstone and sparse conglomerate fluvial deposit. The Temple Mountain Member is altered and marked by purple and white mottles; the combined thicknesses of the Moss Back and Temple Mountain Members ranges from 20 to 55 m [*Witkind*, 1988].

The Upper Triassic Wingate Sandstone [Figure 3] consists of reddish-brown to brown, fine-grained quartzose sandstone with thicknesses ranging from 105 to 135 m [*Witkind*, 1988]. This eolian deposit is thick-bedded to massive and well cemented by calcium carbonate [*Witkind*, 1988].

The Upper Triassic Kayenta Formation [Figure 3] consists of a reddish-brown, fine- to coarse-grained sandstone that is thought to be a fluvial deposit [*Witkind*, 1988]. Its thickness ranges from 30 to 75 m with the unit grading into the overlying and underlying units [*Witkind*, 1988].

Jurassic Units

The Navajo Sandstone [Figure 3] is considered a Lower Jurassic to possibly Upper Triassic unit consisting of a light-tan and reddish-brown quartzose sandstone [*Witkind and Weiss*, 1991]. It can be thick-bedded to massive and fine- to coarse-grained [*Witkind*, 1988]. Variations in the thickness of the eolian deposit, which ranges in thickness form 120 to 305 m [*Witkind*, 1988], indicate the formation was likely deposited on an uneven surface of the Kayenta Formation [*Hood and Patterson*, 1984]. While the top of the Navajo Sandstone is sharply defined, the bottom of the unit is more difficult to distinguish due to a gradational contact with the Kayenta Formation [*Hood and Patterson*, 1984]. The Navajo Sandstone is an aquifer unit that has freshwater where the unit outcrops and saline water where it is buried at depth [*Hood and Patterson*, 1984].

The Middle Jurassic Carmel Formation [Figure 3] can be broken into two units an Upper and a Lower unit with a total thickness ranging from 85 to 105 m [*Witkind*, 1988]. The Upper Unit, which is about 75 m thick, consists of reddish-brown shaly siltstone interbedded with thin sandstone beds and small lenses and beds of gypsum [*Witkind*, 1988]. The Lower Unit is thinner ranging from 9 to 15 m in thickness and consists of light-gray to brownish-gray dense limestone [*Witkind*, 1988].

Coal

The Wasatch Plateau is underlain by significant amounts of coal contained primarily within five Tertiary and Cretaceous age units: the North Horn, Blackhawk, and South Flat Formations, the Sixmile Canyon Formation of the Indianola Group, and the Ferron Sandstone Member of the Mancos Shale [*Witkind et al.*, 2006]. Mining of the seams and beds that outcrop west of the Plateau started with the early settlers of the area and continued until the thicker, higher quality, more continuous and more economic beds were discovered along the eastern side of the Plateau [*Witkind et al.*, 2006]. The coal beds of the Blackhawk Formation of the Spring Canyon area (northwest of Price, Utah), mined until the 1920's and 1930's, were an important source of coal [*Weiss et al.*, 1990].

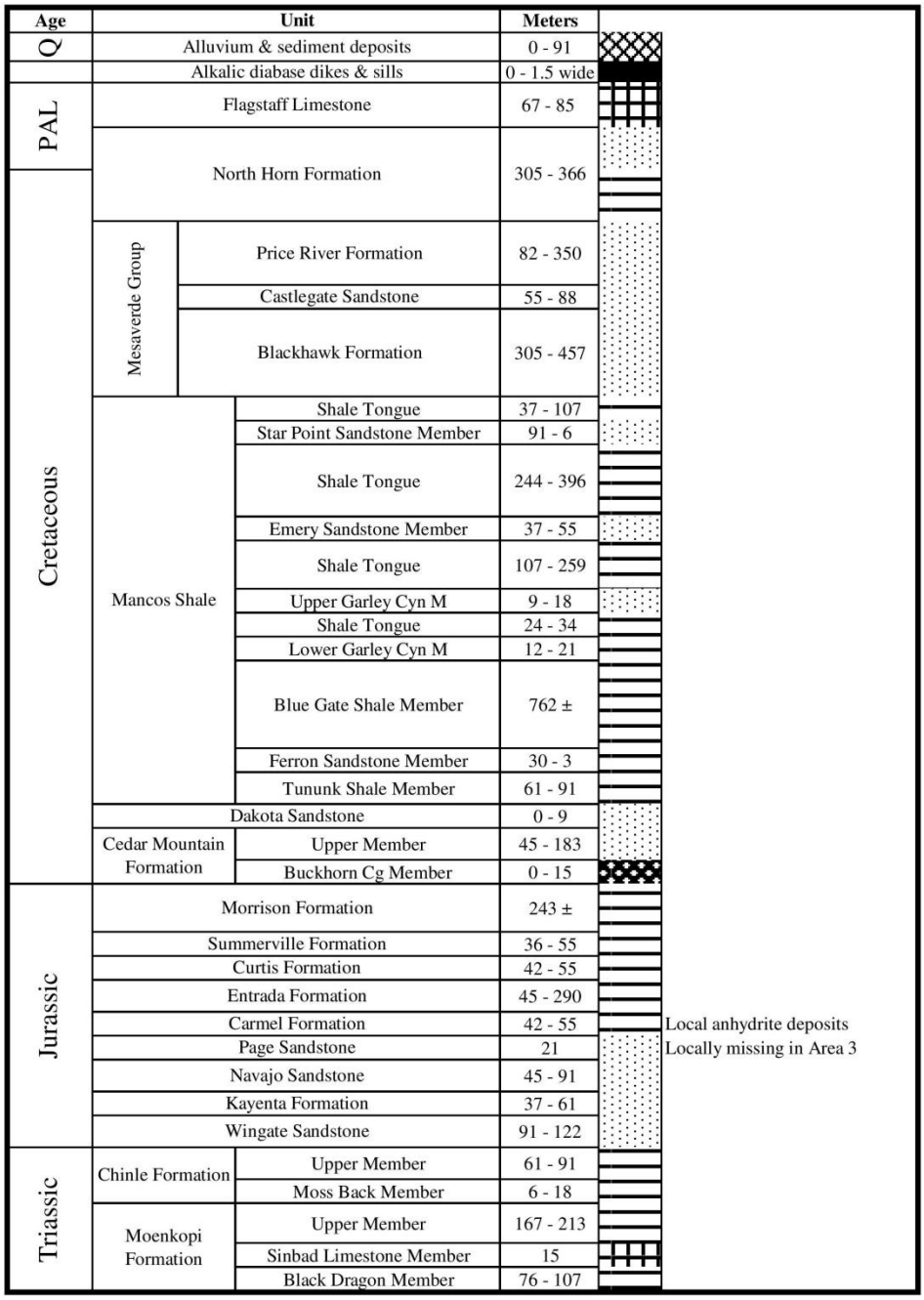

Figure 3: Stratigraphy of Price, Utah, adapted from *Hintze and Kowallis* [2009].

Mining continues in the Wasatch Plateau today. Mining occurs predominately in the beds contained in the Blackhawk Formation, which is at a minable depth within the Wasatch Plateau [*Witkind et al.*, 2006]. The Upper Cretaceous Blackhawk Formation

consists of dominantly light-brown, fine- to medium-grained quartzose sandstone interleaved with shaly siltstone, shale, carbonaceous shale, and coal [*Weiss et al.,* 1990]. The Blackhawk Formation was formed in a wave-dominated delta in a coastal area where flowing streams emptied into swamps, lagoons, and estuaries of a Cretaceous sea and the organic material of the swamps concentrated and gave rise to the thick coal beds [*Weiss et al.,* 1990]. In addition, thick coal beds are found and mined extensively in the western Book Cliffs [*Witkind*, 1988].

Hydrocarbon gas and oil are also present beneath the Wasatch Plateau in significant amounts; the source rock is possibly the Late Cretaceous Mancos Shale and the Middle Jurassic Arapien Shale [*Witkind et al.,* 2006]. The chief reservoir rocks for the economically produced hydrocarbon activity are the Ferron Sandstone Member of the Mancos Shale and the sandstones within the Emery Shale Member.

2.2.3 Seismicity

The majority of the seismicity of Utah [Figure 1] occurs along the Intermountain Seismic Belt (ISB) that is collocated with the approximately 100-km wide transition zone between the Basin and Range Province and the Colorado Plateau [*Arabasz et al.*, 2007]. Focal mechanisms, normal- to strike-slip, show predominantly WNW-ESE extension along the transition zone [*Arabasz et al.*, 2007]. Maximum focal depths of the natural seismicity are approximately 15 – 25 km; however, only a small percentage of the seismicity has well-constrained focal depths due to seismic station spacing [*Arabasz et al.*, 2007].

In addition, there is an area of active coal mining in central Utah that has been suspected of mining induced seismicity (MIS) and has been studied since the 1960s

[*Arabasz et al.*, 2007; *Pechmann et al.*, 2008; *Smith et al.*, 1974]. Monitoring of the MIS by the University of Utah Seismograph Station (UUSS) regional seismic network began in 1978 [*Kubacki et al.*, 2014]. The MIS is mostly a result of partial or complete collapse of underground mine workings and shear-slip motion on rock fractures, but can also be a combination of the two mechanisms [*Pechmann et al.*, 2008]. Most of the MIS is smaller than magnitude 3 and close to the mine depth, which is less than 960 m [*Arabasz et al.*, 2007]. The majority of the MIS with magnitudes greater than local magnitude (M_L) 3 have been caused by sudden roof-floor closure, and, therefore, the mechanism is implosive [*Arabasz et al.*, 2005].

Coal mining in the area is currently executed using longwall mining techniques, at depths less than 960 m [*Arabasz et al.*, 2007], and room and pillar mining [*Boltz et al.*, 2014]. Longwall mining entails the extraction of large panels of coal (200-400 m wide and 1 – 4 km long) using a mechanical shearer that passes back and forth across the width of the panel or the face [*Boltz et al.*, 2014]. As the shearer moves forward extracting the coal, a void is created, and the roof above the mined-out area, purposefully caves into the void; the caved area is known as the gob [*Boltz et al.*, 2014].

Stress, known as the front abutment load, is generated across the panel and ahead of the face. In addition, along the headgate, the road adjacent to the unmined coal panel, and the tailgate, the road adjacent to previously mined panels, stress is generated; the resulting stress change may manifest as coal bursts off pillars in the roads or as heaving in the floors of the mines [*Boltz et al.*, 2014]. In the room and pillar mining process a checkerboard pattern of rooms (openings) and pillars are created, often with the pillars left in place to support the roof of the mine [*Arabasz et al.*, 2005]. Mining induced

seismicity is often closely located to the coalface and the number of seismic events and the coal production amounts are also often correlated [*Boltz et al.,* 2014].

A microearthquake survey completed in 1970 in the Sunnyside coal mining district, approximately 40 km east of Price, Utah, found averages of hundreds of seismic events per day with magnitudes ranging from -0.5 to 2.8 [*Smith et al.*, 1974]. At the time of the study, the coal was extracted using the room and pillar process. The zone of greatest seismicity was located approximately 1 km below the portion of the mine with pillar removal and floor and roof failures [*Smith et al.*, 1974]. This suggests a strong spatial correlation between mining activities and seismicity, and the possibility that unloading and redistribution of the overburden stresses triggers deeper seismicity. The majority of seismic events with magnitudes less than -1 originated as shear failures near the mine walls. Northeast striking reverse faulting was defined by a composite fault-plane solution, which is in agreement with the stress pattern that developed the San Rafael swell in the area, suggesting regional tectonic stress may supply the main energy of the seismic events. Smith et al. [1974] also found evidence that accelerations from the sub-mine seismicity triggered mine failures and rock bursts in the mine above.

Chapter 3: Data

3.1 Utah Service Wells

Utah is one of the top states for hydrocarbon production in the nation. The U.S. EPA UIC program regulates all injection wells in the United States. Often, state agencies administer the UIC program for the EPA, and Utah has administered the program since 1983. Utah's Department of Natural Resources, Division of Oil, Gas and Mining regulates all operations related to the production of oil or natural gas, including the UIC program.

The website for the Division of Oil, Gas and Mining has searchable records for all of the wells in the state. In Utah, service wells include all injection well designations [Figure 4]: water injection wells used in enhanced recovery, water disposal wells, and gas injection wells. Service wells also include water supply wells, which are pumping wells. Many of the records for the wells are public record and available online. Injection volume data for the wastewater disposal wells is available from 1986 to the present. UIC permitting requires reporting of monthly well injection volumes and maximum injection pressure. The Division of Oil, Gas and Mining organizes the information in a searchable database.

I searched Utah's Division of Oil, Gas and Mining website for injection wells and chose four areas of interest based on the service wells in the area [Figure 4]; the boundaries of the four areas are included in Table 1. Area 3 is also located near the active coal mines within the Book Cliffs and Wasatch Plateau.

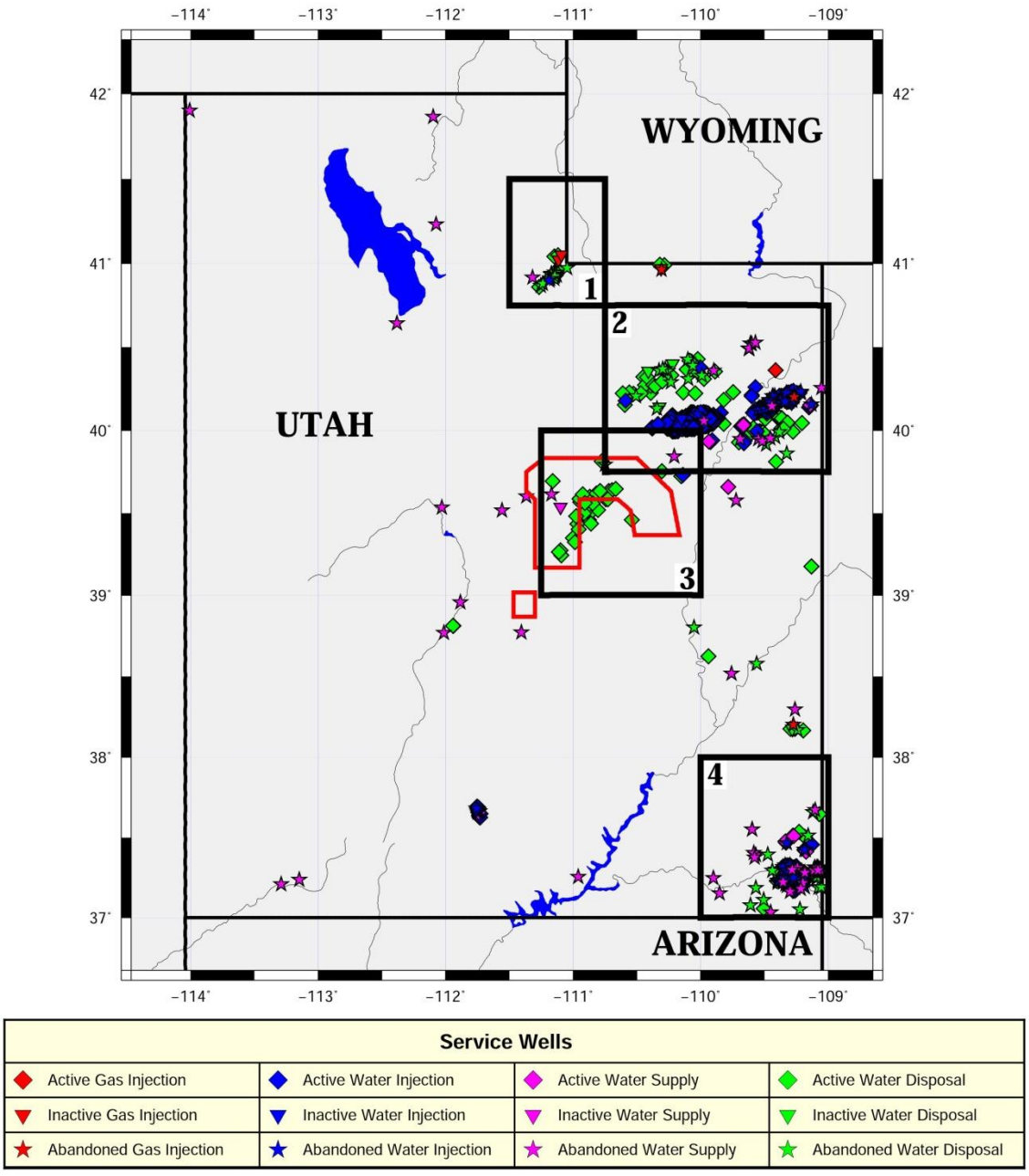

Figure 4: The service wells of Utah. Red polygons outline coal mining areas *[adapted from Arabasz and Pechmann, 2001]*. The four areas of interest are outlined in black and labeled.

Table 1: Boundaries of the Four Areas of Interest

Area	North Boundary	South Boundary	East Boundary	West Boundary
Area 1	41.50°	40.75°	-110.75°	-111.50°
Area 2	40.75°	39.75°	-109.00°	-110.75°
Area 3	40.00°	39.00°	-110.00°	-111.25°
Area 4	38.00°	37.00°	-109.00°	-110.00°

3.2 Coal Production

Area 3 encompasses an area surrounding Price, Utah, which includes Book Cliffs, the northern surface exposure of the San Rafael swell, and a portion of the Wasatch Plateau [Figure 2]. These areas also include a large portion of the coal mining areas of Utah. According to the Utah Coal Program, part of the Utah Department of Natural Resources, Division of Oil, Gas, and Mining, some of the mines in the area have been in use over one hundred years. I downloaded coal production data from the U.S. Department of Labor website (http://www.msha.gov/OpenGovernmentData/OGIMSHA.asp), which supports the Open Government Initiative from the Mine Safety and Health Administration. The annual coal production data, in units of short tons, was collected for each mine by the U.S. Energy Information Administration and the U.S. Mine Safety and Health Administration and covers production from 1983 through 2013. I used this data as a proxy for mining activity on an annual basis in order to evaluate temporal correlations between the mining and seismicity of the area.

3.3 Earthquake Catalog

The The University of Utah Seismograph Station (UUSS) seismic network is a regional element of the Advanced National Seismic System (ANSS). The UUSS operates seismograph stations throughout Utah and in neighboring parts of the ISB in eastern Idaho and western Wyoming. I downloaded the seismic data from the United States Geological Survey (USGS) using the Comprehensive Earthquake Catalog (ComCat) search (http://earthquake.usgs.gov/earthquakes/search/); most of the records were from the UUSS network and included earthquakes from $M < 0$. Having a seismic

network [Figure 5] that includes earthquakes with very small magnitudes is very important to study induced seismicity, as the majority of the induced earthquakes are magnitude less than 3.

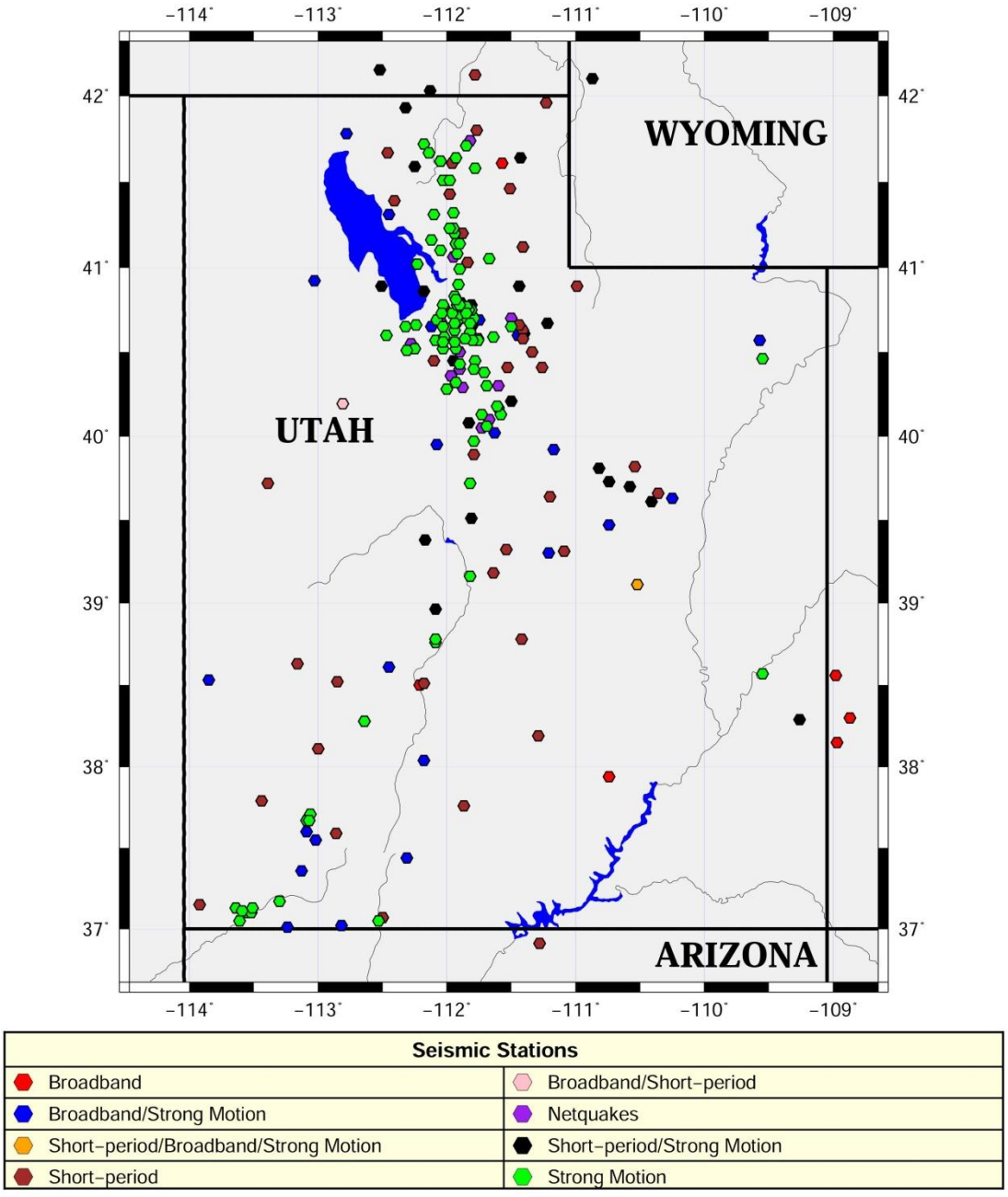

Figure 5: The of Utah Seismograph Station seismic network.

Digital recording of the UUSS regional seismic network began January 1, 1981 and by 1981 there was reasonable seismographic coverage [*Arabasz et al.*, 2007]. Permanent seismic stations have an average spacing of 40-50 kilometers in central Utah [*Arabasz et al.*, 2007], where the majority of my research is focused, causing low focal-depth resolution. Magnitudes in the catalog are mostly based on local magnitude scales [*Arabasz et al.*, 2007] and coda magnitude scales (M_c), which is an empirical estimate of local magnitude. According to Arabasz et al. [2007], the magnitudes are systematically revised to ensure the uniformity of size estimates. Comparisons of revised magnitudes to moment magnitudes (M_w) show that the M_L magnitudes are almost equivalent to M_w magnitudes [*Pechmann et al.*, 2007]. Quarry blasts and other artificial seismic events are routinely identified and removed from the UUSS catalog based on the character of the recorded waveform and information on the location and time of day of the event [*Arabasz et al.*, 2007]. Arabasz et al. [2007] indicated the magnitude threshold for the catalog they used, which includes Area 3 and covers the period 1981 – 2006, was complete for magnitude 2.0 in the Interseismic Belt area and approximately magnitude 2.5 in the other areas.

I downloaded seismic data for Utah from the USGS ComCat search on September 3, 2013. I plotted the seismic data from 1981 to September 2013 for all of Utah in Figure 1 and for the seismicity in Areas 1 – 4 in Figures 6 – 9.

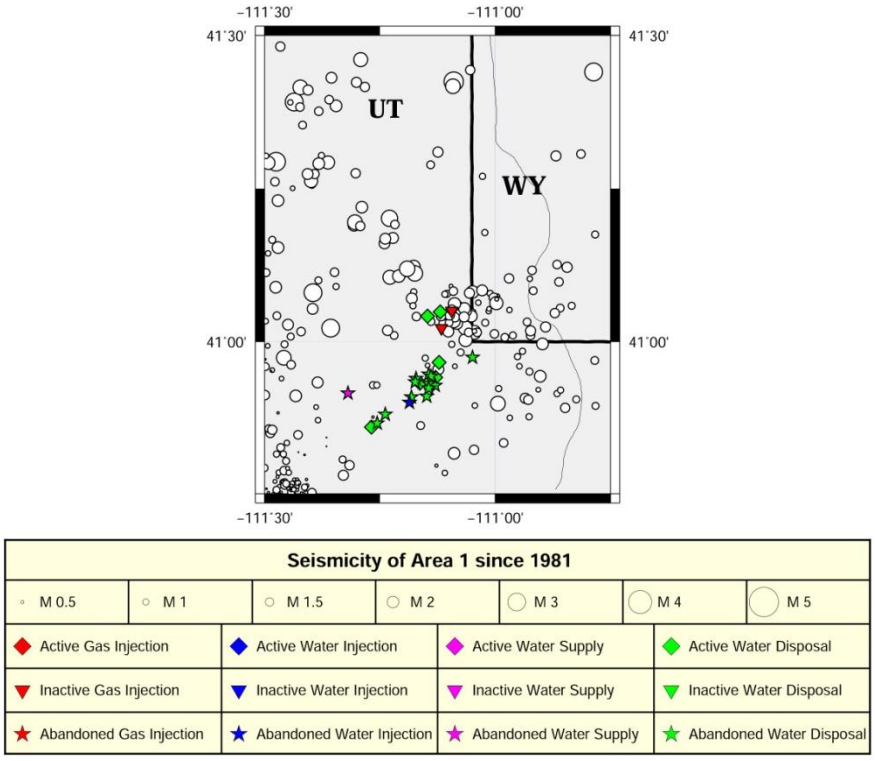

Figure 6: Area 1 seismicity since 1981.

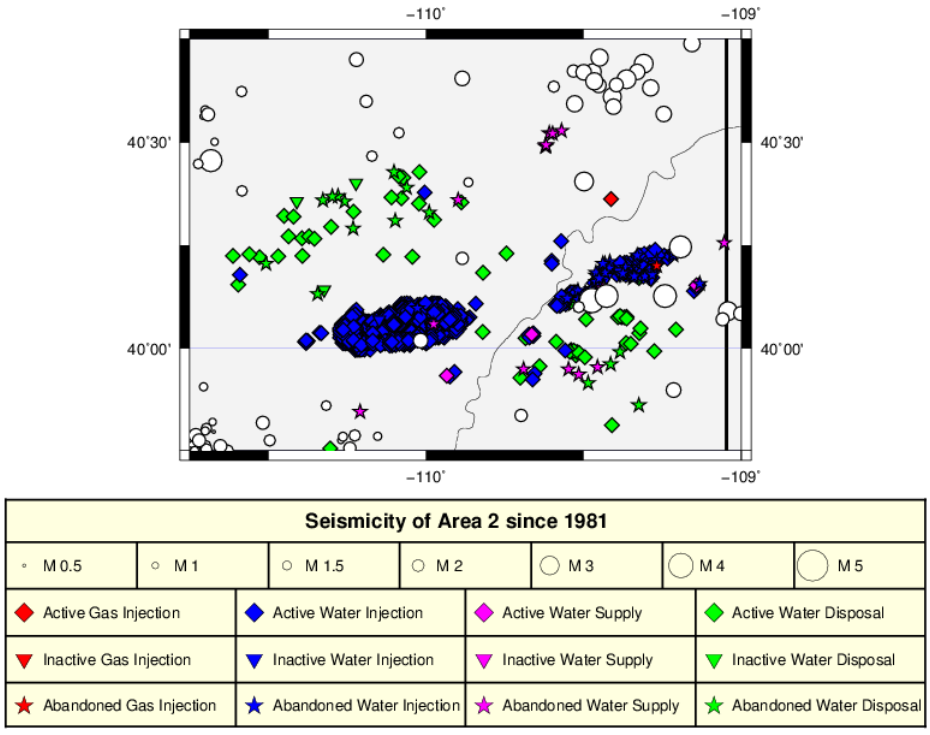

Figure 7: Area 2 seismicity since 1981.

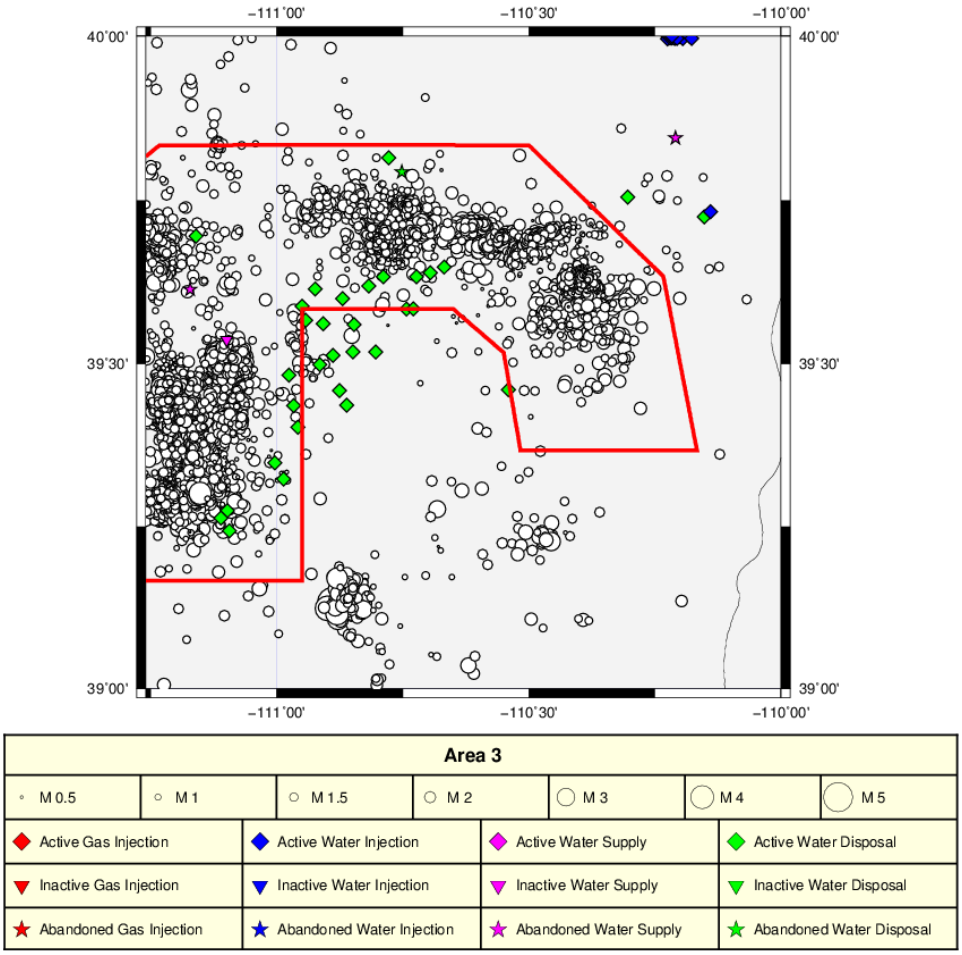

Figure 8: Area 3 seismicity since 1981. Red polygon outlines coal mining areas [adapted from *Arabasz and Pechmann*, 2001].

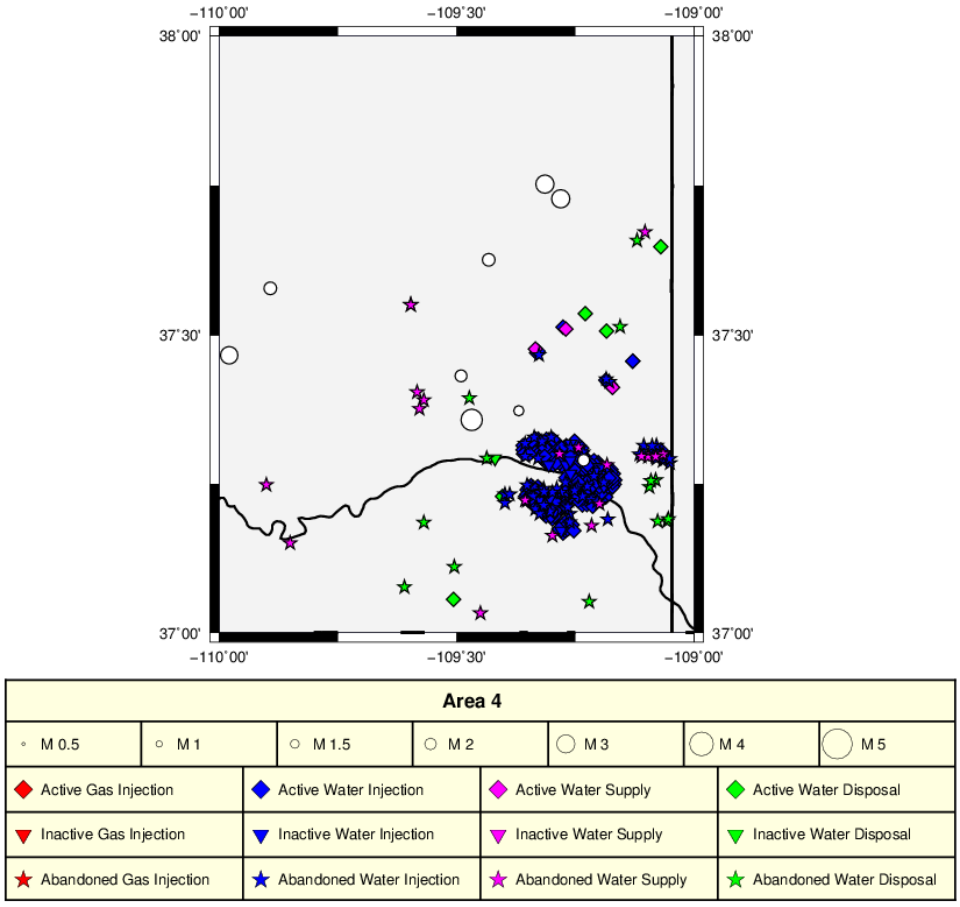

Figure 9: Area 4 seismicity since 1981.

From October 2000 through April 2001, a study was conducted in the Trail Mountain Area, Emery County, Utah evaluating the possible effects of the mining induced seismicity (MIS) on a nearby reservoir [*Arabasz et al.*, 2002]. During the study, the University of Utah installed a temporary seismic array in the Trail Mountain area. As part of the evaluation of MIS on the reservoir, Arabasz et al. [2002] relocated a number of seismic events collected during the deployment of the temporary array. The majority of the seismic events were located at very shallow depths of less than 1 km and within ± 0.6 km of mine level of the Trail Mountain Mine [*Arabasz et al.*, 2002]. Since Arabasz et al. [2002] confirmed their data set of seismic events to be MIS using relocation

techniques, I removed it from my data set. Almost all of the 1,829 seismic events of Arabasz et al.'s [2002] data set for the Trail Mountain local study area [Figure 10] were located within Area 3; upon close inspection, only 1,784 events of the events were included in my data set downloaded from the USGS ComCat search.

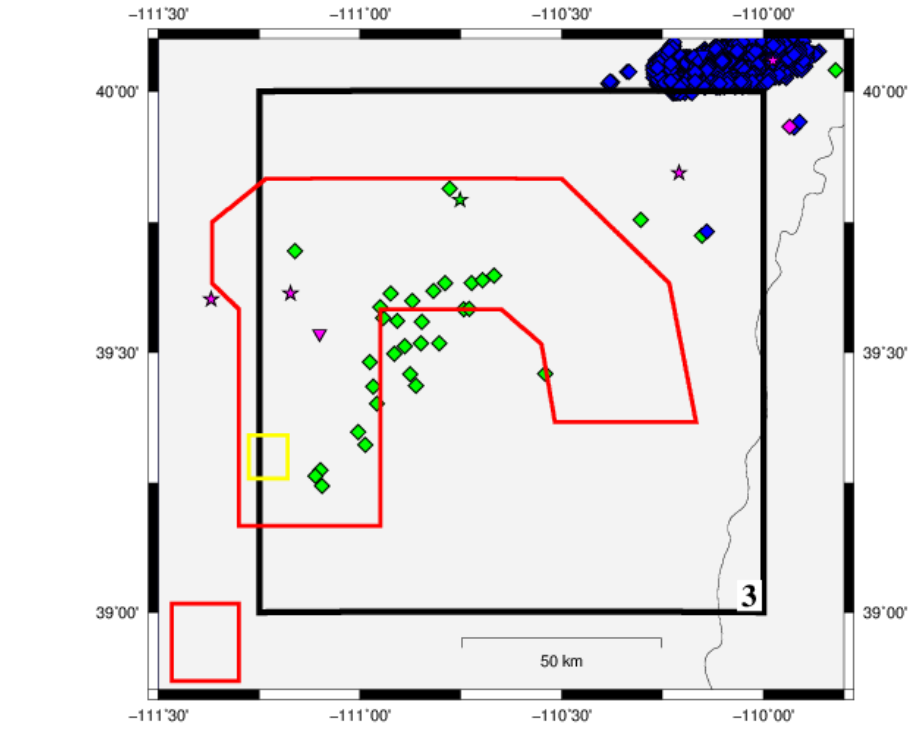

Trail Mountain Local Study Area Location			
Active Gas Injection	Active Water Injection	Active Water Supply	Active Water Disposal
Inactive Gas Injection	Inactive Water Injection	Inactive Water Supply	Inactive Water Disposal
Abandoned Gas Injection	Abandoned Water Injection	Abandoned Water Supply	Abandoned Water Disposal

Figure 10: Trail Mountain local study area is outlined in yellow [adapted from *Arabasz et al.*, 2002]. Area 3 is outlined and labeled in black and the coal mining areas are outlined in red [adapted from *Arabasz and Pechmann*, 2001].

Chapter 4: Spatial and Temporal Correlation

4.1 Seismicity Rate

In order to determine if seismicity changed as a result of the injection wells, I plotted cumulative seismicity of the four areas over time [Figures 11 – 14]. In doing so, the slope of the line is the seismicity rate of the area. If the seismicity rate is consistent, the slope is linear and, using linear regression, the R^2 value is close to one.

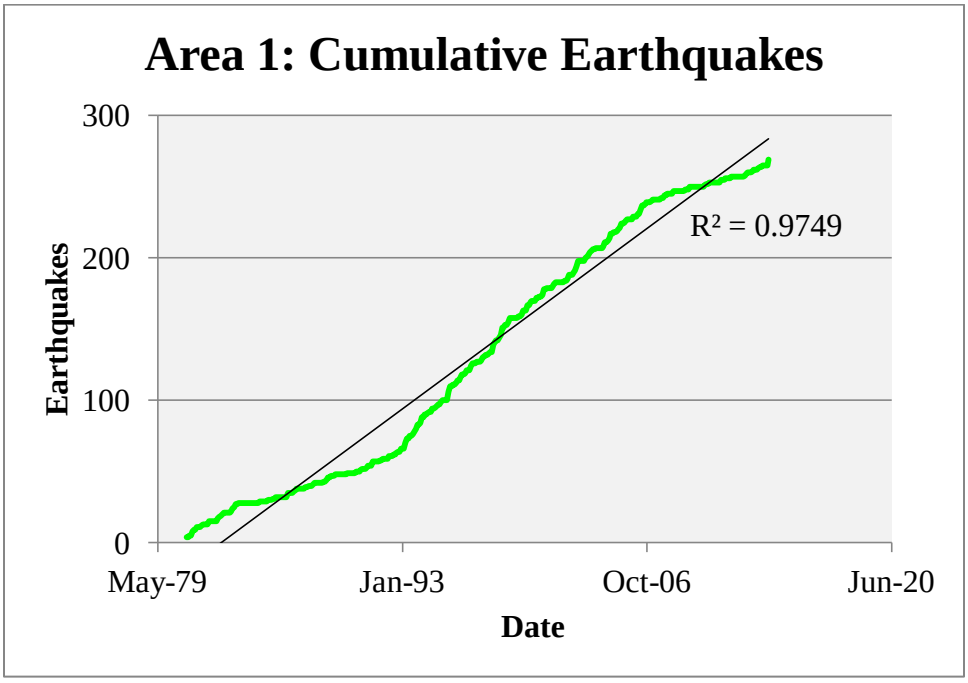

Figure 11: Area 1's cumulative earthquakes since 1981.

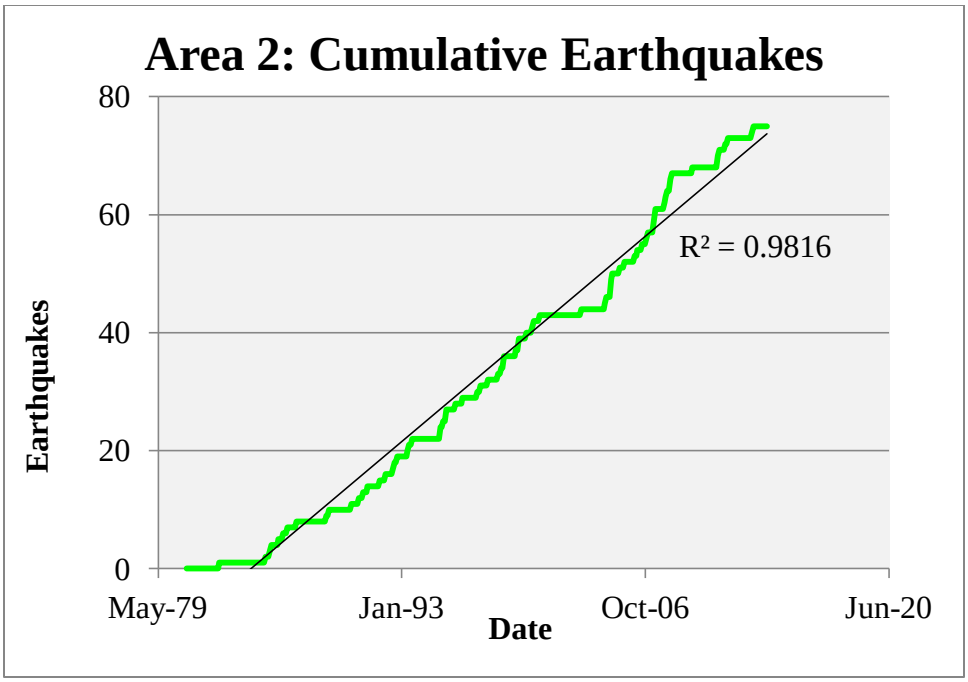

Figure 12: Area 2's cumulative earthquakes since 1981.

Areas 1 and 2 have had a consistent seismicity rate since 1981 [Figures 11 and 12], but Areas 3 and 4 have had seismicity rate variations [Figures 13 and 14]. Area 1 has nineteen wastewater disposal wells, including seven active of which at least two have been active since the 1980s [UIC public record well files]. The wells have injected a reported total of approximately 2.44×10^8 barrels (bbls) of wastewater as of October 2014 [UIC public record well files]. Area 2 has 80 wastewater disposal wells, 61 of which are active, and 1,265 active water injection wells, used for enhanced recovery [UIC public record well files]. The total injected volume from the 80 wastewater disposal wells is 6.3×10^8 bbls as of January 2015 [UIC public record well files].

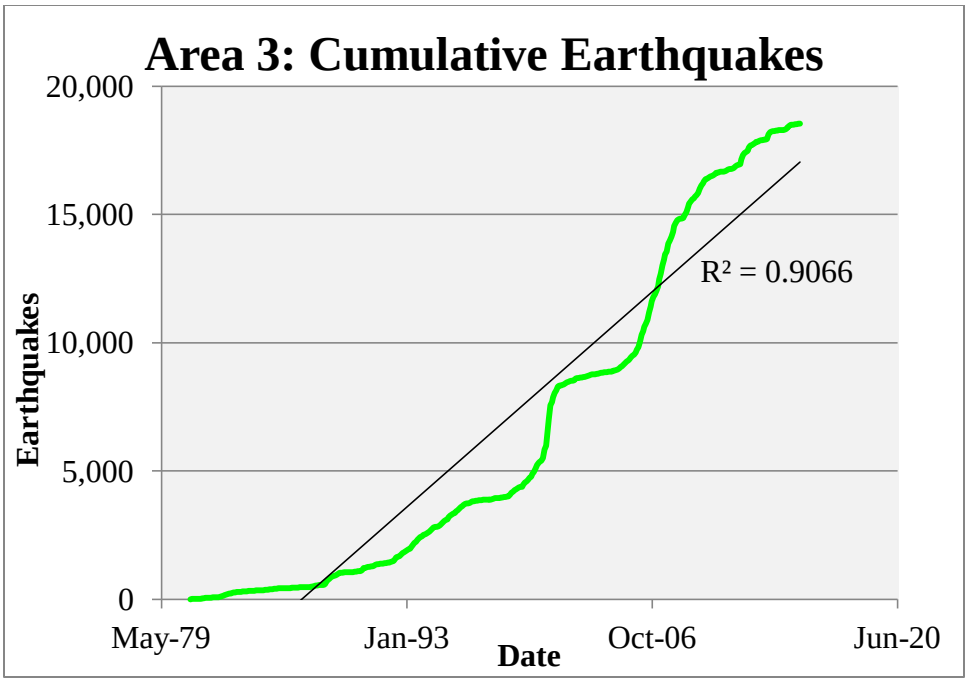

Figure 13: Area 3's cumulative earthquakes since 1981, with confirmed MIS [*Arabasz et al.*, 2002] removed.

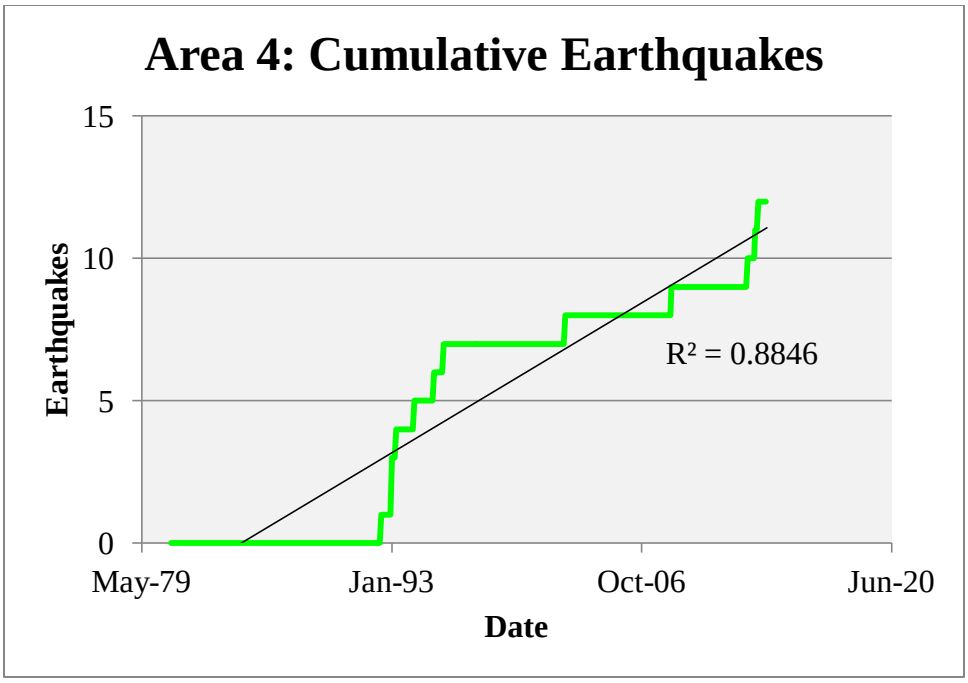

Figure 14: Area 4's cumulative earthquakes since 1981.

Area 3 has had over 20,000 seismic events since 1981, and therefore, the changes in seismicity rate are significant. Area 4 shows variation in seismicity rate since 1981, but it is a very small sample size of events, Figure 14, which is too small to indicate a significant change. Area 4 has twenty-one wastewater disposal wells, seven of which are listed as active wastewater disposal wells [UIC public record well files]. As of January 2015, the wells have injected a reported total volume of 3.3×10^7 bbls [UIC public record well files].

I chose two smaller sections of Area 3 to further test changes in seismicity rates. I include the boundaries of the two clusters [Figure 15], Cluster 1 and Cluster 2, in Table 2. I plotted the cumulative earthquakes since 1981 for Area 3's Cluster 1 and Cluster 2 [Figures 16 and 17]. I removed the MIS identified in Arabasz et al. [2002], which is located within the area of Cluster 2, from the data set.

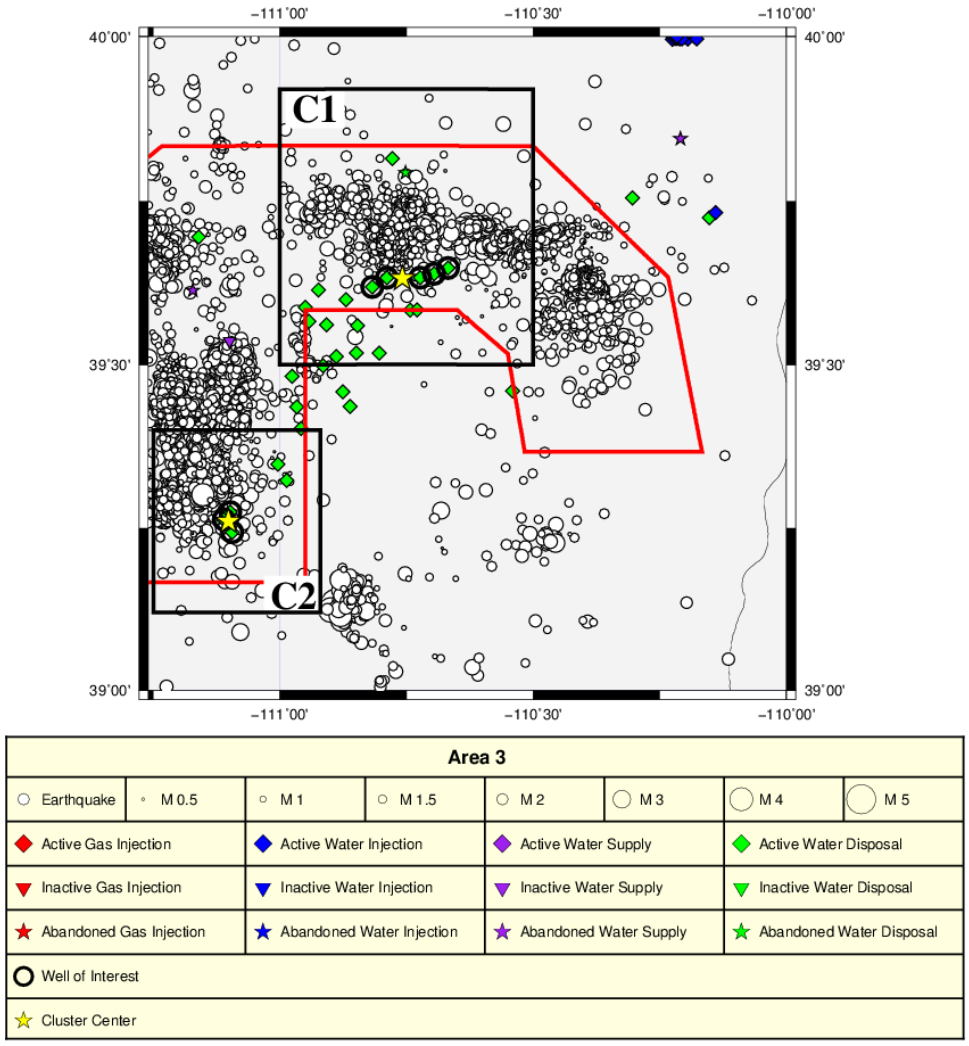

Figure 15: Area 3 with Cluster 1 (C1) and Cluster 2 (C2). The red polygon outlines coal mining areas [adapted from *Arabasz and Pechmann*, 2001].

Table 2: Boundaries for the Two Clusters within Area 3

Area	North Boundary	South Boundary	East Boundary	West Boundary
Cluster 1	39.92°	39.50°	-110.50°	-111.00°
Cluster 2	39.40°	39.12°	-110.92°	-111.25°

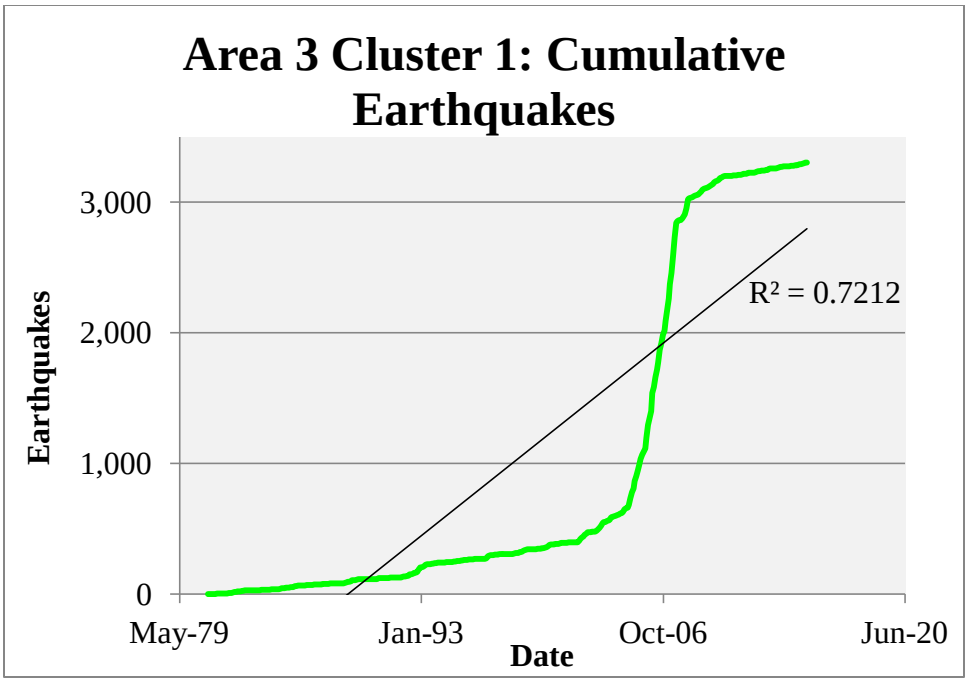

Figure 16: Area 3, Cluster 1 cumulative earthquakes since 1981.

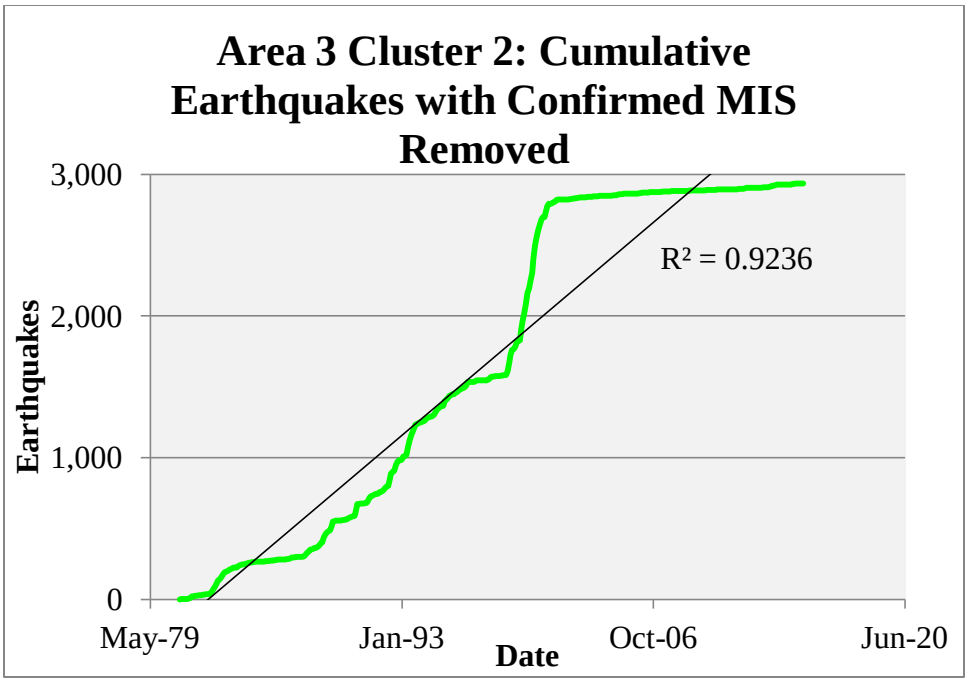

Figure 17: Area 3, Cluster 2 cumulative earthquakes since 1981, with confirmed MIS [*Arabasz et al.*, 2002] removed.

4.2 Temporal Correlation

4.2.1 Injection Wells and Seismicity

Area 3 has 32 active wastewater disposal wells, the majority of which inject into the Navajo Sandstone, Kayenta Formation, and Wingate Sandstone [UIC public record well files]. Disposal well details are included in Table 3. These formations are considered one hydrogeologic unit in the area, the Navajo aquifer [*Freethey and Cordy*, 1991]. Area 3 has 27 wells that inject into the Navajo aquifer; I removed the volumes injected into other formations in the wells that first injected into formations other than the Navajo aquifer. All of the wells in Area 3 injecting into the Navajo aquifer commenced injection after 1986. Only one well in Area 3, which injects into the Moenkopi Formation, started injection in December 1984 [UIC public record well files], and therefore, the 13 months of injection data from this well is missing from the injection volume data. I present the locations of the disposal wells by injection aquifer in Figure 18.

Cluster 1 takes into account the well volumes of five wells of interest (API #s: 43-007-30361; 43-007-30555; 43-007-30912; 43-007-30967; and 43-007-30979) that inject into the Navajo aquifer. Cluster 2 takes into account the well volumes of three wells of interest (API #'s: 43-015-30272; 43-015-30303; and 43-015-30323) that inject into the Navajo aquifer.

Table 3: Area 3 Wastewater Disposal Wells

API	Current Status	Date first active	Latitude	Longitude	Injection formation
43-007-30040	Active	*8/1/1994*	39.5596	-110.8479	Navajo, Kayenta, Wingate
43-007-30093	Active	**9/17/1987**	39.5874	-110.9505	Morrison (until 1996); Navajo, Kayenta, Wingate (since 12/2/1996)
43-007-30100	Active	**9/13/1987**	39.5607	-110.9080	Curtis and Buckhorn (until 1999); Navajo, Kayenta, Wingate (since 1/5/1999)
43-007-30169	Abandoned	N/A	39.7927	-110.7523	Never Used as Injection Well
43-007-30290	Active	*6/12/1996*	39.5177	-110.8494	Navajo, Kayenta, Wingate
43-007-30314	Active	*10/1/1997*	39.5990	-110.8708	Navajo, Kayenta, Wingate
43-007-30351	Active	**11/25/1997**	39.6138	-110.9246	Navajo, Kayenta, Wingate
43-007-30361	Active	**1/28/1998**	39.6332	-110.7891	Navajo, Kayenta, Wingate
43-007-30438	Active	**3/3/2001**	39.5662	-110.9431	Navajo, Kayenta, Wingate
43-007-30520	Active	*10/5/1999*	39.4982	-110.9152	Navajo, Kayenta, Wingate
43-007-30555	Active	*11/15/1999*	39.6187	-110.8190	Navajo, Kayenta, Wingate
43-007-30567	Active	**9/5/2000**	39.5179	-110.8043	Navajo, Kayenta, Wingate
43-007-30656	Active	**8/30/2000**	39.5124	-110.8896	Navajo, Kayenta, Wingate
43-007-30721	Abandoned	**2/8/2001**	39.4822	-110.9767	Navajo, Kayenta, Wingate
43-007-30912	Active	**12/1/2003**	39.6332	-110.7238	Navajo, Kayenta, Wingate
43-007-30913	Active	**9/13/2010**	39.7244	-110.1521	Lower Colton/Wasatch, Dark Canyon Conglomerate, Price River Formation
43-007-30953	Active	*7/31/2008*	39.7545	-110.3043	Middle Wasatch
43-007-30967	Active	**11/19/2005**	39.6390	-110.6968	Navajo, Kayenta, Wingate
43-007-30979	Active	**1/25/2006**	39.6479	-110.6681	Navajo, Kayenta, Wingate
43-007-31182	Active	**1/4/2011**	39.6949	-111.1611	Ferron Sandstone
43-007-31374	Active	**3/4/2009**	39.5833	-110.7433	Navajo, Kayenta, Wingate
43-007-31375	Active	**12/17/2008**	39.5841	-110.7294	Navajo, Kayenta, Wingate
43-013-32308	Active	**12/6/2002**	39.8142	-110.7784	Spring Canyon
43-015-30111	Active	**12/12/1984**	39.4600	-110.5415	Moenkopi
43-015-30272	Active	**6/8/1996**	39.2433	-111.0948	Navajo, Kayenta, Wingate
43-015-30303	Active	**2/7/2008**	39.2739	-111.0990	Navajo, Kayenta, Wingate
43-015-30323	Active	**5/13/1998**	39.2629	-111.1118	Navajo, Kayenta, Wingate
43-015-30338	Active	**11/11/1998**	39.4587	-110.8769	Navajo, Kayenta, Wingate
43-015-30356	Active	*11/1/1999*	39.4361	-110.8615	Navajo, Kayenta, Wingate
43-015-30477	Active	**2/13/2001**	39.4352	-110.9679	Navajo, Kayenta, Wingate
43-015-30490	Active	*4/1/2002*	39.3476	-111.0049	Navajo, Kayenta, Wingate
43-015-30510	Active	*3/1/2010*	39.3229	-110.9871	Navajo, Kayenta, Wingate
43-015-30531	Active	**1/16/2003**	39.4022	-110.9586	Navajo, Kayenta, Wingate

Bold Date = Reported first injection dates.

Italicized Date = Estimated first injection date from well file and reported well volume records.

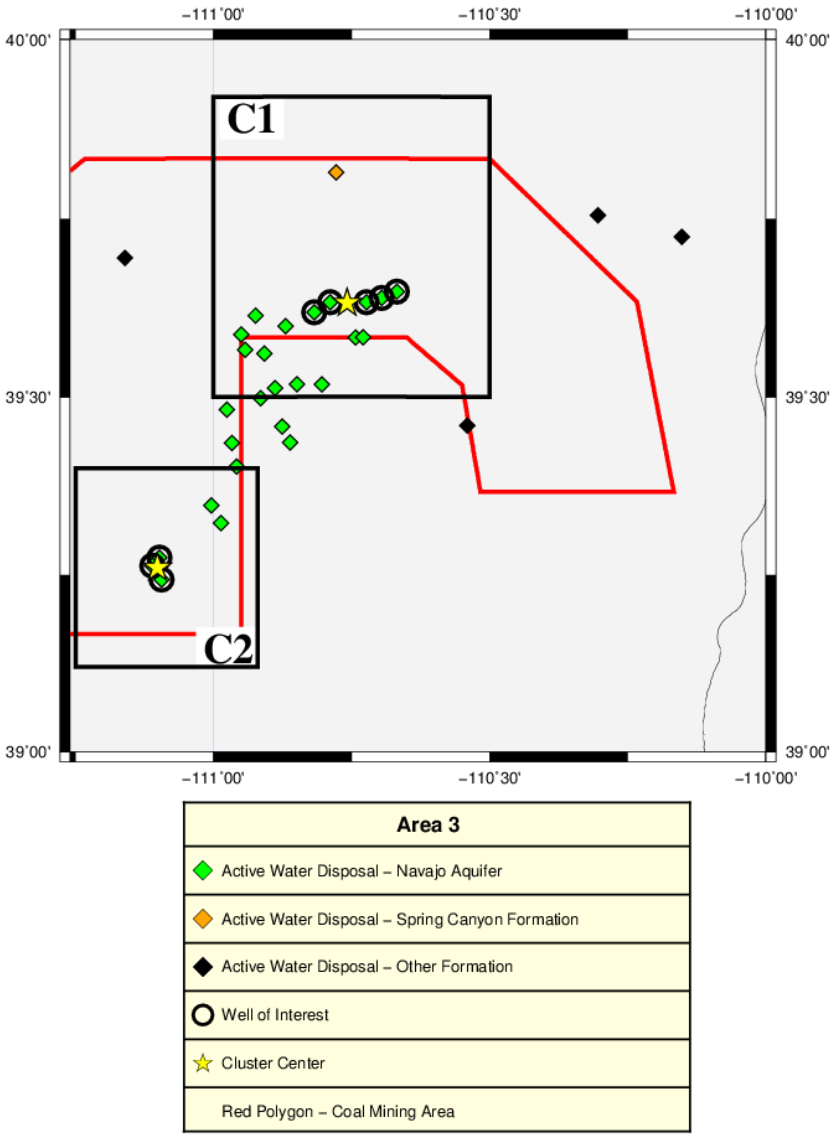

Figure 18: Area 3 disposal wells by injection aquifer.

Due to the consistent seismicity rates since 1981, Areas 1 and 2 did not warrant further evaluation for correlations with wastewater injection. In order to determine the feasibility of injection induced seismicity in the areas with changes in seismicity rate, I plotted the cumulative seismicity and cumulative injection volume for the remaining

areas [Figures 19 – 23]. The injection volume data is available since 1986 via the Utah Department of Natural Resources (DNR), Division of Oil, Gas, and Mining's website. The seismicity rates of Area 3 as a whole, and Clusters 1 and 2 individually, show a correlation with the start of injection when the seismicity and cumulative injection volumes are plotted together.

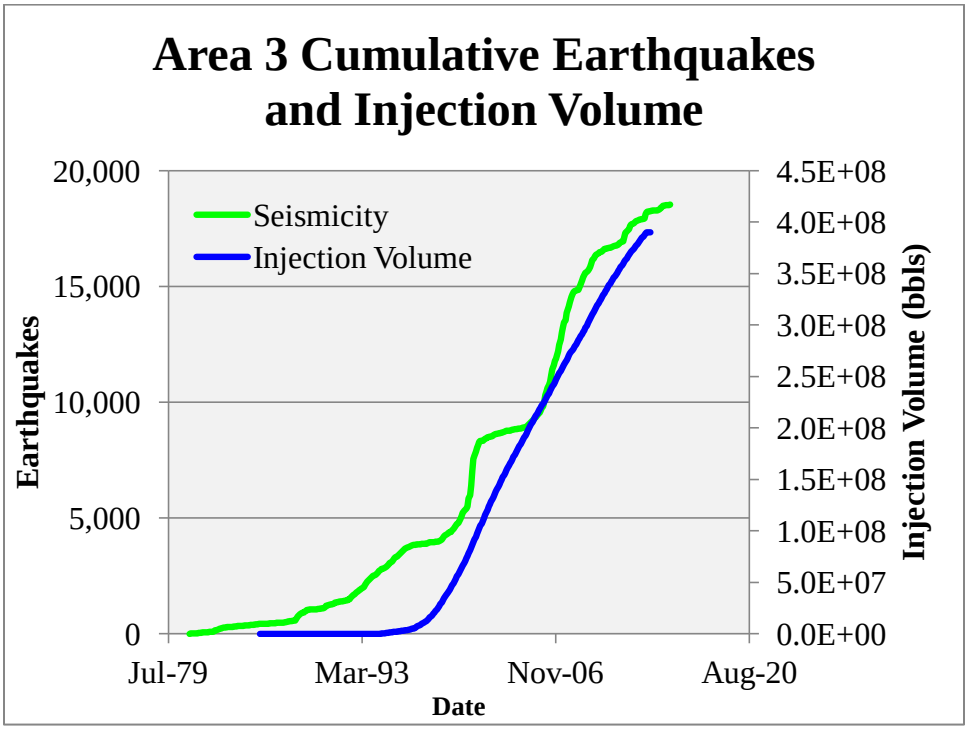

Figure 19: Area 3 cumulative earthquakes since 1981, with confirmed MIS [*Arabasz et al.*, 2002] removed and cumulative injection volume into the Navajo aquifer since 1986.

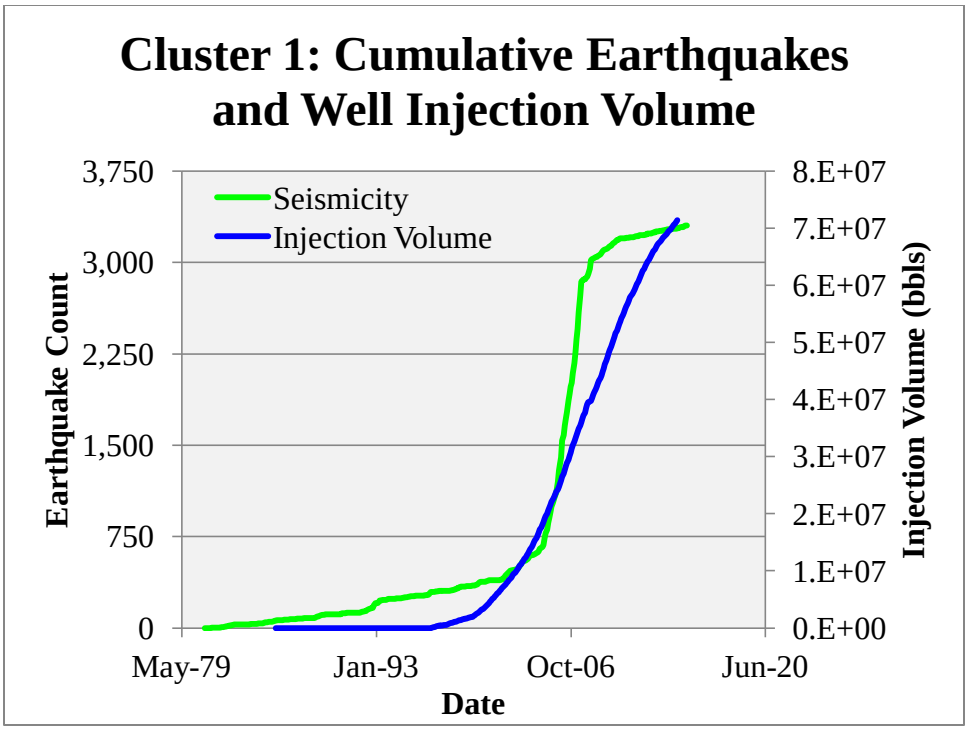

Figure 20: Cluster 1 cumulative earthquakes since 1981 and cumulative well volumes from the five wells of interest since 1986.

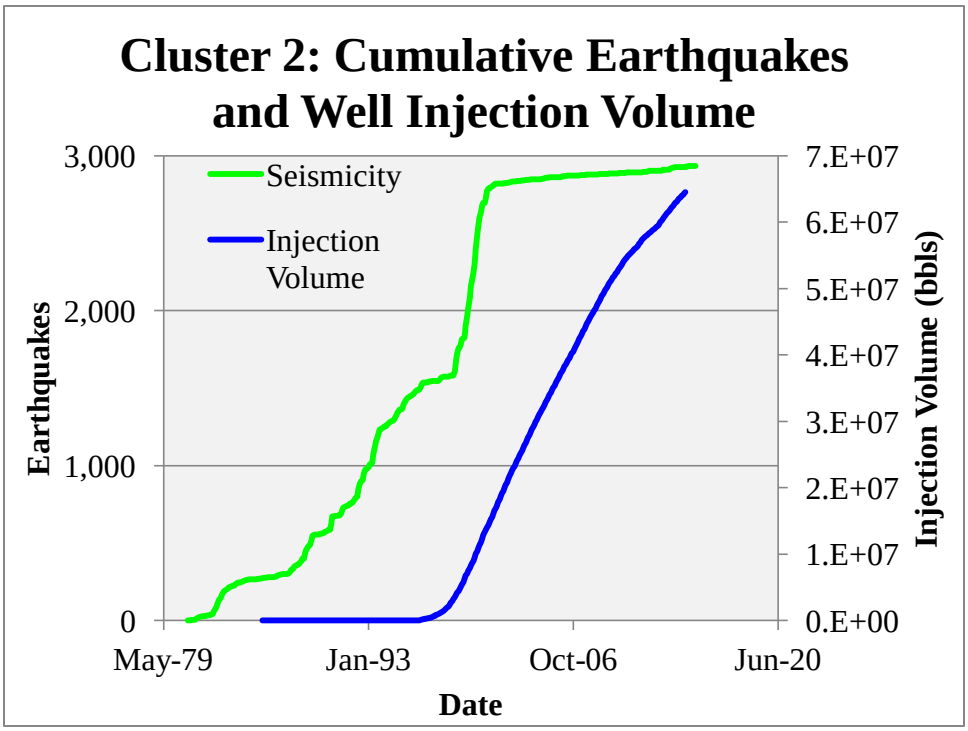

Figure 21: Cluster 2 cumulative earthquakes since 1981, with confirmed MIS [*Arabasz et al.*, 2002] removed and cumulative injection volume from the three wells of interest since 1986.

Cluster 1 also includes a disposal well (API # 43-013-32308) that injects into the Spring Canyon Member of the Blackhawk Formation and is located in the coal mining area. Based on the UIC well file and drilling log, the injection is occurring at approximately 1.7 km below the ground surface. There is a strong correlation between the seismicity of Cluster 1 and the injection volume of this disposal well as indicated in Figure 22.

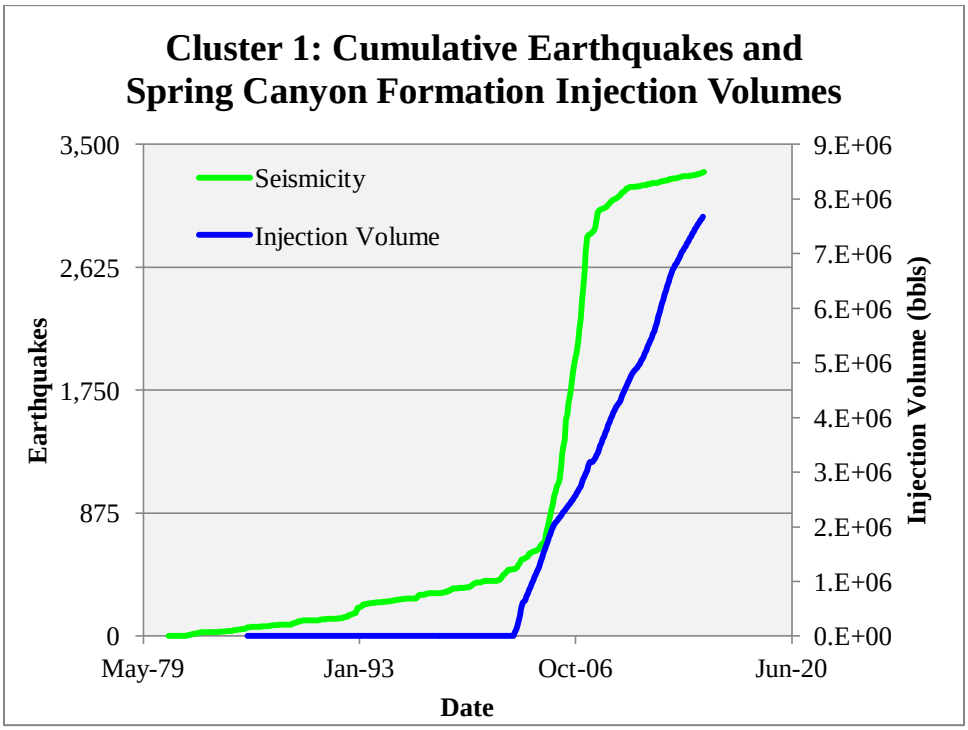

Figure 22: Cluster 1 cumulative earthquakes since 1981 and cumulative injection volume into the Spring Canyon Member of the Blackhawk Formation since 1986.

I also plotted the cumulative earthquakes and injection volumes for Area 4 in Figure 23. Seven wastewater disposal wells are located in Area 4, one of which is now listed as inactive [UIC public record well files]. The seven wells have injected a reported

total of approximately 2.24 x 10^7 bbls of wastewater as of August 2013 [UIC public record well files]. Area 4's variation in seismicity rate is based on a very small number of events, 12, and therefore, I cannot infer correlations.

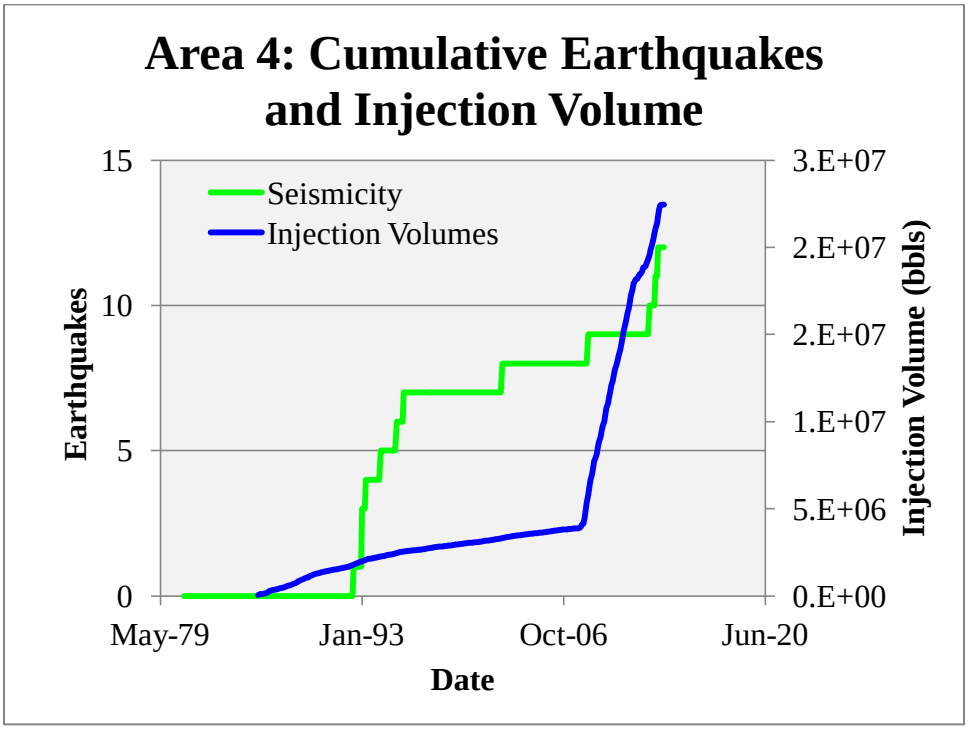

Figure 23: Area 4 cumulative earthquakes since 1981 and cumulative injection volume since 1986.

4.2.2 Coal Production and Seismicity

Area 3 is also located in an area with extensive coal mining [Figure 1]. I compiled annual coal mining production data in order to evaluate correlations between mining activity and increased seismicity. The coal mining production data provided by the U.S. Energy Information Administration (USEIA) and the U.S. Mine Safety and Health Administration (USMSHA) is organized by coal mine. Based on a map of the coal mines of the region [*Utah DNR*, 2014], I separated production data for Cluster 1 and

Cluster 2 as well as evaluating Area 3 as a whole. Coal production is reported in units of short tons, which is the U.S. ton and equivalent to 2,000 pounds. Overall, coal production in Area 3 has been consistent since 1983 [Figure 24].

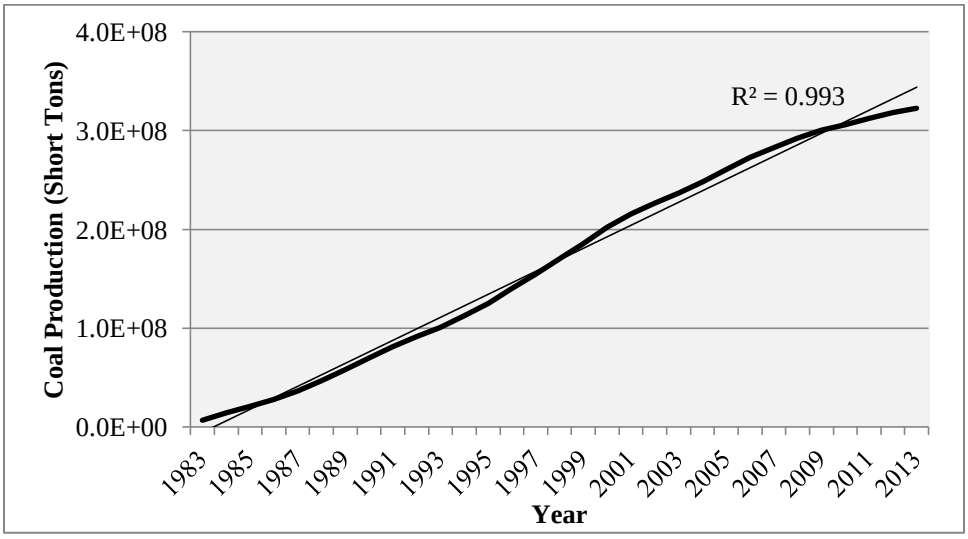

Figure 24: Area 3 cumulative coal production from 1983 to 2013.

Coal production in Clusters 1 and 2 individually has also been fairly consistent since 1983 [Figures 25 and 26].

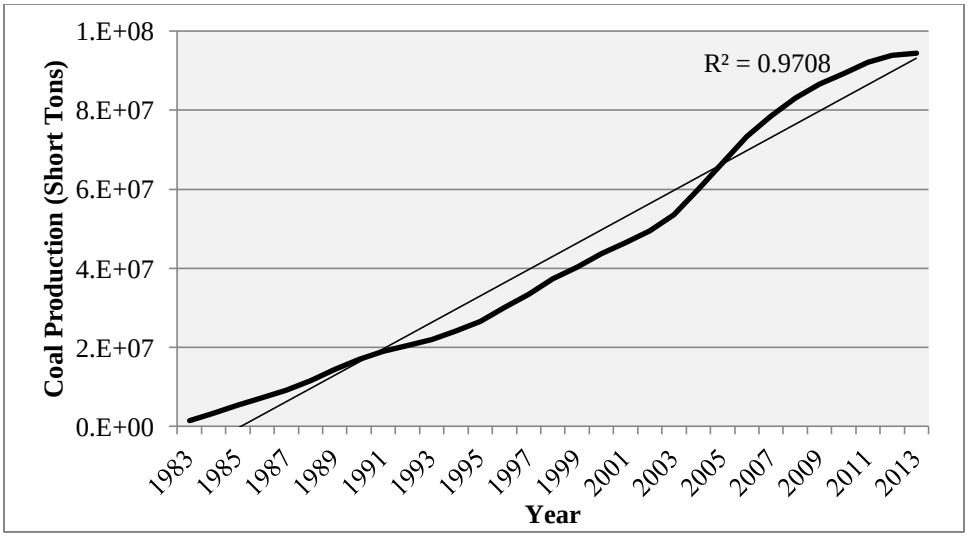

Figure 25: Cluster 1 cumulative coal production from 1983 to 2013.

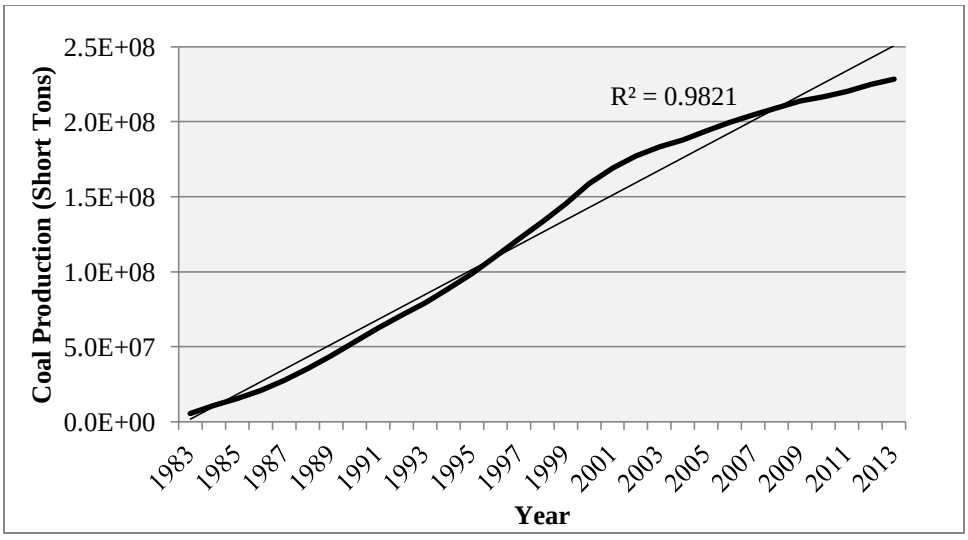

Figure 26: Cluster 2 cumulative coal production from 1983 to 2013.

Coal mining activity has been observed to be highly correlated to mining induced seismicity on the hour, day and week scale [*Arabasz et al.*, 2002]. Strong temporal correlation between MIS and mining activities was observed in Utah during the 2000 to 2001 Trail Mountain Area study [*Arabasz et al.*, 2002; *Arabasz et al.*, 2005]. Arabasz et al. [2005] observed the MIS was highly correlated with mining shifts. In addition, there were observations of decreased seismicity during weekend days. I evaluated the MIS events that I removed based on the relocations completed by Arabasz et al. [2002] by creating histograms of the number of seismic events during each hour of the day. The MIS events are strongly correlated with reported mining shifts during the Trail Mountain Area study [*Arabasz et al.*, 2005]; the shifts were reported as 7:30 a.m. to 4:30 p.m. and 4:30 p.m. to 1:30 a.m. with an off-shift from 1:30 a.m. to 7:30 a.m. The off-shift corresponds to UTC hours 9 through 14 and the period of decreased seismicity [Figure 27].

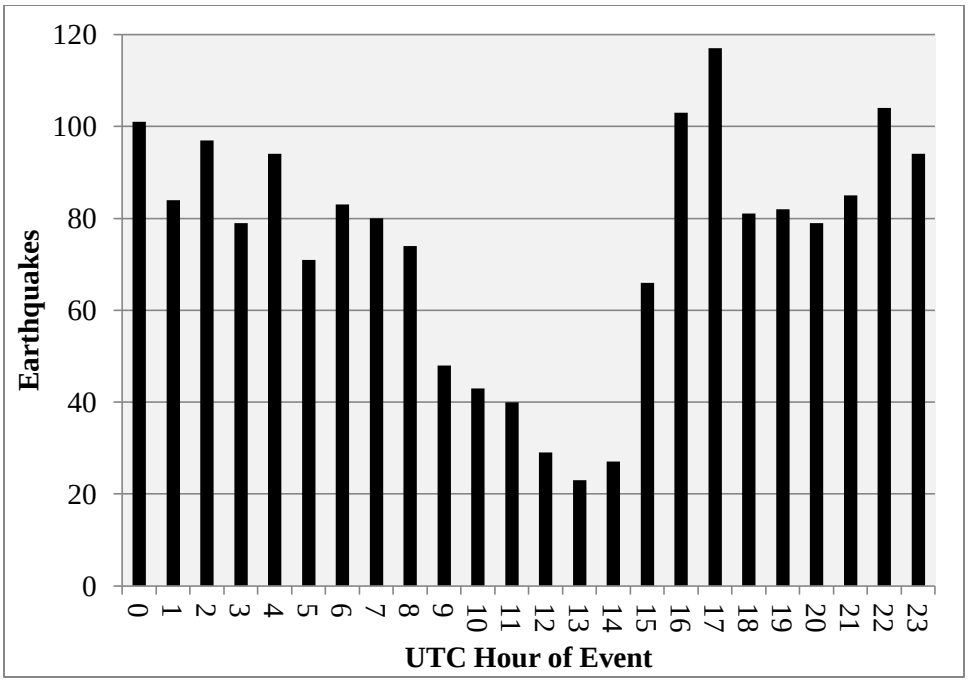

Figure 27: Hourly distribution of confirmed mining induced seismicity from Arabasz et al. [2002] in my data set.

I then evaluated the distribution of the timing of the seismicity of Area 3, and Cluster 1 and Cluster 2 separately, by creating histograms of the number of seismic events during each hour of the day since 1981 to test for a correlation with mining shifts [Figures 28 to 30]. A decrease in seismicity during the likely mining off-shift is present in all areas to varying degrees, indicating a strong correlation between mining activity and seismicity.

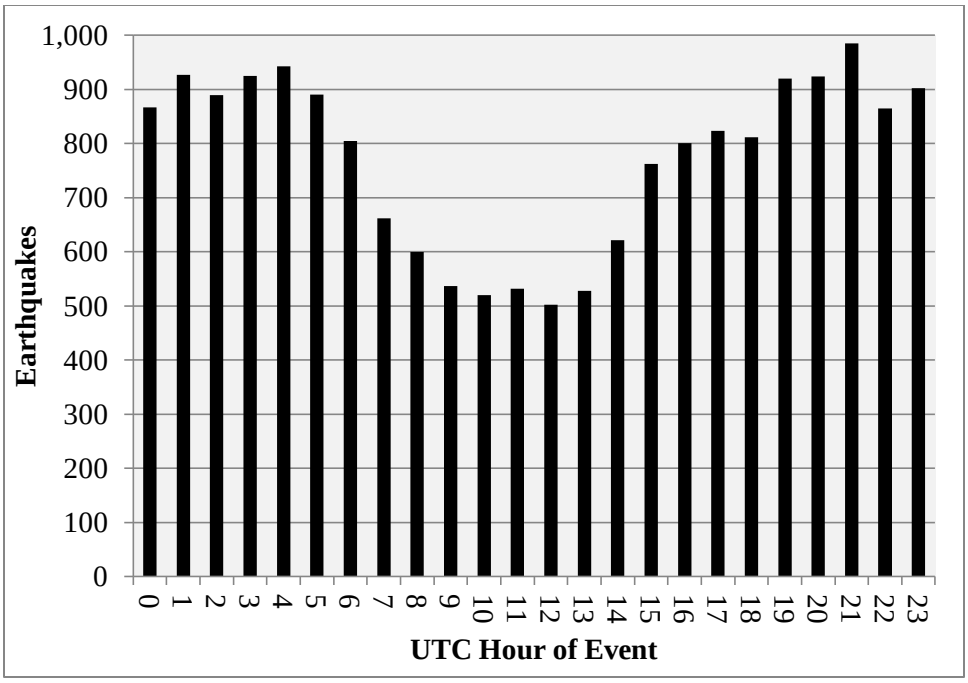

Figure 28: Hourly distribution of earthquakes in Area 3 with confirmed MIS [*Arabasz et al.*, 2002] removed.

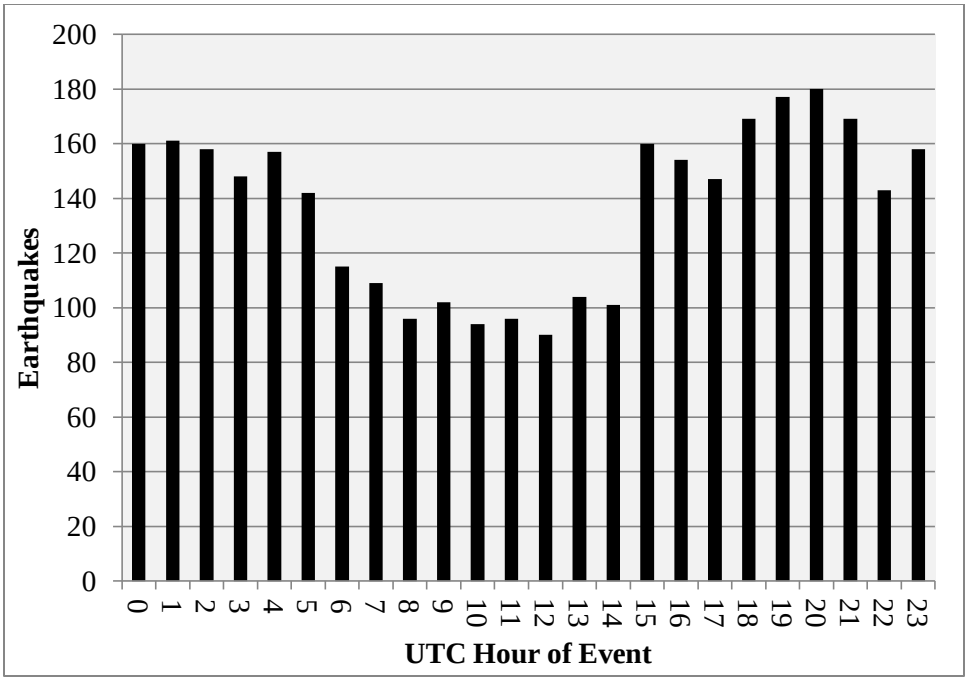

Figure 29: Hourly distribution of earthquakes in Cluster 1.

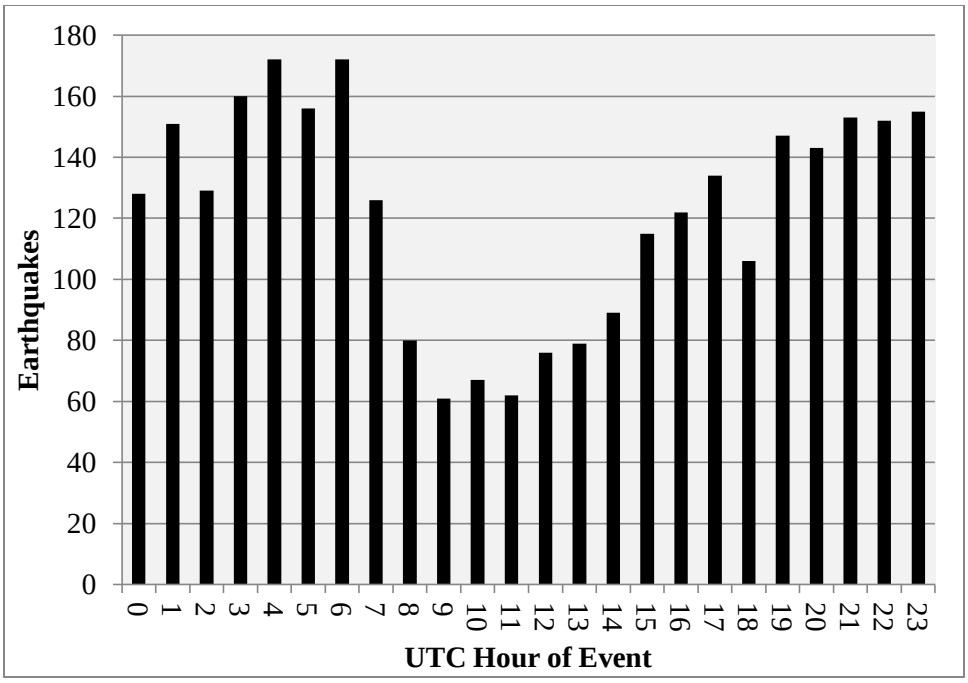

Figure 30: Hourly distribution of earthquakes in Cluster 2 with confirmed MIS [*Arabasz et al.*, 2002] removed.

4.2.3 Injection Wells, Coal Production, and Seismicity

When I compare cumulative coal production, well volumes and earthquakes, temporal correlation between the well volumes and seismicity appears more pronounced than correlation between coal production and seismicity [Figures 31 – 33]. I include the confirmed MIS [*Arabasz et al.*, 2002] in the data set for this comparison since I include coal mining activity in the correlation evaluation.

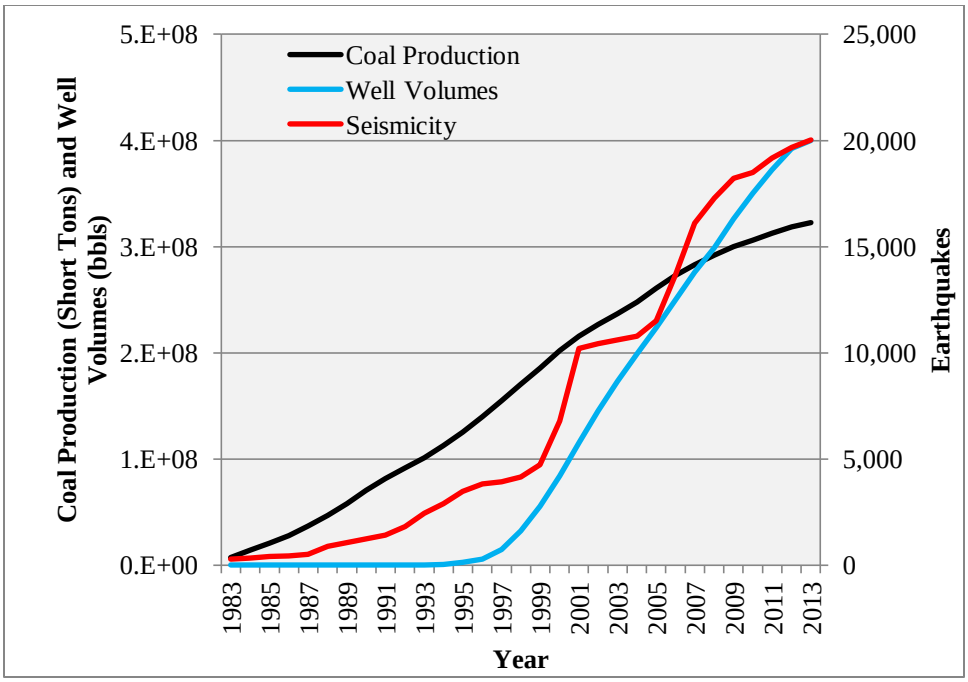

Figure 31: Area 3 cumulative coal production, injection volumes and earthquakes.

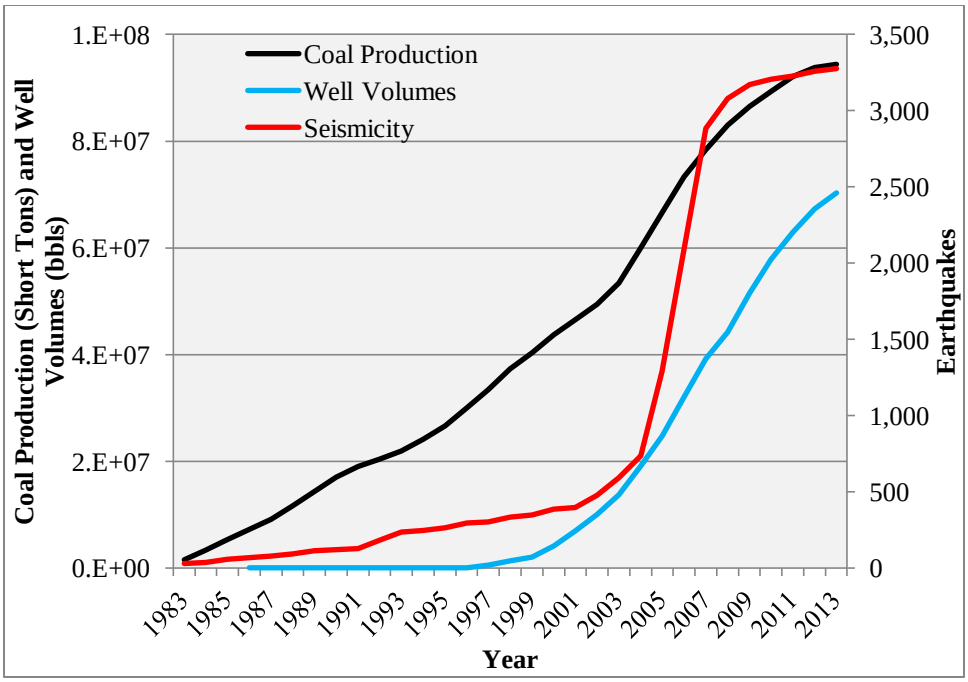

Figure 32: Cluster 1 cumulative coal production, injection volumes and earthquakes.

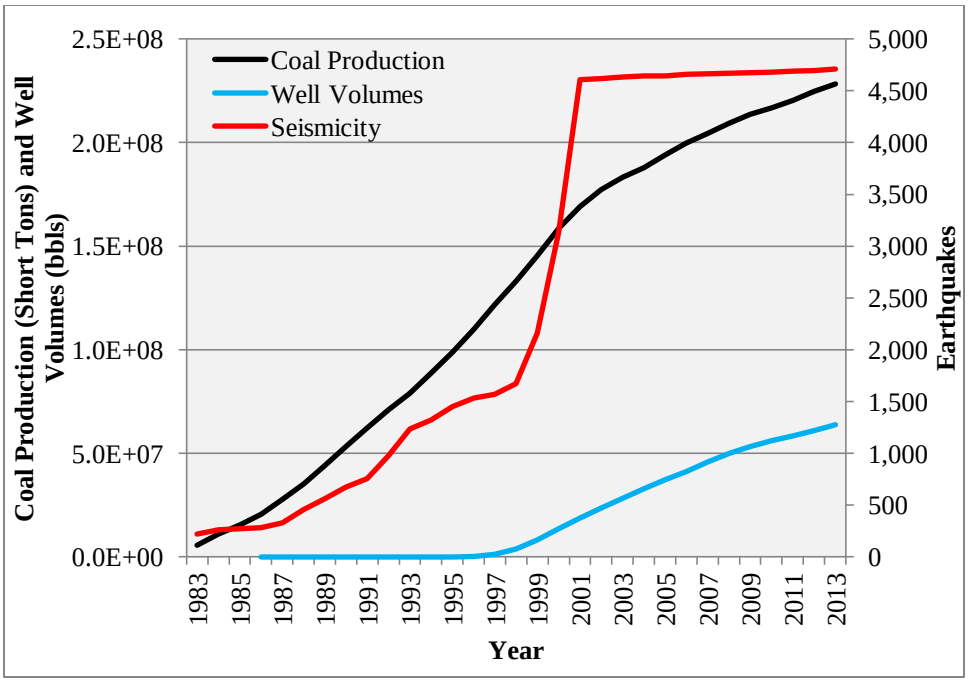

Figure 33: Cluster 2 cumulative coal production, injection volumes and earthquakes.

Comparing annual coal production to annual earthquake amounts and annual well volumes to annual earthquake amounts provides a finer detail comparison and a more complicated correlation between the two anthropogenic activities and the seismicity of the area [Figures 34 – 39]. For Area 3 as a whole, the annual earthquakes appear to correlate very well with the coal production, but with an approximately 1-year shift [Figure 34], while the annual injection volumes also correlate well with the annual earthquakes [Figure 35].

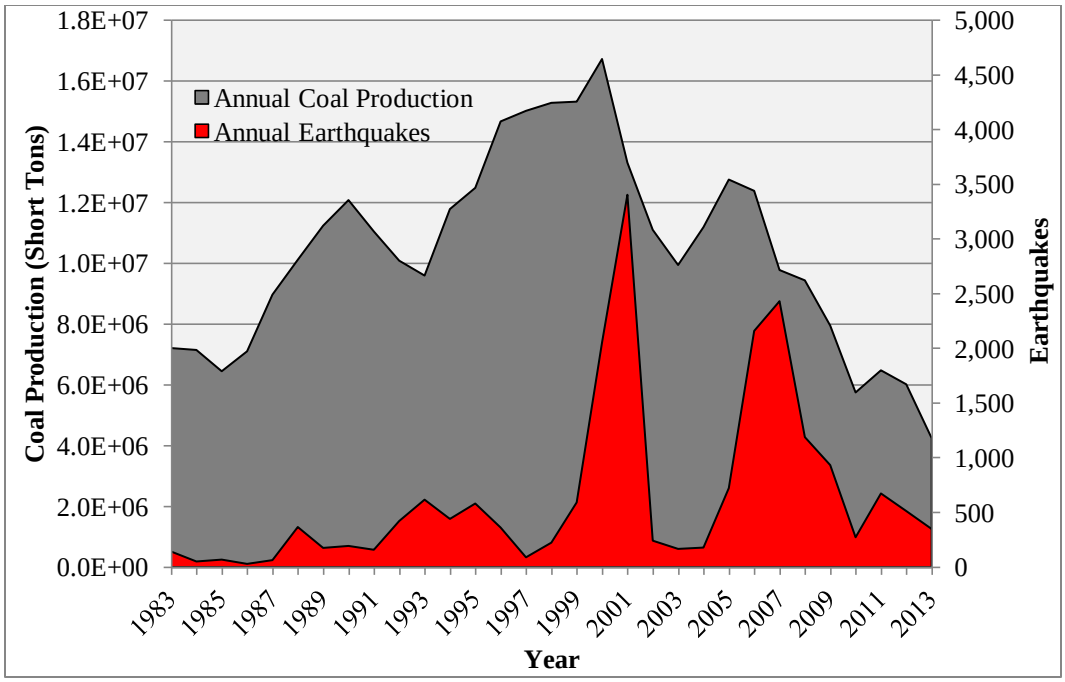

Figure 34: Area 3 annual coal production and earthquakes.

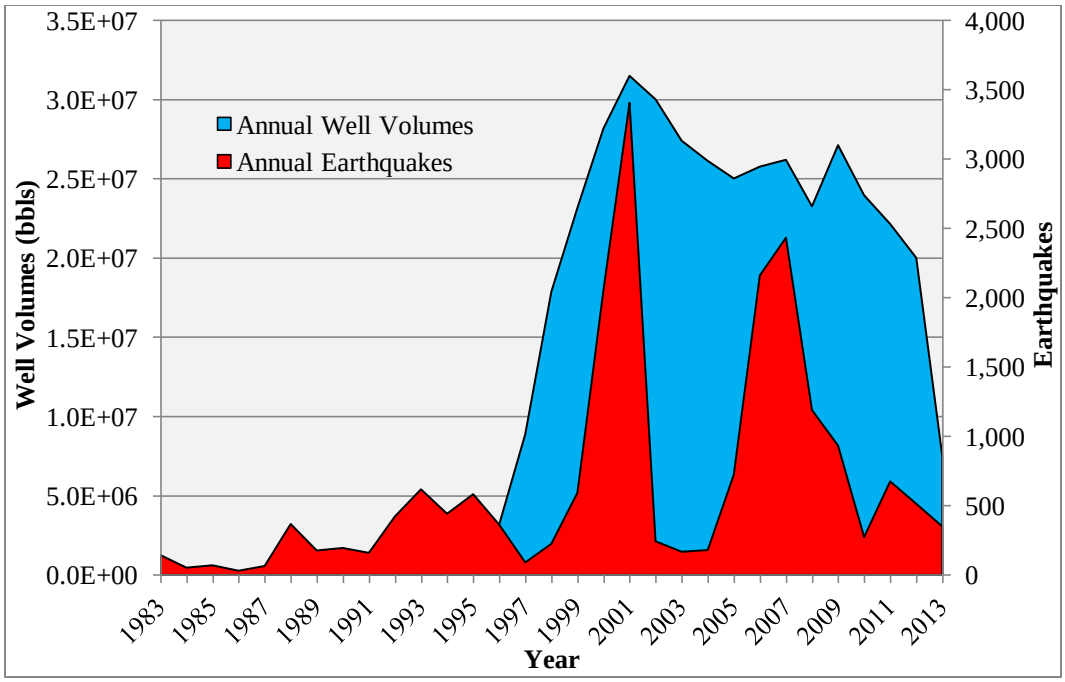

Figure 35: Area 3 annual injection volumes and earthquakes.

Cluster 1 also has a strong correlation between the increased seismicity around 2006 – 2008 and coal mining activity, but with a 2-year shift [Figure 36], while the annual injection volumes correlate very well with the increased seismicity [Figure 37]. In addition, variations in coal production occurred throughout the 1980s and 1990s with little variation in the seismicity [Figure 36].

Cluster 2 has a strong correlation between the increased seismicity that occurred around 2001 and the coal production and injection volumes. Interestingly, there is a 1-year shift between both the coal production and increased seismicity [Figure 38] and the injection volumes and increased seismicity [Figure 39]. Again, there is variation in coal production during the 1980s and 1990s with little to no correlation with variations in the seismicity in the area [Figure 38].

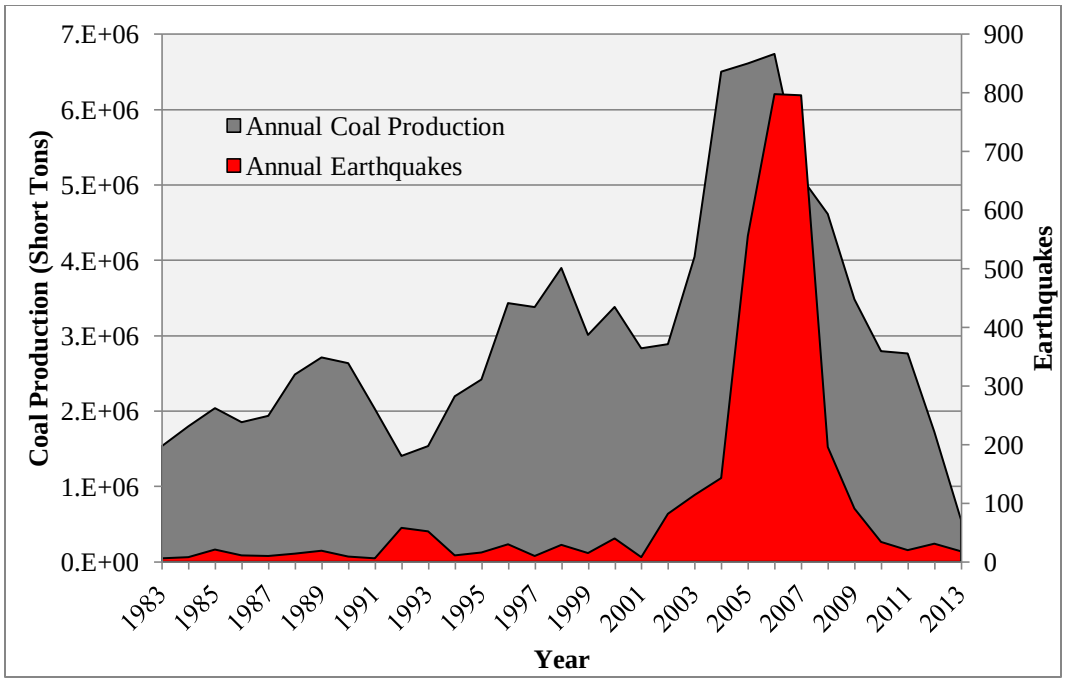

Figure 36: Cluster 1 annual coal production and earthquakes.

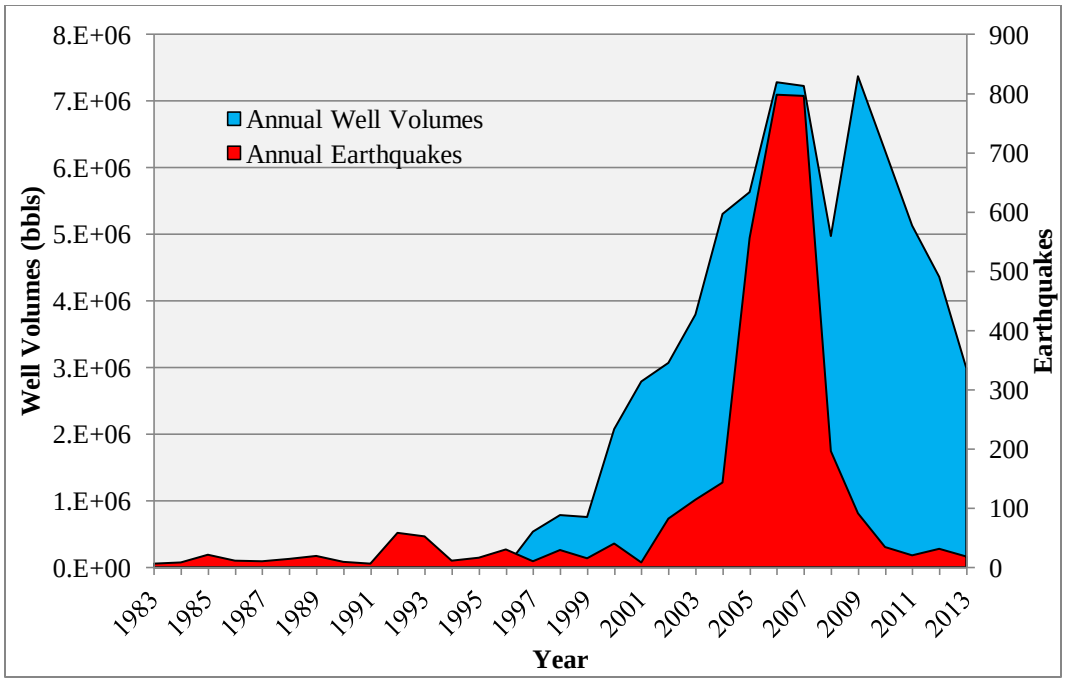

Figure 37: Cluster 1 annual injection volumes and earthquakes.

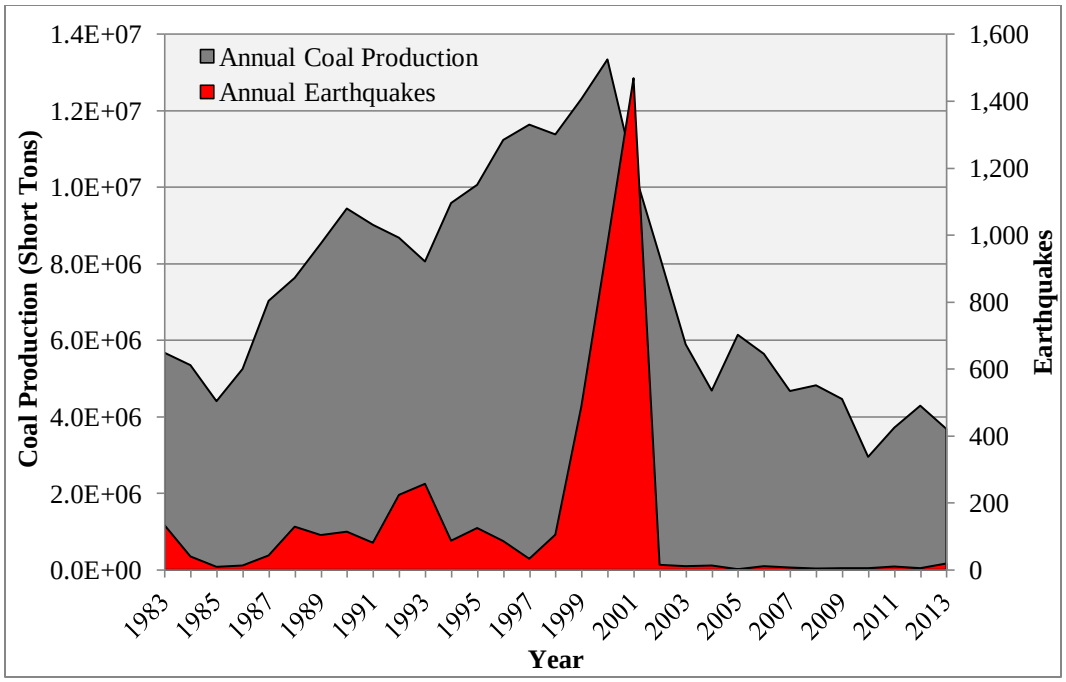

Figure 38: Cluster 2 annual coal production and earthquakes.

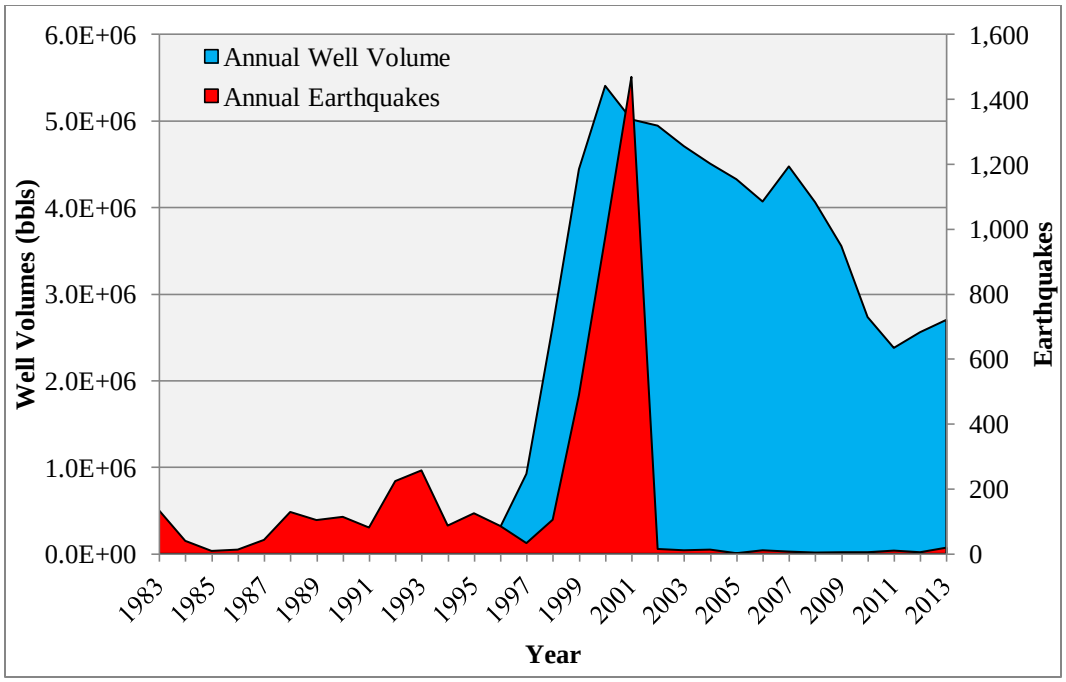

Figure 39: Cluster 2 annual injection volume and earthquakes.

4.3 Spatial Correlation

To further investigate the spatial distribution of the seismicity, I calculated and plotted the surface distance between each seismic event and the center point of the cluster of wastewater disposal wells for Clusters 1 and 2 [Figures 40 – 41]. To accomplish this, I created a script using MATLAB to determine the surface distance between two points on a sphere. The equations used are as follows [*Turcotte and Schubert*, 2002]:

$$(1) \qquad a = \cos^{-1}\left[\sin\lambda_x \sin\lambda_p + \cos\lambda_x \cos\lambda_p \cos\left(\phi_p - \phi_x\right)\right],$$

where in equation (1) a is the angle between the two points at the center of the earth; $\lambda_{(x,p)}$ is the latitude; and $\phi_{(x,p)}$ is the longitude of each point in equation, and

$$(2) \qquad S = aR,$$

where in equation (2) S is the surface distance, R is the radius of the earth, and a is the value from equation (1) in radians. I assumed an average value of 6371 km for the radius of the earth.

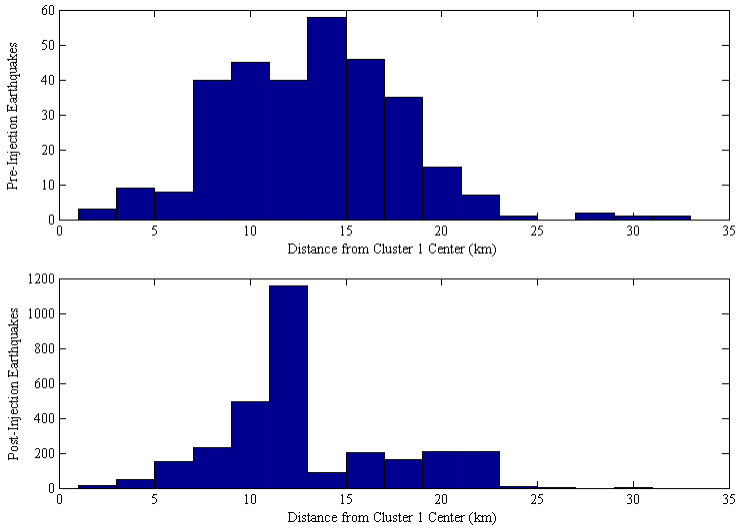

Figure 40: Cluster 1 distance distributions, pre- and post-injection.

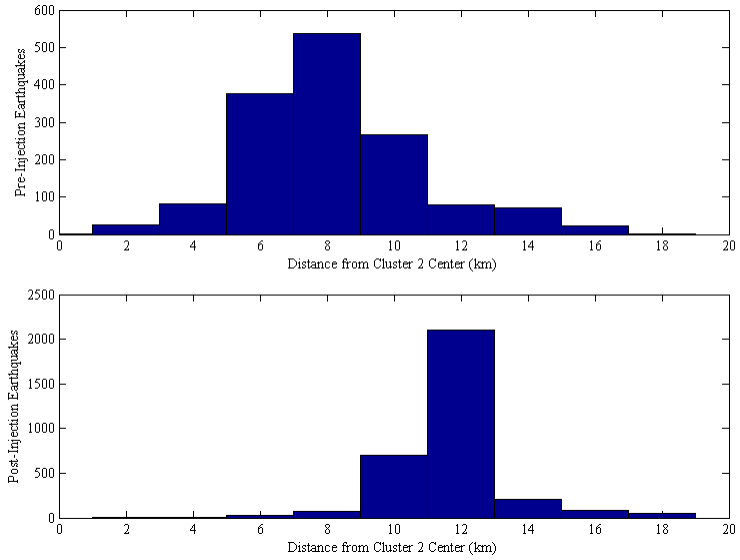

Figure 41: Cluster 2 distance distribution, pre- and post-injection.

Following the start of injection, the seismicity appears to cluster at distances around 10 km from the cluster centers. Box and whisker plots of the distances for pre-injection seismicity and post-injection seismicity [Figures 42 and 43] further illustrate the apparent clustering of seismicity especially in Cluster 2. Cluster 1 does not exhibit the same level of localization during the entire post-injection period, but has significant localization for the time of increased seismicity from 2003 to 2007. Cluster 2 post-injection distances are much more clustered than Cluster 1, as is the time of increased seismicity from 1999 to 2001. I did not remove the confirmed MIS [*Arabasz et al.*, 2002] for the distance evaluation.

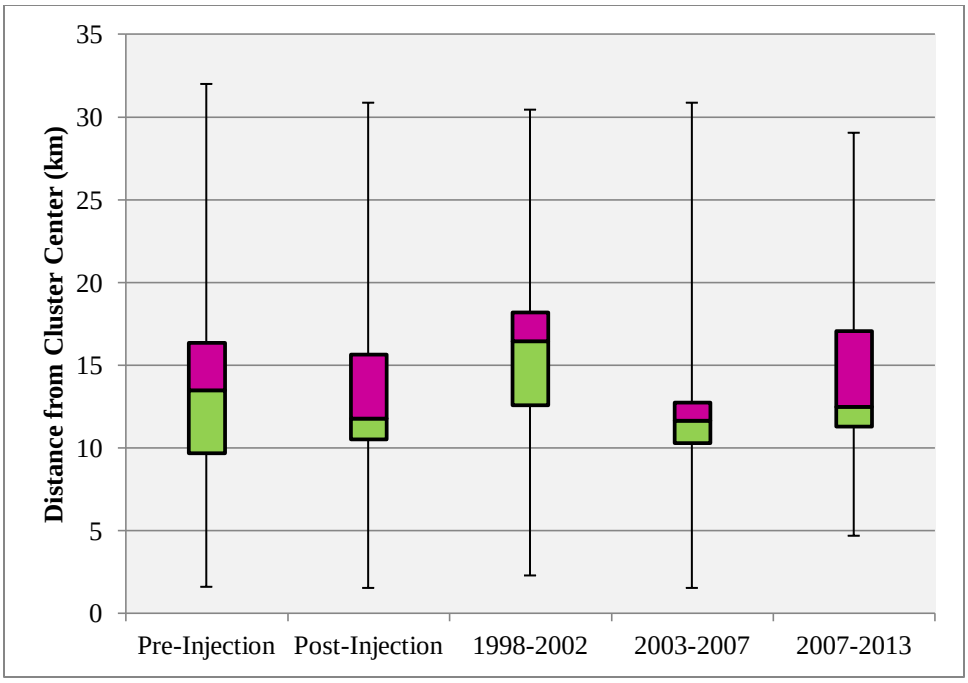

Figure 42: Cluster 1 distance evaluation box and whisker diagram. Post-injection begins in 1998 when the first well of interest started injection.

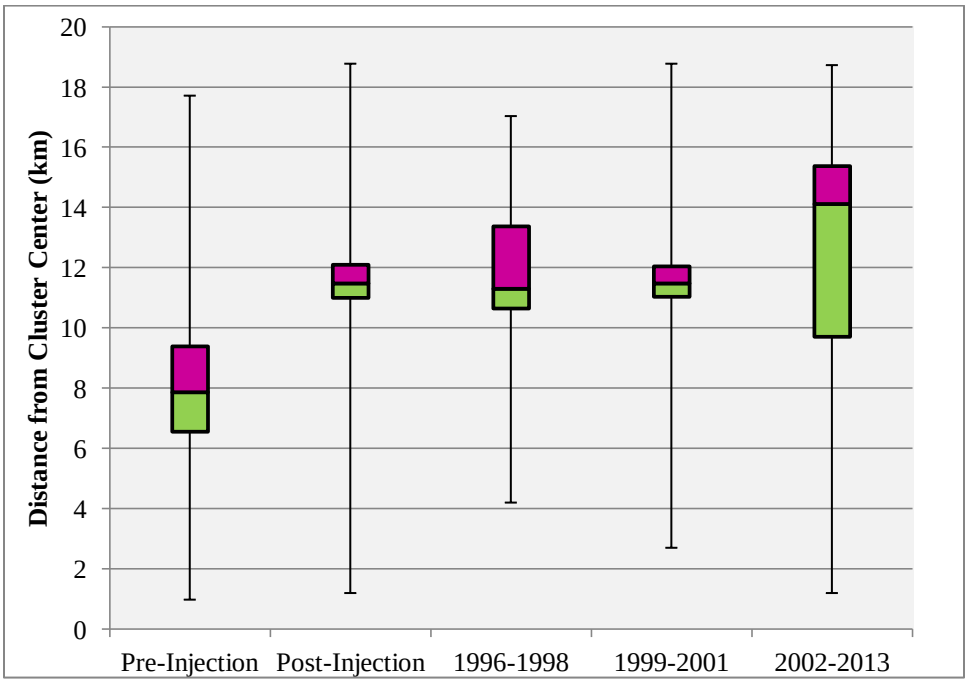

Figure 43: Cluster 2 distance evaluation box and whisker diagram. Post-injection began in 1996 when the first well of interest started injection.

Chapter 5: Pore Pressure Increase

I found a temporal correlation between the wastewater injection and the seismicity with a time gap of approximately 1 – 5 years between the start of wastewater injection and the increase in the seismicity rate. In addition, I found a spatial correlation between the location of the injection wells and the seismicity and a clustering of the increased seismicity at specific distances, approximately 10 – 12 km from the injection wells. I hypothesize that pore pressure increase along pre-existing faults induced the increased seismicity. This is also consistent with the time and spatial gap. To test the hypothesis, I created a generic groundwater model based on hydrogeologic parameters reported in the literature.

5.1 Groundwater Model

5.1.1 Aquifer Parameters

The majority of the wastewater disposal wells inject into the Navajo Sandstone, Kayenta Formation, and Wingate Sandstone [UIC public record well files]. These formations are considered one hydrogeologic unit in the area, the Navajo aquifer [*Freethey and Cordy*, 1991]. Well logs indicate the aquifer is overlain by the Carmel Formation, which consists of limestone, siltstone, and shale [*Freethey and Cordy*, 1991] and locally anhydrite deposits, which provide a confining layer [UIC public record well files]. The aquifer is underlain by the Chinle Formation [UIC public record well files] that consists of siltstones, claystones, and limestones [*Freethey and Cordy*, 1991], which with a much lower hydraulic conductivity than the Navajo aquifer provides a basal confining layer. Artesian conditions were observed in several wells drilled in the Navajo

Sandstone [*Hood and Patterson*, 1984]. Therefore, I executed the model domain as a confined aquifer.

Thirty-three designated wastewater disposal wells are located within Area 3; one well was never utilized as an injection well and is now abandoned [UIC public record well files]. Five of the remaining thirty-two wells inject into aquifers other than the Navajo aquifer. One of the wells that injects into the Navajo aquifer was abandoned in 2013. Details of the wastewater disposal wells in Area 3 are included in Table 3. Based on well records, the average thickness of the Navajo aquifer is approximately 250 m; therefore, I used a thickness of 250 m for the model domain. The Navajo aquifer is a saline aquifer at depth [*Hood and Patterson*, 1984]; this is confirmed in the UIC well files by groundwater laboratory testing. The wastewater disposed in the injection wells is also saltwater [UIC public record well files]. Therefore, there are no issues with density variations and I made no modifications to the model.

Hydrogeologic properties of the Navajo Sandstone, which makes up the majority of the aquifer, were obtained using laboratory sampling on core samples and from drill stem tests [*Freethey and Cordy*, 1991; *Hood and Danielson*, 1979; *Hood and Patterson*, 1984]. The hydraulic conductivity of the Navajo aquifer ranges from 0.001 – 1.6 meters per day (m/d) according to Hood and Patterson [1984]. Freethey and Cordy [1991] and Hood and Danielson [1979] referenced hydraulic conductivity values within that range. Transmissivity values, which is hydraulic conductivity multiplied by aquifer thickness, also have a large range: 0.46 – 464 square meters per day (m^2/d) [*Freethey and Cordy*, 1991]; 2.5 – 60.1 m^2/d [*Hood and Patterson*, 1984]; and 42 – 395 m^2/d [*Hood and Danielson*, 1979]. The storage coefficient for the Navajo aquifer ranges from 0.0003 to

0.008 [*Freethey and Cordy*, 1991]; which converts to specific storage values of 1.2 x 10^{-6} m^{-1} to 3.2 x 10^{-5} m^{-1}. I utilized these ranges of values for the groundwater model.

5.1.2 Groundwater Model Set-Up

The groundwater model was created with Groundwater Modeling System (GMS), which is a graphical user interface marketed by Aquaveo™ that utilizes MODFLOW 2000 software. MODFLOW was developed at the U.S. Geological Survey and solves for groundwater flow using the finite difference method. MODFLOW solves the transient groundwater flow equation:

$$\frac{\partial h}{\partial t} = \frac{K}{S_s}\left[\frac{\partial^2 h}{\partial x^2} + \frac{\partial^2 h}{\partial y^2} + \frac{\partial^2 h}{\partial z^2}\right], \quad (3)$$

where h is hydraulic head, t is time, K is hydraulic conductivity for an isotropic aquifer, and S_s is specific storage of the aquifer.

I created a generic, isotropic, homogeneous, one-layer grid model with a thickness of 250 m, the average thickness of the Navajo aquifer, and a model domain of 50,000 m by 50,000 m [Figure 44]. The model grid was set up with spacing of 250 m by 250 m by 250 m. I chose to create such a large model domain to account for the lack of boundary conditions.

A single injection well was located in the center of the model domain and set with a constant injection rate of 1,370 cubic meters per day (m^3/d), approximately three times the average injection rate of the injection wells in Area 3. I chose a value three times the average injection rate to represent three injection wells, which is consistent with the wells

of interest in Area 3's Cluster 2. Area 3's Cluster 1 has five injection wells of interest operating.

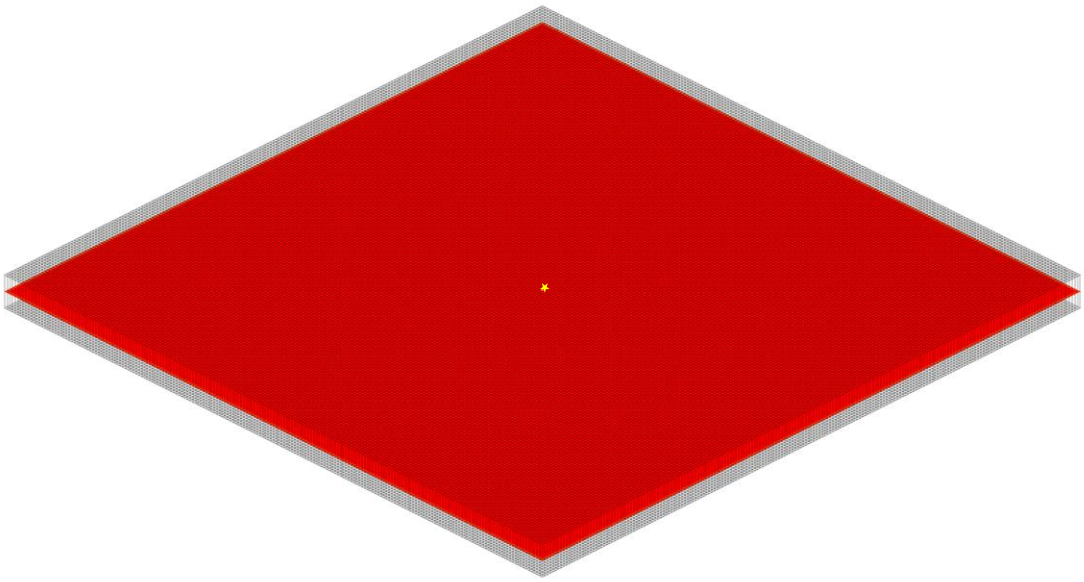

Figure 44: Model domain in an oblique view with single injection well in center.

I set the model as a confined aquifer and initial conditions as hydrostatic. The entire thickness of the Navajo aquifer is saturated when the thickness is greater than 100 feet [*Freethey and Cordy*, 1991]. By choosing a hydrostatic initial condition, I can attribute any resulting change in hydraulic head to the injection well point source. I gave the boundary cells of the model domain specified head designations of hydrostatic; this allows groundwater flow out of the model domain. I set the transient model to run for approximately thirty years (10,950 days) with sixty time steps; each time step is approximately a half year. I ran the model using Layer Property Flow (LPF) flow package and the Preconditioned Conjugate-Gradient 2 (PCG2) Solver. I executed the

model with varying hydraulic conductivity and specific storage values in order to determine the sensitivity of the model to specific parameters.

5.2 Groundwater Model Results

I ran the groundwater model using four different hydraulic conductivity (K) values at two different specific storage (S_s) values each. The specific storage and hydraulic conductivity values used and the corresponding transmissivity (T) are included in Table 4.

Table 4: Model Run Parameters

Model Run	Hydraulic Conductivity (m/d)	Transmissivity (m^2/d)	Specific Storage (m^{-1})
1	0.001	0.25	1.2×10^{-6}
2	0.001	0.25	3.2×10^{-5}
3	0.01	2.5	1.2×10^{-6}
4	0.01	2.5	3.2×10^{-5}
5	0.5	125	1.2×10^{-6}
6	0.5	125	3.2×10^{-5}
7	1.6	400	1.2×10^{-6}
8	1.6	400	3.2×10^{-5}

The lowest reported hydraulic conductivity for the Navajo aquifer was 0.001 m/d [*Hood and Patterson*, 1984]. I ran the model [Figures 45 and 46] with this value of K and the lowest reported specific storage and the highest reported specific storage for the Navajo aquifer, 1.2×10^{-6} m^{-1} and 3.2×10^{-5} m^{-1}, respectively [*Freethey and Cordy*, 1991].

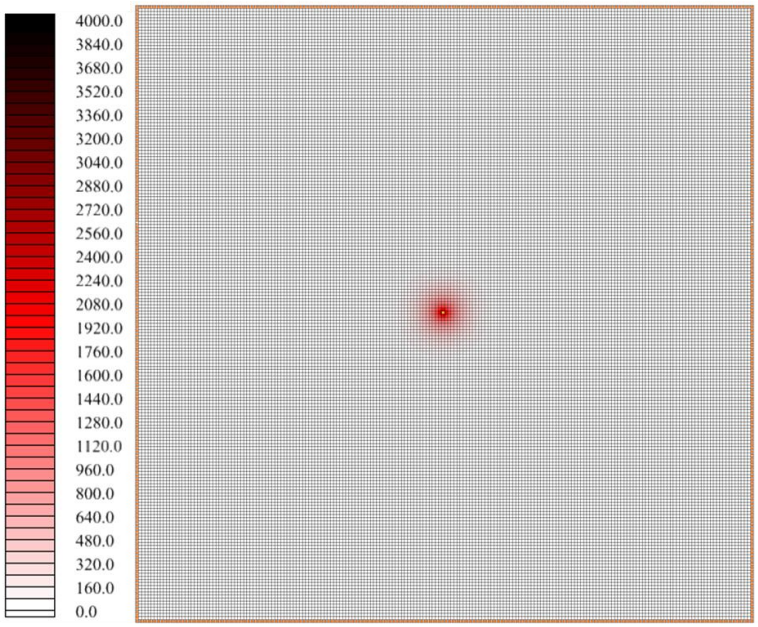

Figure 45: Model Run 1 change in hydraulic head (meters), shown in red, following 10 years of continuous injection.

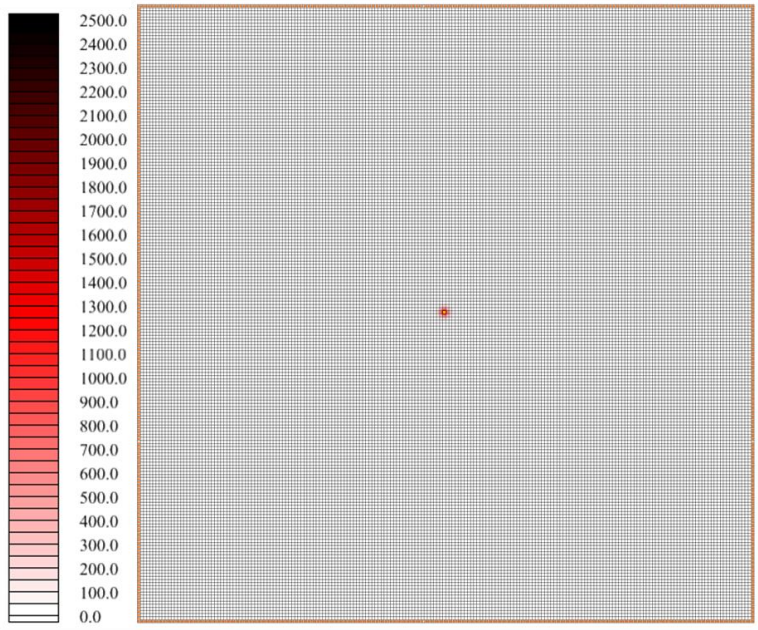

Figure 46: Model Run 2 change in hydraulic head (meters), shown in red, following 10 years of continuous injection.

Injection with these parameter values results in extremely high changes in hydraulic head at the injection well and directly adjacent to the well. I plotted the change in hydraulic head with time at the injection well for the two model runs [Figures 47 and 48]; the change in hydraulic head is large enough at the injection well that these parameters are not reasonable for the aquifer. In addition, the transmissivity 0.25 m^2/d is far lower than the values reported [*Freethey and Cordy*, 1991; *Hood and Danielson*, 1979; *Hood and Patterson*, 1984].

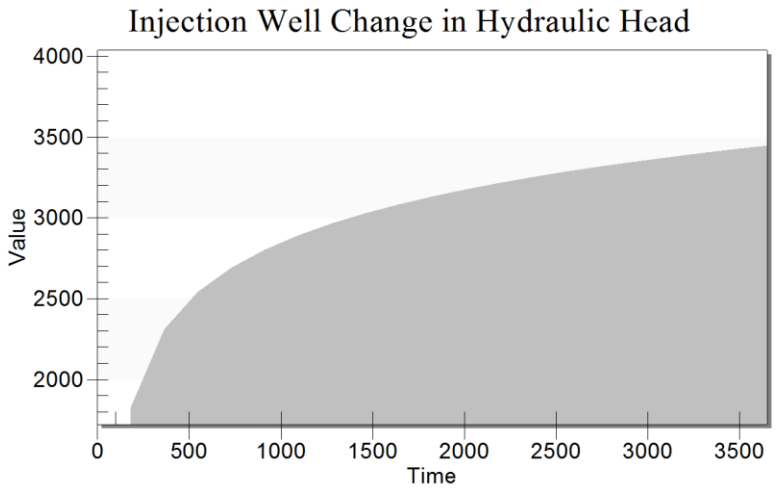

Figure 47: Model Run 1 change in hydraulic head (meters) in time (days) at the injection well.

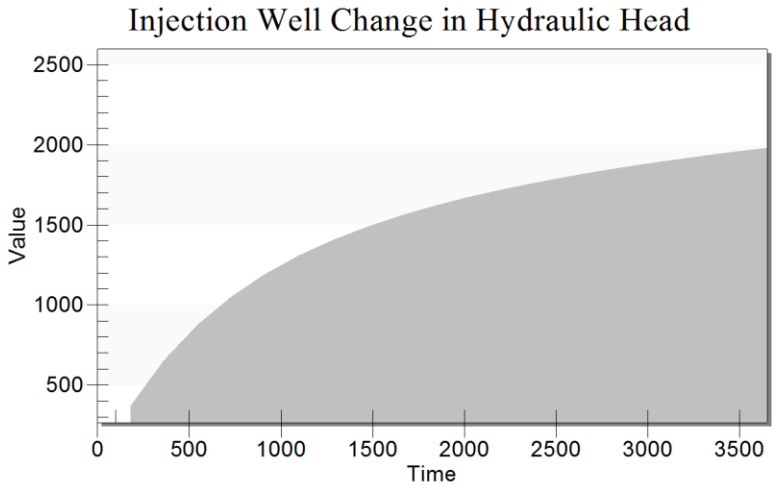

Figure 48: Model Run 2 change in hydraulic head (meters) in time (days) at the injection well.

I ran Model Runs 3 and 4 [Figures 49 and 50] at a hydraulic conductivity of 0.01 m/d (T = 2.5 m^2/d), which is in the range of values reported for the Navajo aquifer [*Freethey and Cordy*, 1991; *Hood and Danielson*, 1979; *Hood and Patterson*, 1984].

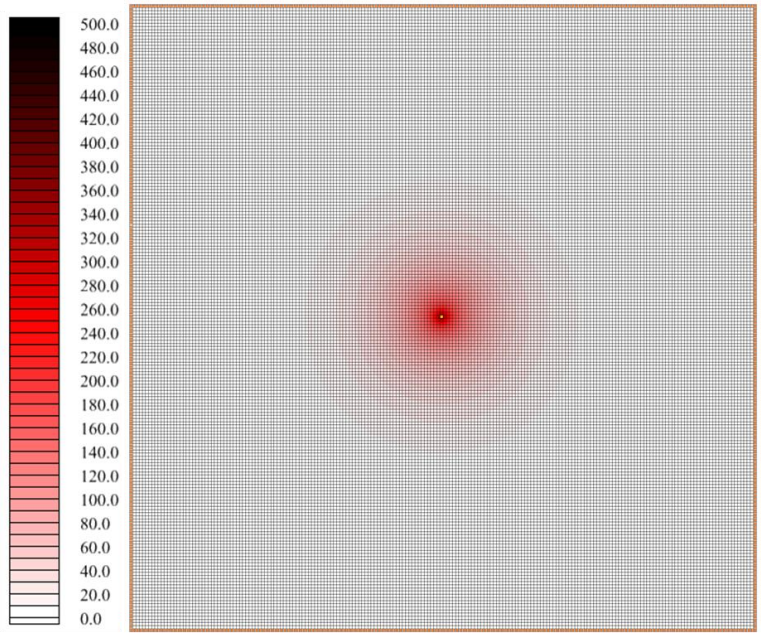

Figure 49: Model Run 3 change in hydraulic head (meters), shown in red, following 10 years of continuous injection.

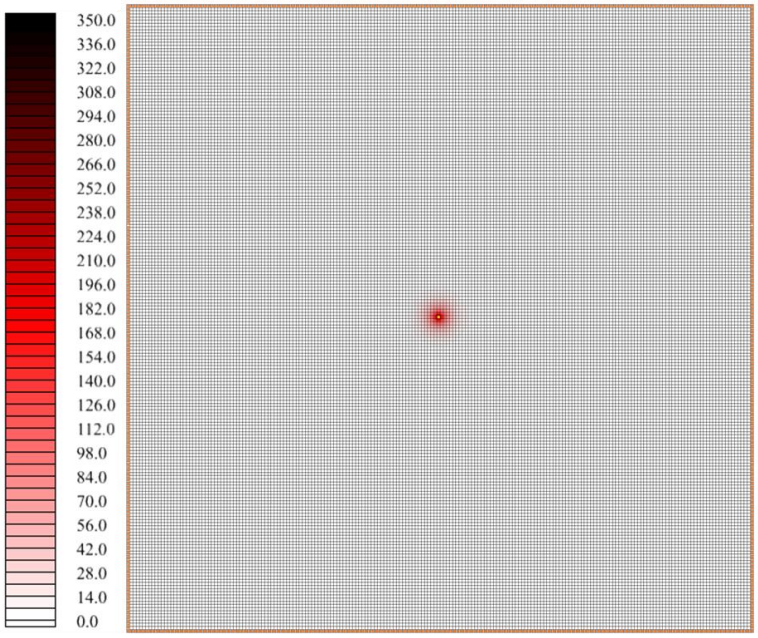

Figure 50: Model Run 4 change in hydraulic head (meters), shown in red, following 10 years of continuous injection.

Model Runs 5 and 6 with K = 0.5 m/d [Figures 51 and 52] and Runs 7 and 8 with K = 1.6 m/d [Figures 53 and 54], also have transmissivity values, 125 m^2/d and 400 m^2/d, respectively, which fall within the reported ranges of transmissivity values [*Freethey and Cordy*, 1991; *Hood and Danielson*, 1979; *Hood and Patterson*, 1984].

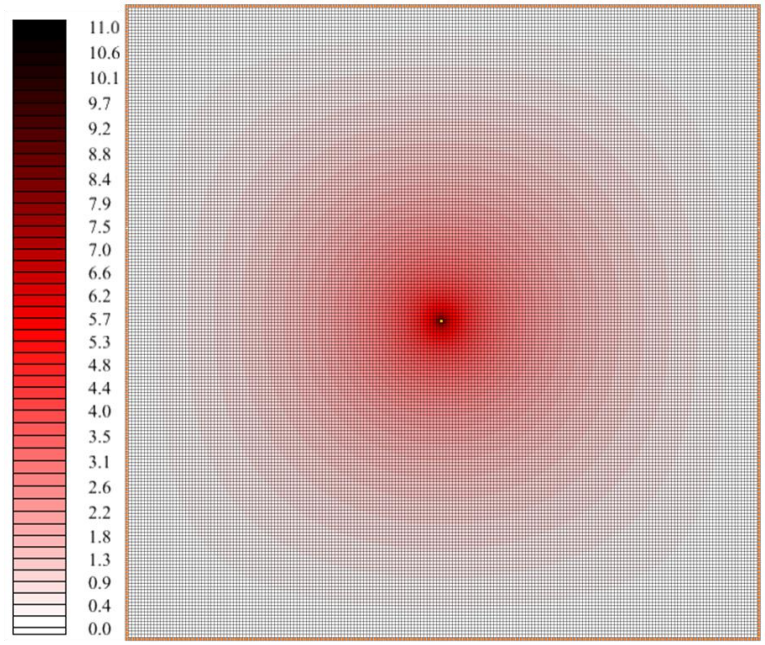

Figure 51: Model Run 5 change in hydraulic head (meters), shown in red, following 10 years of continuous injection.

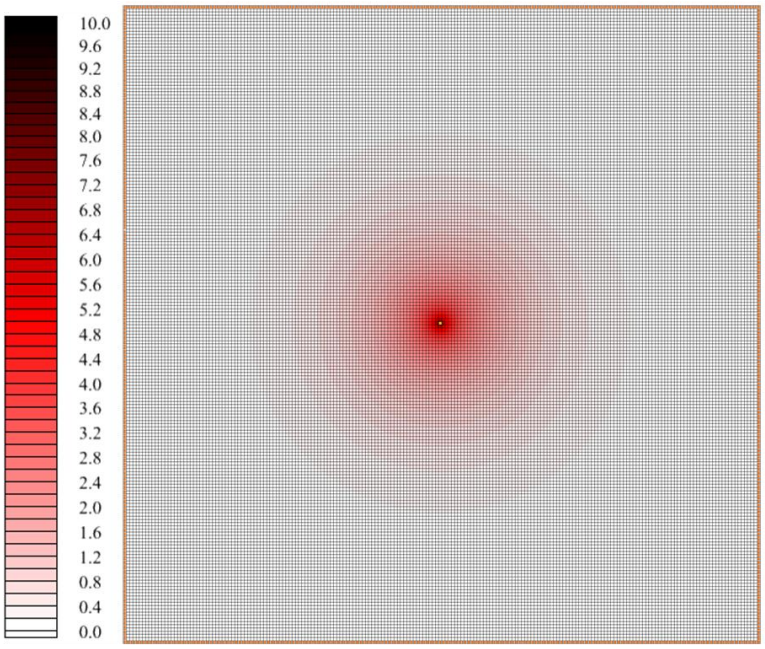

Figure 52: Model Run 6 change in hydraulic head (meters), shown in red, following 10 years of continuous injection.

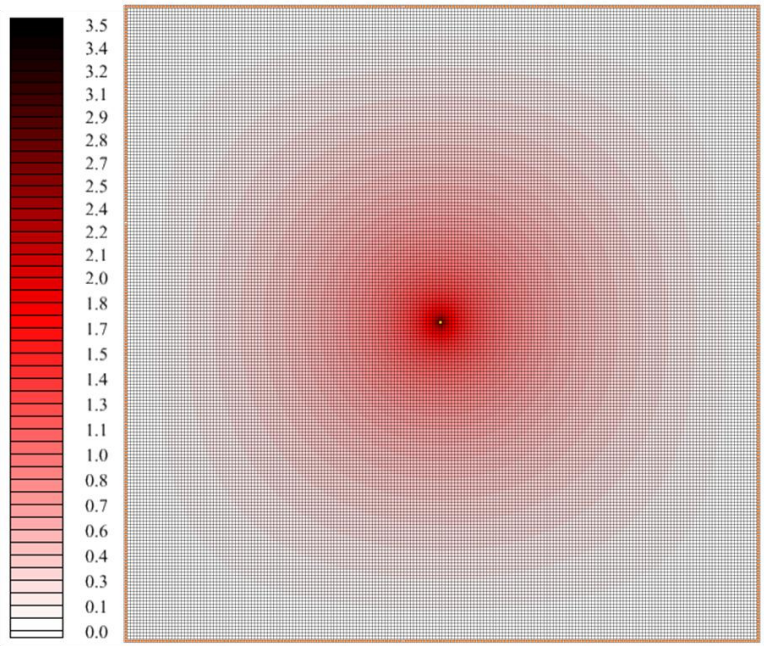

Figure 53: Model Run 7 change in hydraulic head (meters), shown in red, following 10 years of continuous injection.

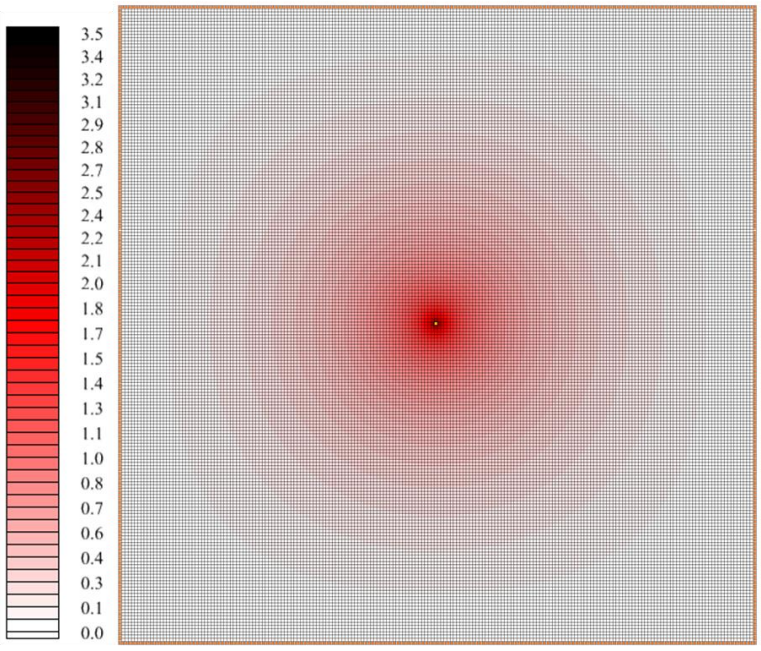

Figure 54: Model Run 8 change in hydraulic head (meters), shown in red, following 10 years of continuous injection.

As the model domain is an isotropic, homogeneous aquifer, the change in hydraulic head is the same radially in all directions from the injection well. To illustrate the spatiotemporal changes, I created plots [Figures 55 – 60] for each feasible model run, Runs 3 – 8. In these figures, the y-axis represents the location of the injection well and time increases away from the origin of the plots. When I compare the model results, it is clear changes in hydraulic head and the diffusivity of the system are most affected by changes in the hydraulic conductivity. Changes in specific storage also significantly affect diffusivity of the system, but have limited effects on changes in hydraulic head.

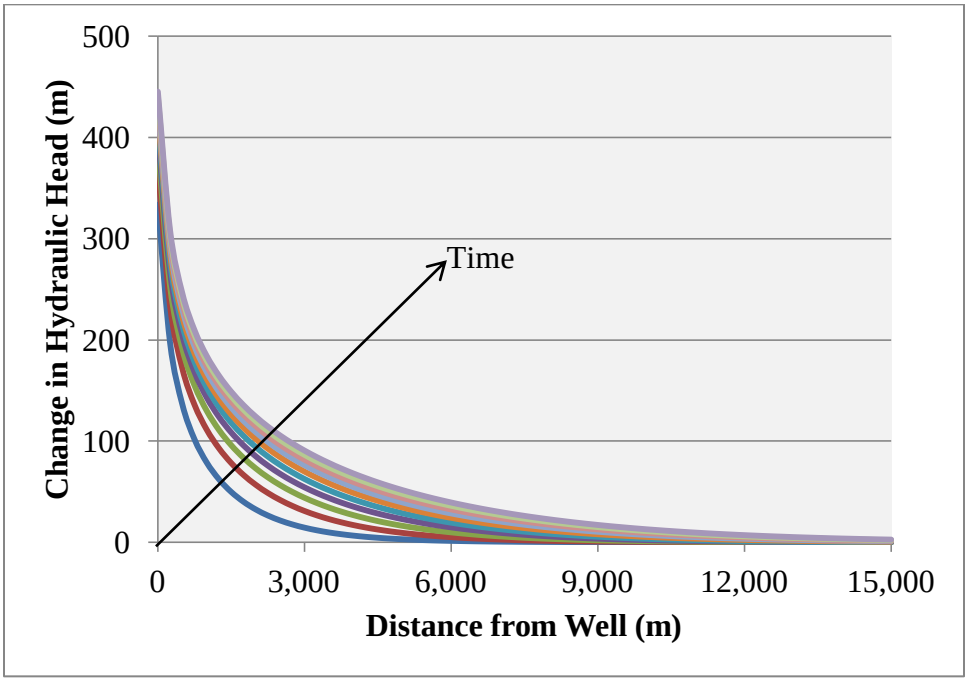

Figure 55: Model Run 3 spatiotemporal changes in hydraulic head with distance from injection well.

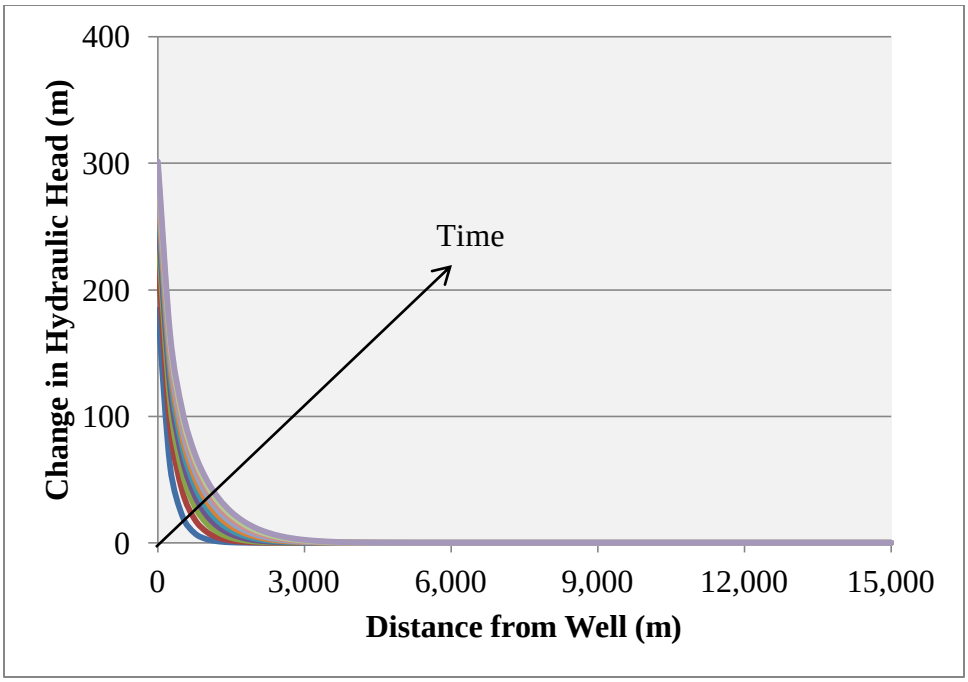

Figure 56: Model Run 4 spatiotemporal changes in hydraulic head with distance from injection well.

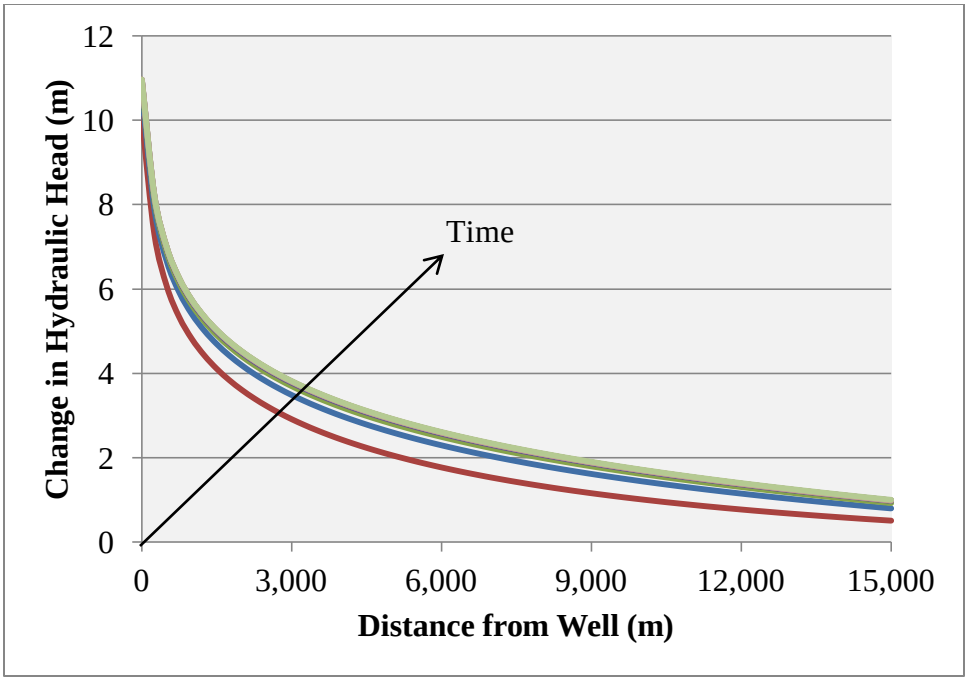

Figure 57: Model Run 5 spatiotemporal changes in hydraulic head with distance from injection well.

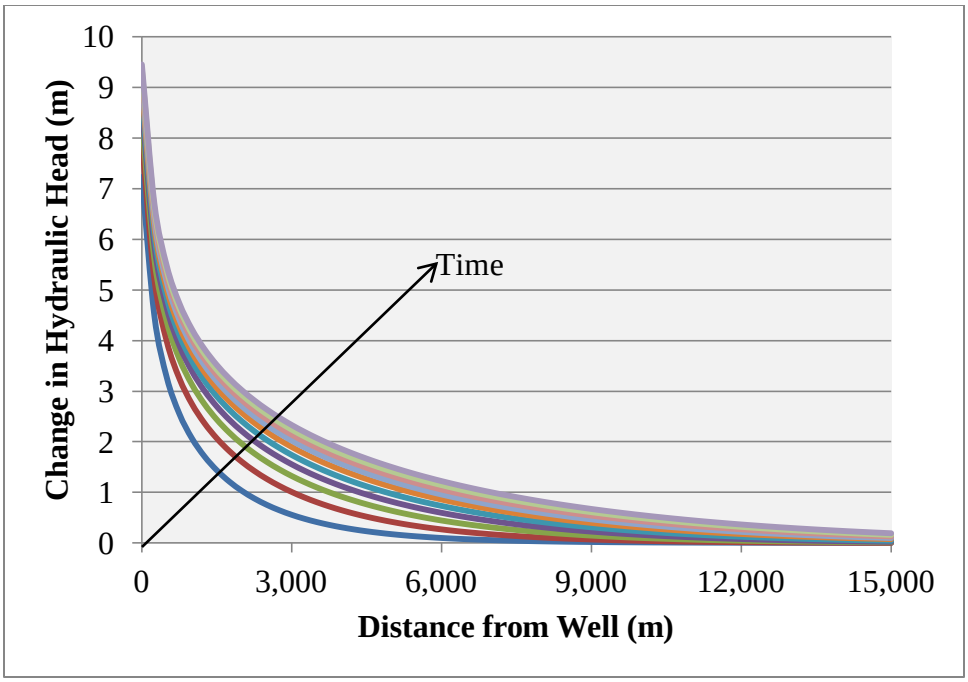

Figure 58: Model Run 6 spatiotemporal changes in hydraulic head with distance from injection well.

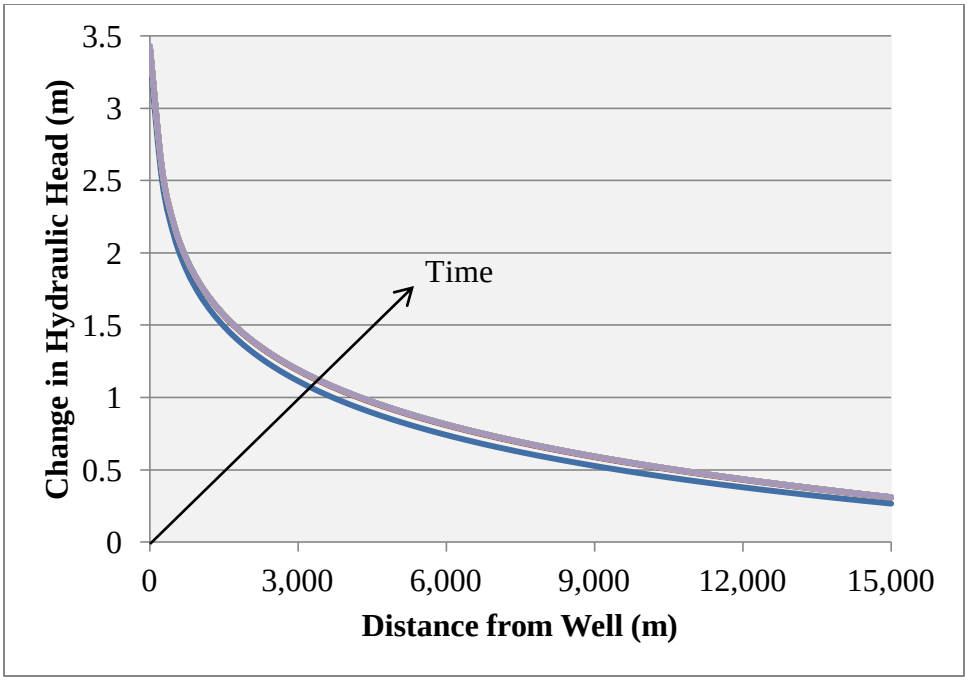

Figure 59: Model Run 7 spatiotemporal changes in hydraulic head with distance from injection well.

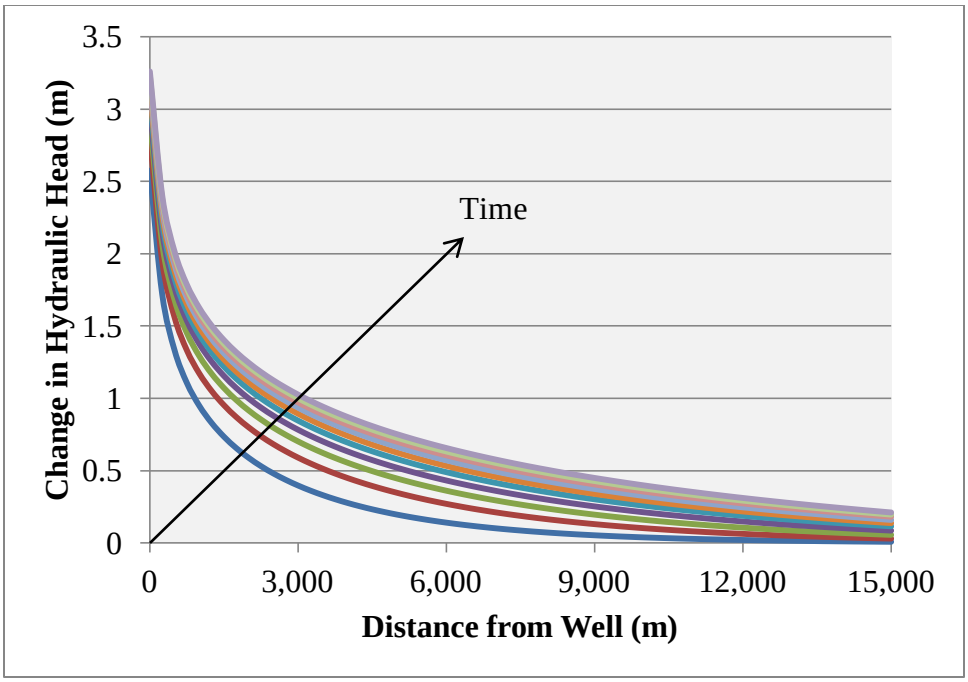

Figure 60: Model Run 8 spatiotemporal changes in hydraulic head with distance from injection well.

Seismic events have been induced or triggered by a change in pressure equivalent to 0.01 Mega-Pascals (MPa) or greater [*Keranen et al.*, 2014; *Stein*, 1999]. I used the change in hydraulic head as a proxy for pore pressure change by converting the change in hydraulic head to units of pressure. If you use the standard conversion of 1 foot of water (ft-H2O) equals approximately 0.4335 pounds per square inch (psi), then 0.01 MPa is approximately equal to 1 m of hydraulic head change. Another way to use change in hydraulic head as a proxy for pressure is to use the specific weight to calculate pore pressure change [*Keranen et al.*, 2014]:

(4) $\Delta P = \gamma * \Delta h,$

where ΔP is the change in pore-pressure, γ is the specific weight of water, and Δh is the change in hydraulic head. As the specific weight of water is equal to 9.807

kilonewtons per cubic meter (kN/m^3), 1 m change in hydraulic head is equal to 0.0098 MPa. Therefore, I used 1 m of hydraulic head change as the threshold for possible pore pressure induced seismicity. In Area 3, the 25^{th} percentile to 75^{th} percentile distance from the center of the well clusters to the earthquakes after the start of injection is approximately 10.5 to 15.6 km for Cluster 1 and 11 to 12 km for Cluster 2 [Figures 39 and 43]. The increase in seismicity rate occurred approximately one to five years following the start of injection activities.

As can be seen in Figures 55 – 60, Model Runs 3 and 5 fit the spatiotemporal observations of the increased seismicity in Area 3's Clusters 1 and 2, while Model Runs 4 and 6 – 8 fall short of the threshold increase in hydraulic head (1 m) in the temporal and/or spatial observations. The model is a generic, isotropic, homogenous model, while the Navajo aquifer is far more complex in actuality. However, the modeling shows using the parameters reported in the literature [*Freethey and Cordy*, 1991; *Hood and Danielson*, 1979; *Hood and Patterson*, 1984], an adequate increase in pore pressure to induce earthquakes is possible with the average injection volumes.

Chapter 6: Earthquake Statistics

6.1 b-value Evaluation

During the course of the research, I noticed a decrease in the magnitude of seismicity for Area 3, Cluster 1, and Cluster 2 following the start of injection. I utilized the Gutenberg-Richter relation [*Gutenberg and Richter*, 1944] to identify temporal variations in magnitude-frequency. I calculated the b-values of background seismicity and the seismicity after the start of injection by fitting the Gutenberg-Richter relation: $Log_{10}(N) = a - bM$, where M is the magnitude, N is the number of observed events greater than or equal to magnitude M, and a and b are constants [*Gutenberg and Richter*, 1944].

I binned the magnitudes of the seismicity data, using various bin sizes to test for bias, and fit the Gutenberg-Richter relation to the data using Microsoft Excel's linear regression. The b value of a set of seismicity data is often used to indicate changes in conditions spatially and temporally. A b-value of 1 is the global average for tectonic earthquakes, while injection induced earthquakes have been reported to have larger b-values ranging closer to 2 [*National Research Council of the National Academies*, 2013].

6.1.1 Area Three

The magnitudes in Area 3 decrease following the start of consistent injection in 1994 [Figure 61]. While there was injection in the late 1980s and early 1990's it was

inconsistent and low volumes [UIC public record well files]; therefore, I evaluated temporal variation in b-value for pre- and post-start of consistent injection.

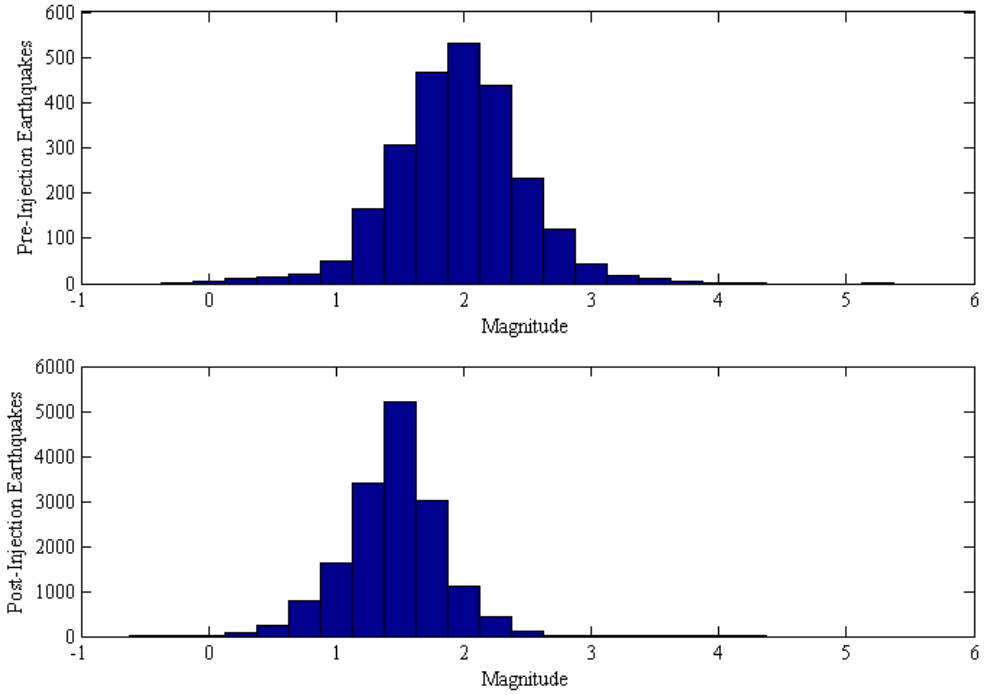

Figure 61: Area 3's earthquakes magnitude distribution pre- and post-injection, with confirmed MIS [*Arabasz et al*., 2002] removed.

The b-value for Area 3, prior to the start of consistent injection, is approximately 1.12 to 1.14 depending on bin size [Figures 62 and 63].

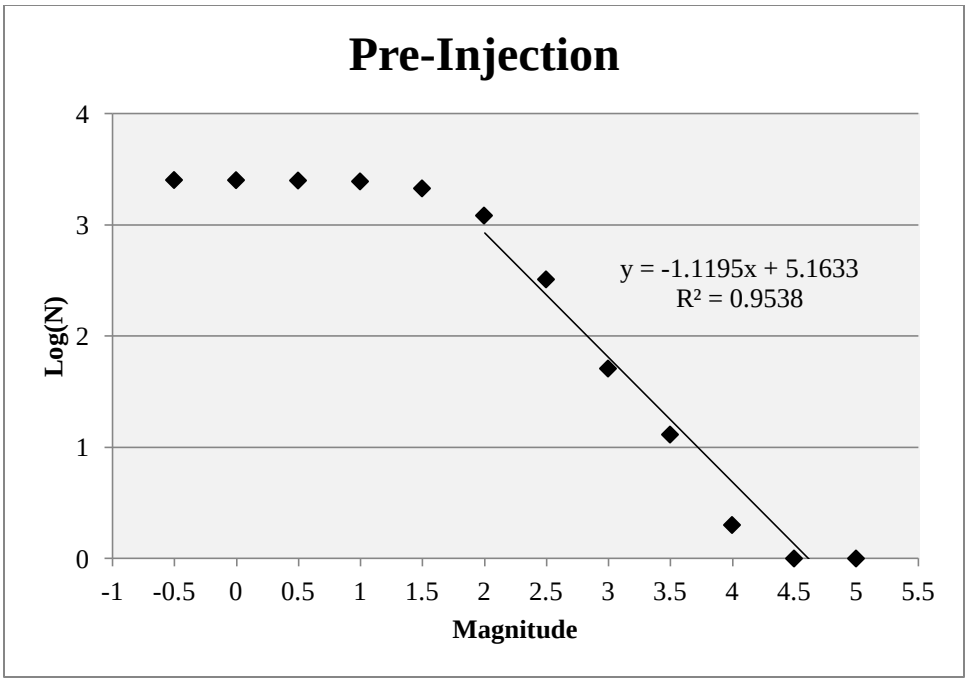

Figure 62: Area 3 pre- consistent injection magnitude-frequency relationship. N represents the number of events larger than or equal to the given magnitude. The b-value calculated for the linear portion (M > 2), using 0.5 sized bins, is approximately 1.12.

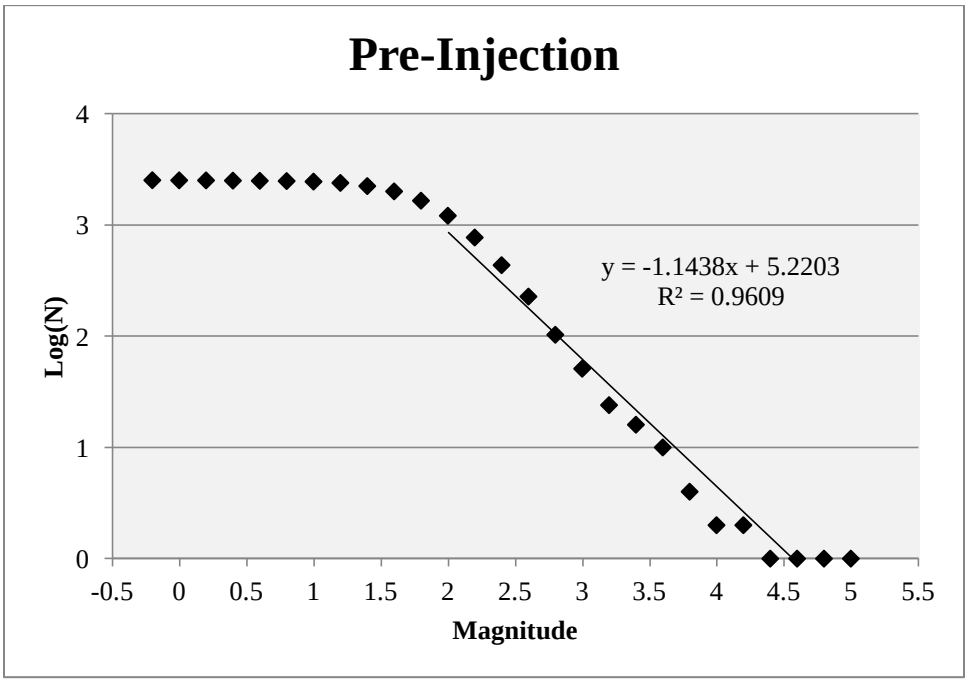

Figure 63: Area 3 pre- consistent injection magnitude-frequency relationship. N represents the number of events larger than or equal to the given magnitude. The b-value calculated for the linear portion (M > 2), using 0.2 sized bins, is approximately 1.14.

The b-value calculated for Area 3 following the start of consistent injection in 1994 is approximately 1.49 to 1.54 depending on bin size [Figures 64 and 65]. I removed the confirmed MIS [*Arabasz et al.*, 2002] for the b-value evaluation. I evaluated the confirmed MIS separately and I present the results in a later section.

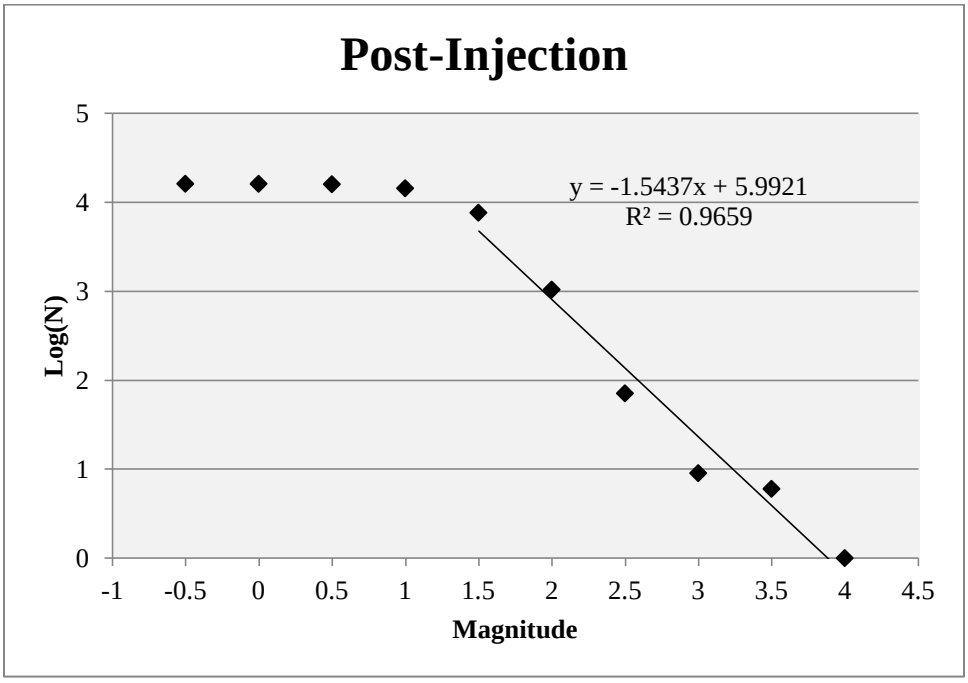

Figure 64: Area 3 post- consistent injection magnitude-frequency relationship. N represents the number of events larger than or equal to the given magnitude. The b-value calculated for the linear portion (M > 1.5), using 0.5 sized bins, is approximately 1.54.

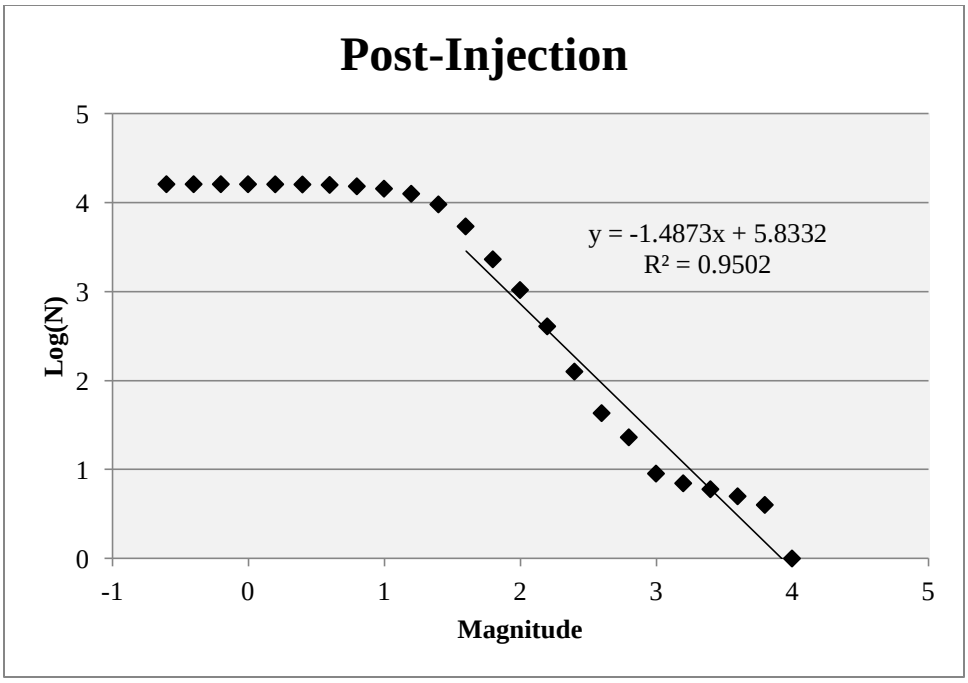

Figure 65: Area 3 post- consistent injection magnitude-frequency relationship. N represents the number of events larger than or equal to the given magnitude. The b-value calculated for the linear portion (M > 1.6), using 0.2 sized bins, is approximately 1.49.

The magnitude-frequency relationship shown in the post-injection plot with a 0.2 bin size indicates a possible bimodal distribution where the events with magnitude greater than 3 follow a different power relation than the events ranging from magnitude 1.6 to 3. Bimodal distributions have been observed in other coal mining regions [*Fritschen*, 2010; *Sen et al.*, 2013] and is often observed with mining induced seismicity [*Gibowicz*, 2009]. If I calculate the b-value for only the linear section from magnitude 1.6 to 3, [Figure 66] the b-value is approximately 2.03.

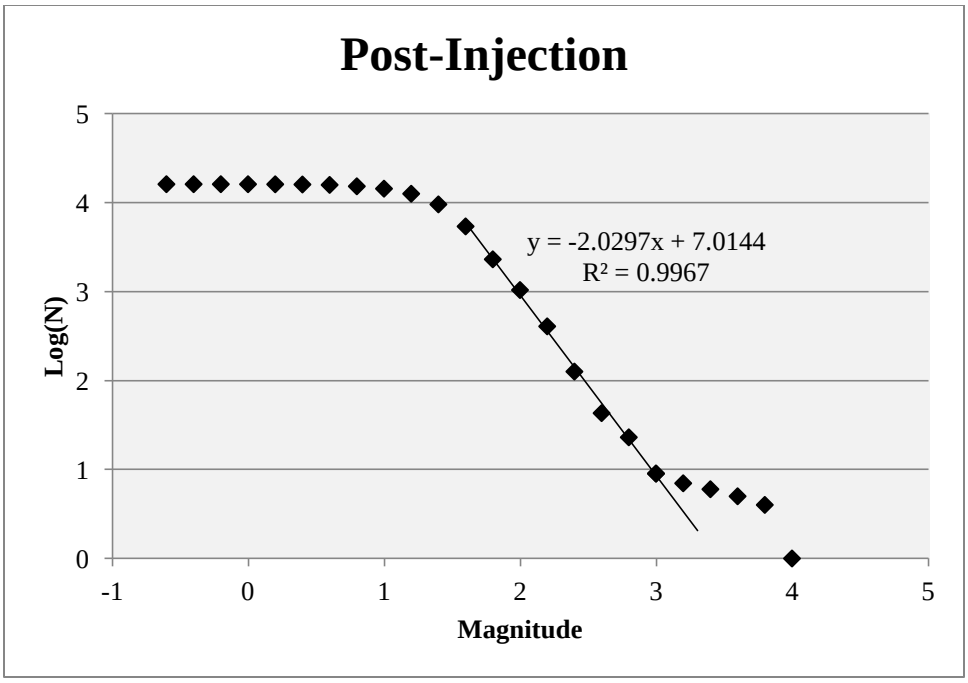

Figure 66: Area 3 post- consistent injection magnitude-frequency relationship. N represents the number of events larger than or equal to the given magnitude. The b-value calculated for the linear portion ($1.6 < M < 3$), using 0.2 sized bins, is approximately 2.03.

6.1.2 Cluster 1

Cluster 1 also has a decrease in magnitude during the increased seismicity post the start of injection. The first of the five wells of interest in Cluster 1 started injection in January 1997; the second well started injection in November 1999; the third in December 2003; the fourth in November 2005; and, the fifth in January 2006 [UIC public record well files]. The magnitude drop appears to begin just after the start of the third well in December 2003 [Figure 67].

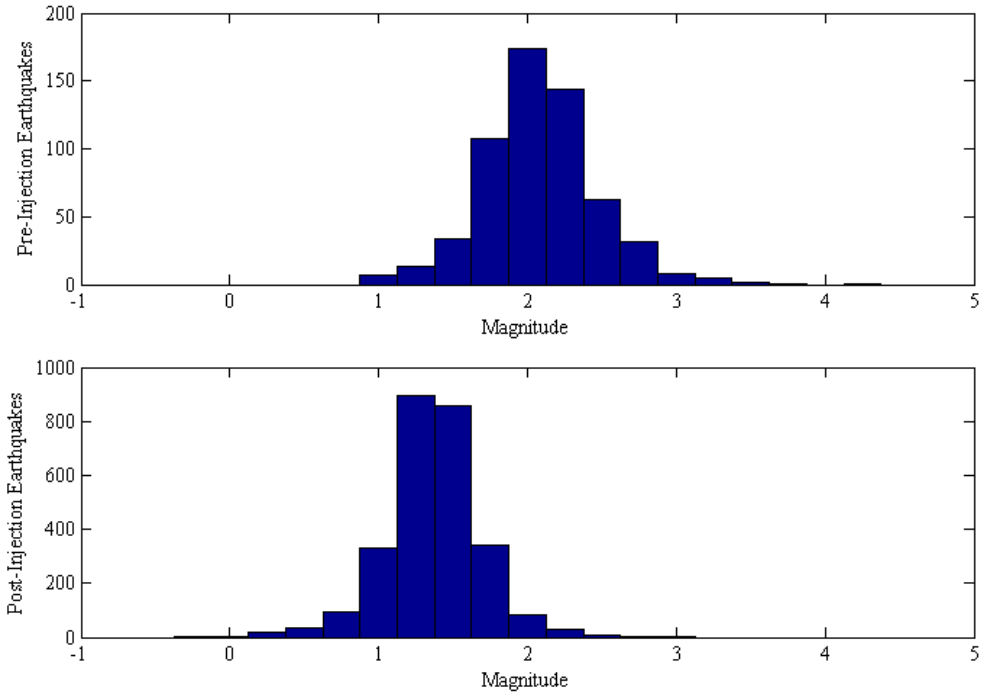

Figure 67: Cluster 1's earthquake magnitude distribution, pre- and post-injection. Post-injection begins at the start of the third well of interest.

The b-value for Cluster 1, prior to the start of the third well of interest and the shift in magnitudes, is approximately 1.34 to 1.37 depending on bin size [Figures 68 and 69].

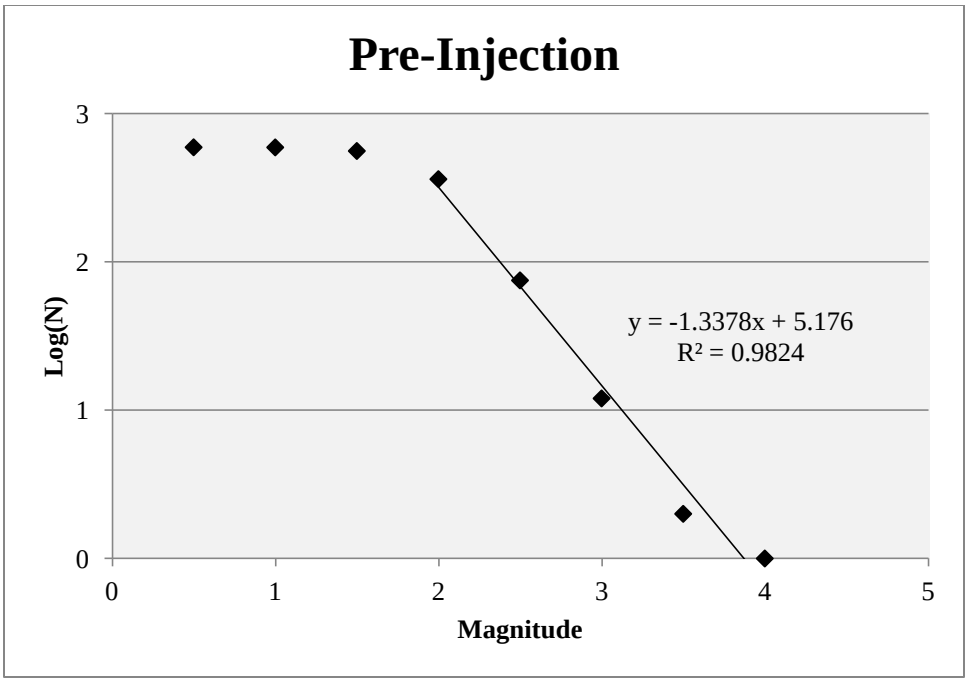

Figure 68: Cluster 1 pre- third well of interest start of injection magnitude-frequency relationship. N represents the number of events larger than or equal to the given magnitude. The b-value calculated for the linear portion (M > 2), using 0.5 sized bins, is approximately 1.34.

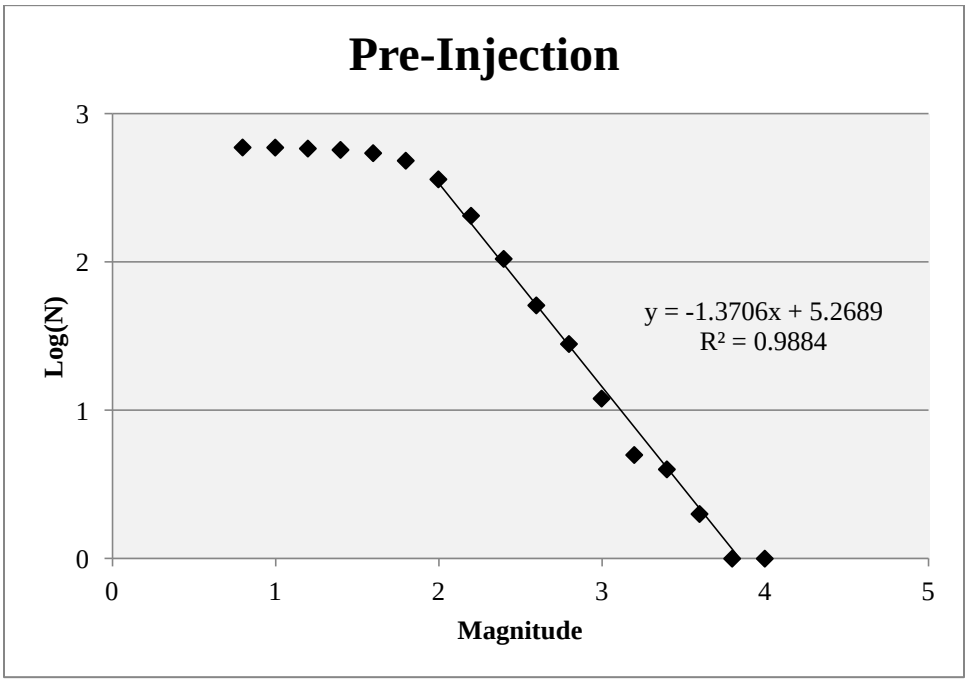

Figure 69: Cluster 1 pre- third well of interest start of injection magnitude-frequency relationship. N represents the number of events larger than or equal to the given magnitude. The b-value calculated for the linear portion (M > 2), using 0.2 sized bins, is approximately 1.37.

The b-value calculated for Cluster 1 following the start of the third injection well of interest in December 2003 is approximately 2.17 to 2.32 depending on bin size [Figures 70 and 71].

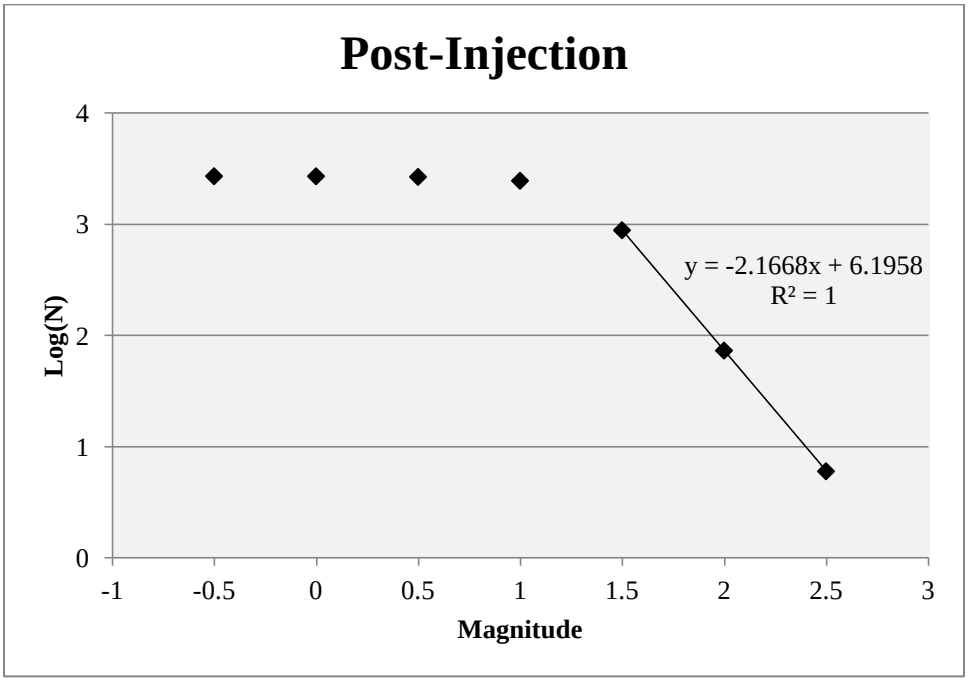

Figure 70: Cluster 1 post- third well of interest start of injection magnitude-frequency relationship. N represents the number of events larger than or equal to the given magnitude. The b-value calculated for the linear portion (M > 1.5), using 0.5 sized bins, is approximately 2.17.

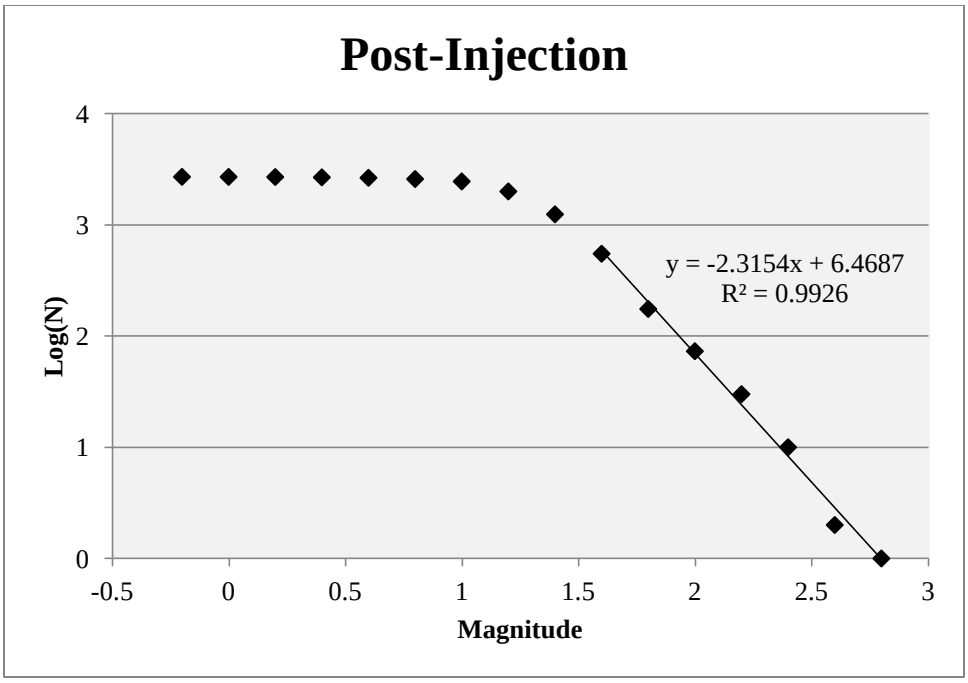

Figure 71: Cluster 1 post- third well of interest start of injection magnitude-frequency relationship. N represents the number of events larger than or equal to the given magnitude. The b-value calculated for the linear portion (M > 1.6), using 0.2 sized bins, is approximately 2.32.

6.1.3 Cluster 2

Cluster 2 appears to have a decrease in magnitude during the increased seismicity post the start of injection. The first of the three wells of interest in Cluster 2 started injection in February 1996; the second well started injection in December 1997; and, the third in July 2000 [UIC public record well files]. The magnitude drop appears to coincide with the start of injection of the first well in February 1996 [Figure 72]. I removed the confirmed MIS [*Arabasz et al.*, 2002] from the data set for the b-value evaluation.

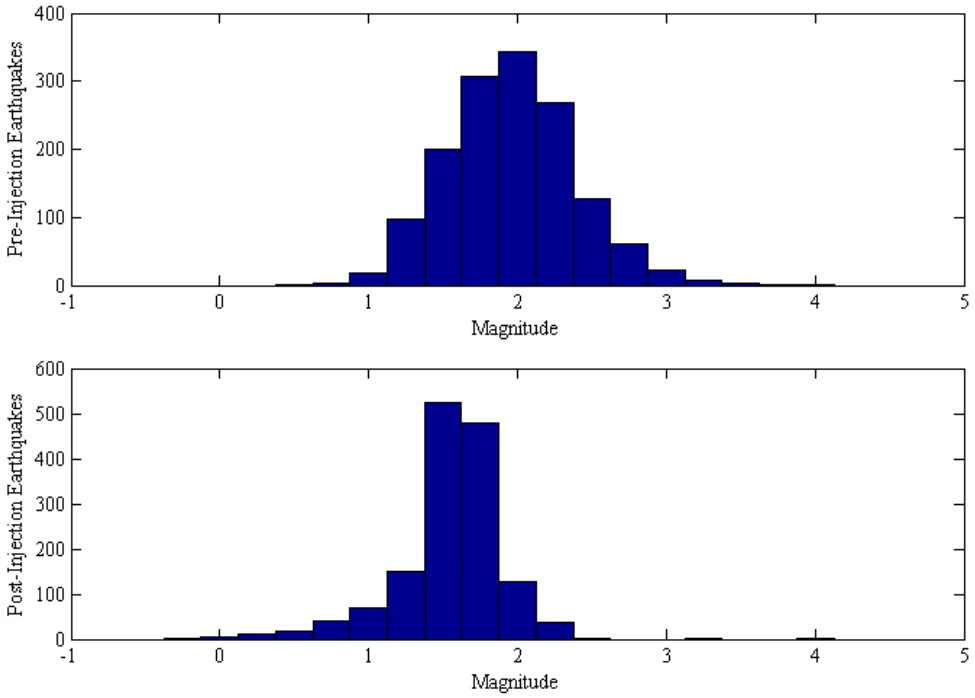

Figure 72: Cluster 2's earthquake magnitude distribution, pre- and post-injection, with confirmed MIS [*Arabasz et al.*, 2002] removed.

While the magnitudes appear to drop following the start of injection, the b-values for Cluster 2 stay consistent pre- and post- start of injection. The b-value prior to injection is 1.46 to 1.56 depending on bin size [Figures 73 and 74]; the b-value after the start of injection is 1.42 to 1.52 depending on bin size [Figures 75 and 76].

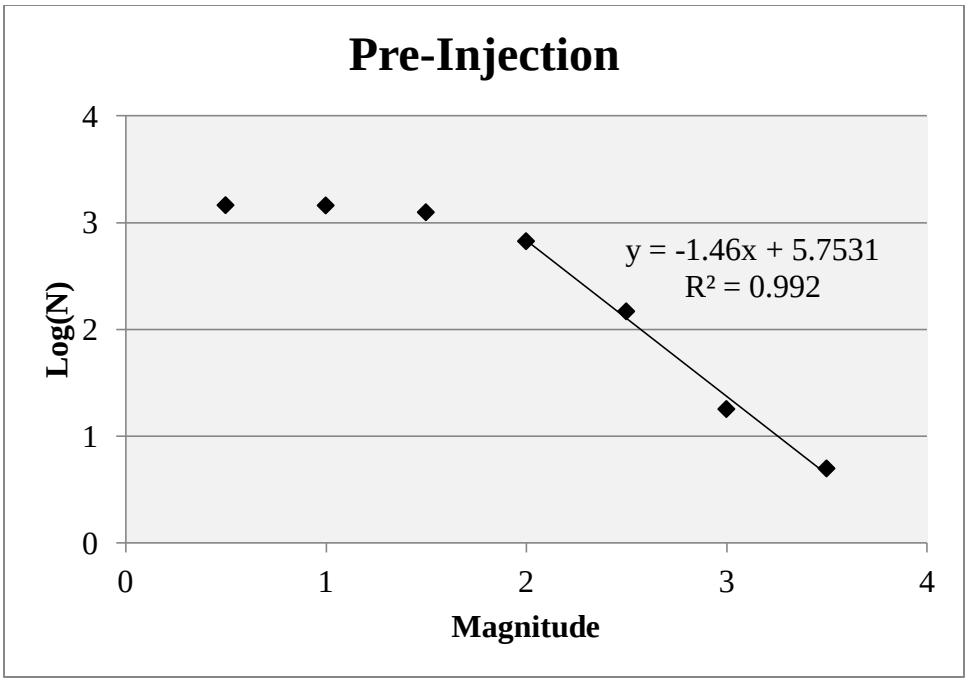

Figure 73: Cluster 2 pre-injection magnitude-frequency relationship. N represents the number of events larger than or equal to the given magnitude. The b-value calculated for the linear portion (M > 2), using 0.5 sized bins, is approximately 1.46.

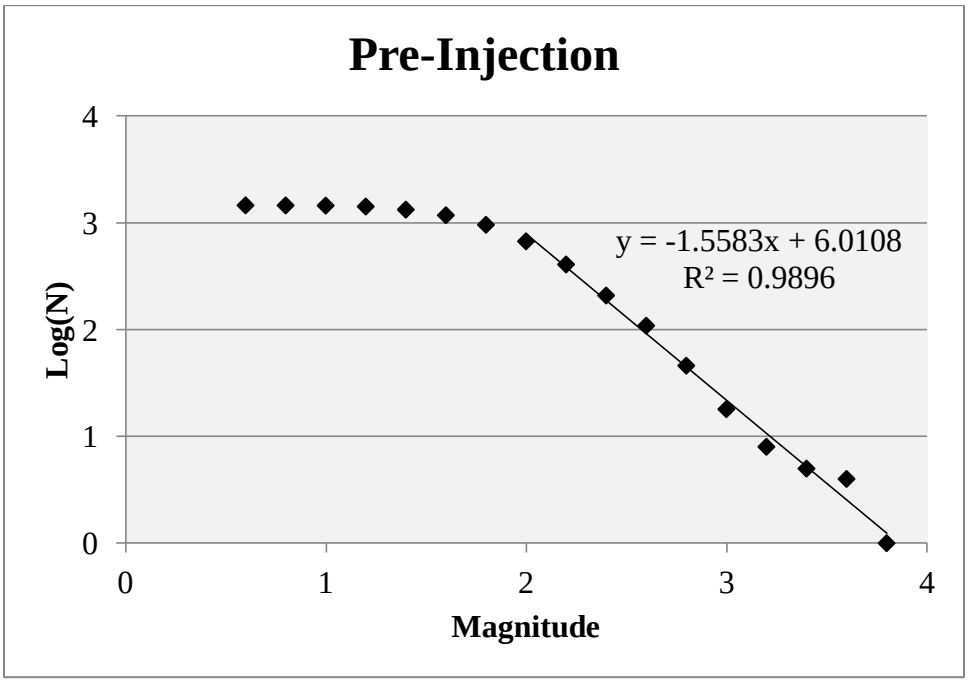

Figure 74: Cluster 2 pre-injection magnitude-frequency relationship. N represents the number of events larger than or equal to the given magnitude. The b-value calculated for the linear portion (M > 2), using 0.2 sized bins, is approximately 1.56.

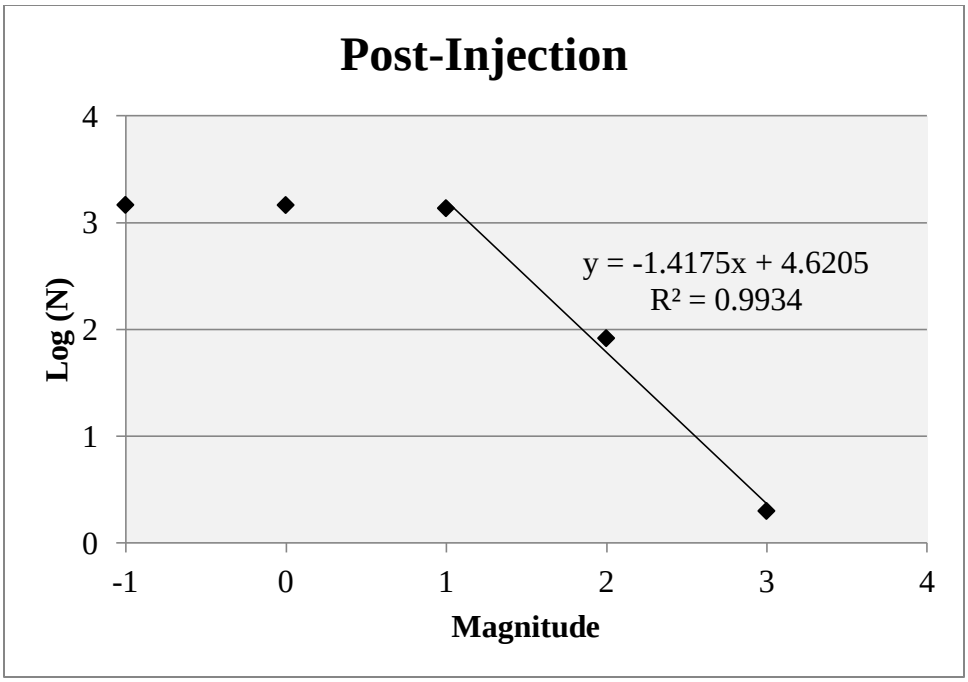

Figure 75: Cluster 2 post-injection magnitude-frequency relationship. N represents the number of events larger than or equal to the given magnitude. The b-value calculated for the linear portion (M > 1), using 1 sized bins, is approximately 1.42.

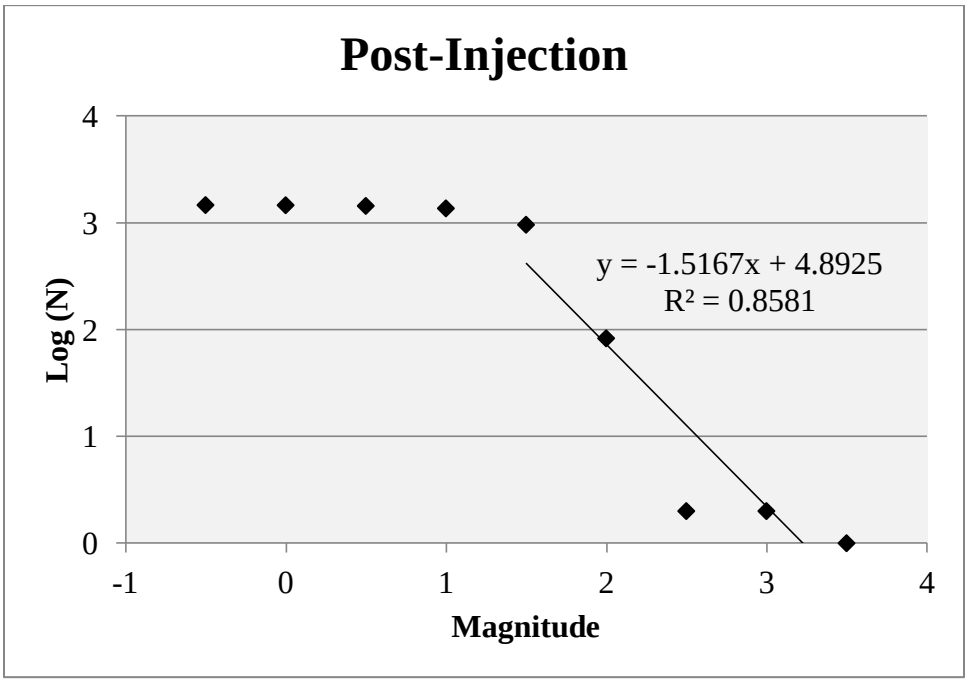

Figure 76: Cluster 2 post-injection magnitude-frequency relationship. N represents the number of events larger than or equal to the given magnitude. The b-value calculated for the linear portion (M > 1.5), using 0.5 sized bins, is approximately 1.52.

The post-injection magnitude-frequency distribution for Cluster 2 also appears to have a possible bimodal distribution where the events with magnitude greater than 2.5 follow a different power relation than the events with magnitudes from 1.5 to 2.5. You can observe this more clearly with smaller bin sizes [Figure 77]. Calculating the b-value for just the linear portion of the bimodal distribution from magnitude 1.5 to 2.5 gives a b-value of approximately 2.68 [Figure 77].

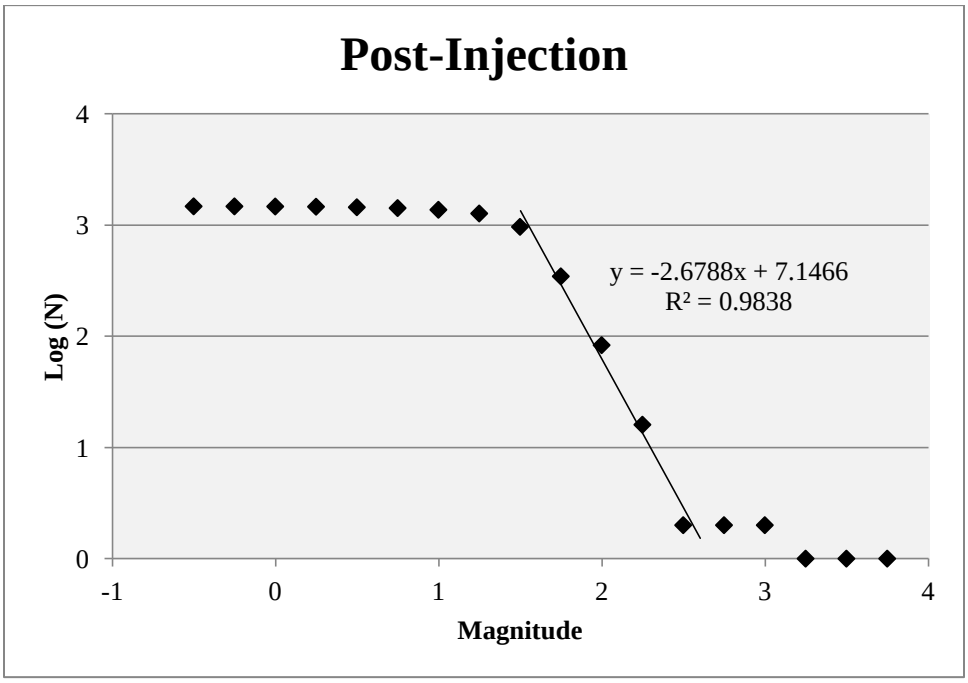

Figure 77: Cluster 2 post-injection magnitude-frequency relationship plotted using 0.25 sized bins. N represents the number of events larger than or equal to the given magnitude. The b-value calculated for the linear portion ($1.5 < M < 2.5$), using 0.25 sized bins, is approximately 2.68.

6.1.4 Mining Induced Seismicity

I removed the confirmed MIS [*Arabasz et al.*, 2002] for the b-value evaluations of Area 3 and Cluster 2. I evaluated the confirmed MIS separately using the revised magnitudes in Arabasz et al. [2002]. During the Trail Mountain Mining Area study in

2000 to 2001, a significant decrease in the magnitudes of the seismicity was noted for the last quarter of 2000 and the first quarter of 2001 [*Arabasz et al.*, 2005]. The decrease is noted in Arabasz et al. [2005], but was not further investigated or explained. I calculated the b-value for the 1,784 events that were in the USGS ComCat search and removed from my data set. The b-value ranged from 1.89 to 2.18 depending on bin size [Figures 78 and 79].

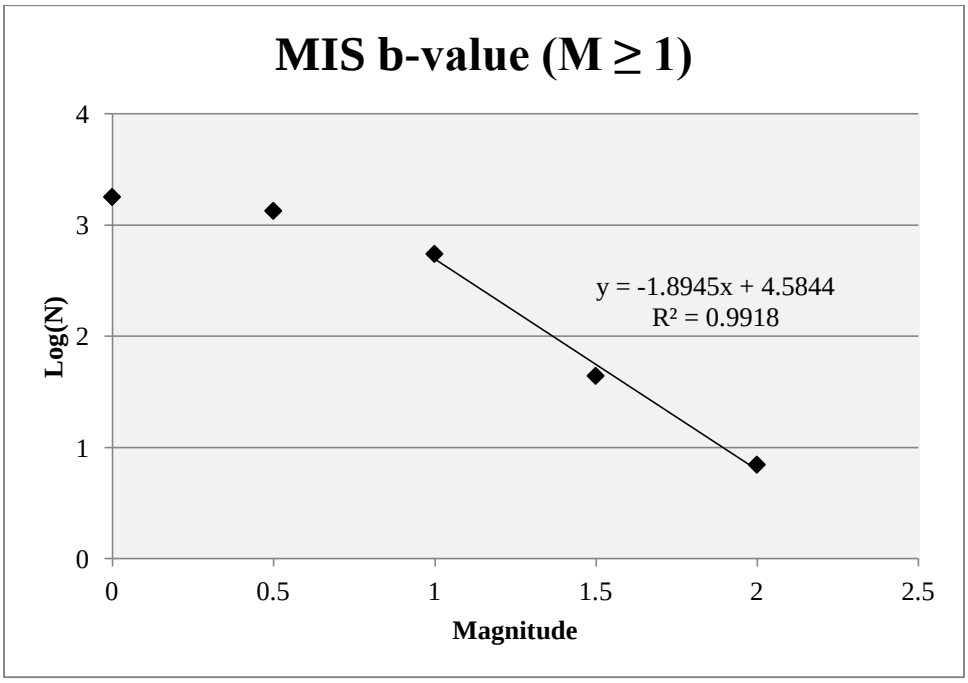

Figure 78: Mining induced seismicity magnitude-frequency relationship. N represents the number of events larger than or equal to the given magnitude. The b-value calculated for the linear portion (M > 1), using 0.5 sized bins, is approximately 1.89.

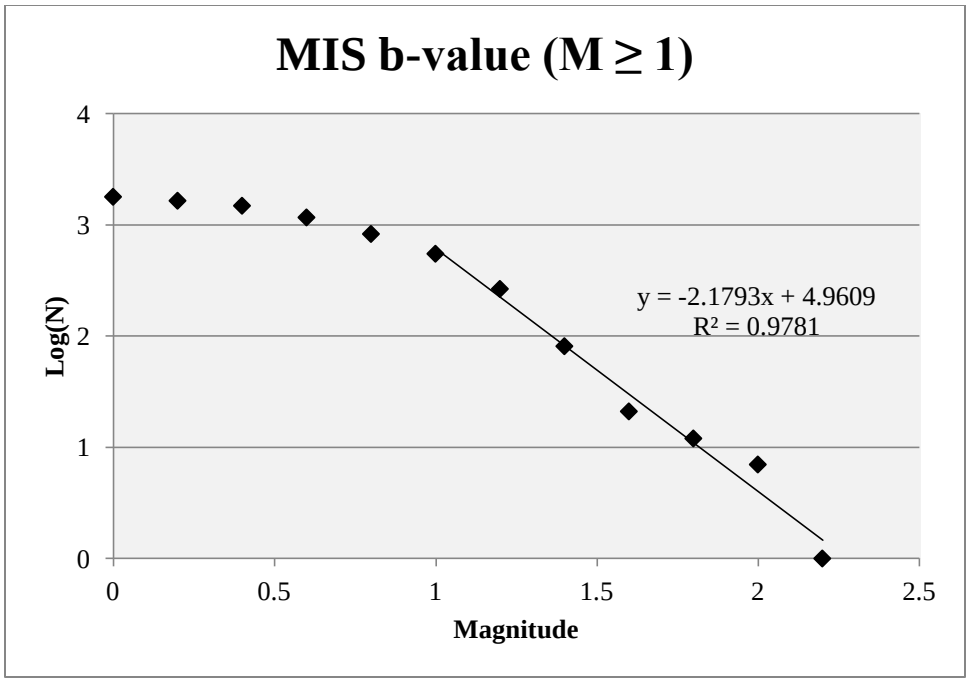

Figure 79: Mining induced seismicity magnitude-frequency relationship. N represents the number of events larger than or equal to the given magnitude. The b-value calculated for the linear portion (M > 1), using 0.2 sized bins, is approximately 2.18.

Chapter 7: Discussion

7.1 Spatial and Temporal Correlations

The correlation between seismicity and mining activity is evident in Area 3 in both time and space. The strong correlation between the mining shifts and the decrease in seismicity during off-shift hours [Figures 28 – 30], indicates much of the seismicity of Area 3 is mining induced. However, I cannot explain the significant increase in seismicity during the 2000s by the mining activity alone. There also appears to be a strong correlation between the increased seismicity in Area 3 and the injection in the wastewater disposal wells [Figures 31 – 33]. In addition, the increased seismicity appears to cluster at specific distances [Figures 40 – 43] from the wells, which would be consistent with pore-pressure induced seismicity along pre-existing faults.

Due to the focal depths of the seismicity not being well constrained, it is not possible to determine how close to the mining activity the majority of the seismic events are located. The disposal wells injecting into the Navajo aquifer in Area 3 are injecting at depths of approximately 1 – 2 km below the ground surface [UIC public record well files]. Based on UIC well logs and average thicknesses of stratigraphy, the Navajo aquifer is approximately 4 – 5 km below the coal mining areas in Book Cliffs to the north of the majority of the injection wells. In addition, there is a disposal well located in the coal mining area of Book Cliffs (Cluster 1 area) that injects into the Spring Canyon Formation [Figures 18 and 19], which is located approximately 1.7 km below ground surface [UIC public record well files], only a short distance below the coal mining.

7.2 Groundwater Models

The groundwater models I created are very basic models that indicated, with the known parameters for the Navajo aquifer and the average well volumes injected by the disposal wells, that it is possible the pore pressure could increase enough to trigger seismicity. The model I created is homogenous and isotropic; in actuality, the Navajo aquifer is dipping based on the local geology and is likely not homogenous or isotropic. There are faults in the area [*Weiss et al.*, 1990; *Witkind*, 1988; *Witkind and Weiss*, 1991; *Witkind et al.*, 2006] as well as joints [*Kubacki et al.*, 2014] that likely produce anisotropy based on either increased or decreased hydraulic conductivity along the features.

I chose to make my model flat and for the model's initial condition be hydrostatic. Based on well logs [UIC public record well files], I know the Navajo aquifer is dipping in the area of the disposal wells. In addition, while the Navajo aquifer in Area 3 is fully saturated [*Freethey and Cordy*, 1991; *Hood and Patterson*, 1984], it also has a groundwater gradient that predominantly moves away from the San Rafael swell in a complicated pattern [*Hood and Patterson*, 1984].

7.3 b-values

Studies have indicated that larger b-values, sometimes ranging closer to 2 [*National Research Council of the National Academies*, 2013], and spatial and temporal variations can be associated with fluid-induced activity whether anthropogenic injection or related to magma intrusion [*Bachmann et al.*, 2014]. In contrast, mining induced seismicity is often characterized by bimodal magnitude-frequency distributions [*Gibowicz*, 2009].

A study of the seismicity in the Crandall Canyon Mine area, Utah, following the tragic mine collapse August 6, 2007 that killed 6 miners, found the magnitude of completeness for their data set to be 1.6 (coda magnitude) [*Pechmann et al.*, 2008]. This is consistent with the linear sections of my b-value evaluations for Area 3, Cluster 1 and Cluster 2. The b-value was calculated for just the Crandall Canyon Mine area from March 2005 through just before the main collapse event on August 6, 2007; the b-value prior to the collapse was found to be approximately 1.74 [*Pechmann et al.*, 2008]. The b-value for the aftershocks associated with the collapse was also calculated and was approximately 0.9.

Kubacki et al. [2014] completed a closer examination of temporal changes in b-value for the Crandall Canyon Mine area for the period surrounding the main collapse. A b-value of approximately 1.23 was calculated for July 26 through August 4, 2007; a b-value of approximately 1.12 was calculated for the 48 hours prior to the collapse; and a b-value of approximately 0.92 was calculated for the seismicity following the collapse through August 20, 2007 [*Kubacki et al.*, 2014]. The b-values for two separate periods of data collection, during a 1970 survey of microseismicity in mines in the eastern section of the Book Cliffs mining area, Utah, were calculated and found to be 1.1 for the first period and 0.5 for the second [*Smith et al.*, 1974]. Excluding the very low 0.5 b-value, these values are close to the values I calculated for the area.

Sen et al. [2013] found variations in the frequency-magnitude relationship for different sets of focal mechanisms for mining induced seismicity in a coal mine in the Ruhr region, Germany and that the overall frequency-magnitude distribution did not fit

the Gutenberg-Richter relation, but rather has a bi-modal distribution. This area is not considered tectonically active and, therefore, all seismicity is inferred to be induced by mining operations [*Sen et al.*, 2013]. The bimodal frequency-magnitude distribution may be caused by structural heterogeneities or the combination of tectonic and induced acting stresses [*Sen et al.*, 2013].

The Saar mine in Germany also has mining induced seismicity that does not fit the Gutenberg-Richter relation [*Fritschen*, 2010]. This area has a bimodal distribution, where the smaller events do not have the same power relation as the larger events [*Fritschen*, 2010]. Mines in the Upper Kama potash deposits of Western Ural, Russia also have induced seismicity with bimodal magnitude-frequency relations [*Gibowicz*, 2009]. Coal mining induced events in the Edwinstowe area in England, however, do follow the Gutenberg-Richter relation and have a b-value of 0.8 [*Bishop et al.*, 1993].

The b-values previously calculated for the Utah mining region [*Kubacki et al.*, 2014; *Pechmann et al.*, 2008; *Smith et al.*, 1974] did follow the Gutenberg-Richter magnitude-frequency distribution. These calculations, however, were completed over short periods of time, the longest being a little over two years [*Pechmann et al.*, 2008]. The b-values I calculated for Area 3, Cluster 1, and Cluster 2 spanned longer periods, at least 9 years. My results show temporal and spatial variations. Area 3 and Cluster 1 show an increase in b-value following the start of injection, while Cluster 2's b-value remains consistent. The increase in b-value following the start of injection could indicate changes in stress distribution consistent with pore-pressure increase along pre-existing faults.

The b-value of Cluster 1 compared to Cluster 2 indicates spatial variations in the area. Cluster 1 had a b-value of 1.34 – 1.37 prior to injection, while Cluster 2 had a b-value of 1.46 – 1.56. Following injection, Cluster 1's b-value increased to 2.17 – 2.32, while Cluster 2's remained consistent, 1.42 – 1.52. Area 3 and Cluster 2, especially in the post-injection calculations appear to have a bimodal distribution to the b-value. The bimodal distribution of Area 3 could be due to the spatial variations that are included in the area. When the b-value is calculated for the linear portions of the bimodal distributions in post-injection Area 3 and Cluster 2, the resulting b-values are much higher, approximately 2.03 and 2.68, respectively.

The b-values larger than 2 are consistent with injection induced seismicity [*National Research Council of the National Academies*, 2013]. However, the b-value calculated for the mining induced seismicity, confirmed by relocation [*Arabasz et al.*, 2002], that was removed from my data set has a b-value of 1.89 to 2.18, depending on bin size. Therefore, the higher b-value alone does not indicate injection induced seismicity. However, the temporal change in b-value in Cluster 1 from approximately 1.5 to greater than 2 does indicate a significant change in stress conditions that could signify a variation in the induced seismicity. This is consistent with the mining induced seismicity being enhanced by pore-pressure increase due to injection from the wastewater disposal wells.

Chapter 8: Conclusions

There are thousands of wastewater disposal wells in the United States and only a small percentage are known to induced seismicity, typically the wells that inject large volumes of fluid and/or communicate pressure changes into basement faults [*Ellsworth*, 2013]. Seismicity in Areas 1 and 2 remained consistent since 1981 despite injection of fluids in the area. Area 1 has nineteen wastewater disposal wells, seven of which are active wastewater disposal wells [UIC public record well files]. The wells have injected a reported total of approximately 2.44×10^8 bbls of wastewater as of October 2014 [UIC public record well files], which is approximately 61% of the amount injected into Area 3. It is possible that the lower cumulative injection volume could be responsible for the lack of induced seismicity in Area 1.

Area 2 has 80 wastewater disposal wells, 61 of which are active, and 1,265 active water injection wells, used for enhanced recovery [UIC public record well files]. The total reported injected volume from the 80 wastewater disposal wells is 6.3×10^8 bbls as of January 2015 [UIC public record well files], which is approximately 1.6 times the amount injected into Area 3. The injection volume of Area 2 compared to Area 3 cannot explain the lack of injection induced seismicity in Area 2, as it is larger than the volume injected into Area 3. Ellsworth [2013] suggests that, since only a small percentage of wastewater disposal wells induced seismicity, the ambient conditions in the majority of the injection formations may not be close enough to failure to induce seismicity; this may be the case in Area 2. This could also contribute to the lack of induced seismicity in Area 1.

Area 4 shows variation in seismicity rate since 1981, but it is a very small sample size of events, which is too small to indicate a significant change. Area 4 has twenty-one wastewater disposal wells, seven of which are listed as active wastewater disposal wells [UIC public record well files]. As of January 2015, the wells have injected a reported total volume of 3.3×10^7 bbls [UIC public record well files], which is approximately 8.3% of the volume injected in Area 3.

Seismicity in the region of Area 3 has long been inferred to be mining induced seismicity due to the strong correlation with the active coal mining in the region and the very shallow focal depths [*Pechmann et al.,* 2008]. Mining induced seismicity studies have been conducted in the area since the 1960's [*Pechmann et al.,* 2008]. Area 3 also has numerous UIC Class II wastewater disposal wells. Thirty-three designated wastewater disposal wells are located within Area 3; twenty-seven of which inject into the Navajo aquifer [UIC public record well files]. Five of the wells inject into aquifers other than the Navajo aquifer and one well was never utilized and is now abandoned.

I conclude the increased seismicity in Area 3 that occurred from 2000 through 2010, and in Cluster 1 in particular, is mining induced seismicity and injection induced seismicity. There is a strong correlation between the seismicity of the area and the coal mining activity in both time and space; in addition, there is a strong spatial and temporal correlation between the wastewater injection wells and the seismicity. The time gap between the beginning of injection and the large increases in the seismicity rate in Clusters 1 and 2 could be consistent with pore-pressure diffusion from the injection wells to the area of seismicity. The clustering of the increased seismicity at certain distances

from the wells is also consistent with pore-pressure increase along pre-existing faults. In addition, the groundwater models I created confirm it is possible, with the known parameters for the aquifer and the average injection rate, to produce a pore-pressure increase large enough to trigger seismicity.

The temporal changes in b-value, especially in Cluster 1, indicate a change in the stress distribution in the area that is consistent with injection induced seismicity. The bimodal magnitude-frequency distribution of Cluster 2 post-injection could indicate the seismicity is only mining induced, as bimodal distributions are common [*Gibowicz*, 2009]. However, as bimodal distribution can indicate multiple types of seismicity, friction-dominated versus fracture-dominated [*Gibowicz*, 2009], are occurring, it is also conceivable that both mining induced seismicity and injection induced seismicity occurring together could create a bimodal magnitude-frequency distribution as well.

Coal mining in Utah has been active for over 100 years [*Wong and Humphrey*, 1989] and consistently active from 1983 through 2013 as seen in the production data [Figures 24 – 26] collected by the U.S. Energy Information Administration and the U.S. Mine Safety and Health Administration. If all the seismicity remained mining induced seismicity as it has been observed for decades, I would not expect temporal changes in seismicity rate or b-value. The changes I observed indicate a strong possibility that the mining induced seismicity has been augmented by pore-pressure changes caused by wastewater disposal injection. Increased seismicity and changes in seismicity should be taken into account during mine safety assessment and planning. In addition, the location of wastewater injection wells near active mines may need to be more carefully considered in the future in regards to the possibility of induced seismicity.

REFERENCES

Arabasz, W. J., and J. C. Pechmann (2001), Seismic characterization of coal-mining seismicity in Utah for CTBT monitoring, Technical *Rep. UCRL-CR-143772*, 120 pp, LLNL Research Agreement No. B344836, Livermore, California.

Arabasz, W. J., R. Burlacu, and K. L. Pankow (2007), An overview of historical and contemporary seismicity in central Utah, in *Central Utah - Diverse Geology of a Dynamic Landscape*, edited by G. C. Willis, M. D. Hylland, D. L. Clark and J. Chidsey, T.C., pp. 236-253.

Arabasz, W. J., S. J. Nava, M. K. McCarter, and K. L. Pankow (2002), Ground-Motion Recording and Analysis of Mining-Induced Seismicity in the Trail Mountain Area, Emery County, Utah, Technical *Rep.*, 168 pp, University of Utah Seismograph Stations, Salt Lake City, Utah.

Arabasz, W. J., S. J. Nava, M. K. McCarter, K. L. Pankow, J. C. Pechmann, J. Ake, and A. McGarr (2005), Coal-Mining Seismicity and Ground-Shaking Hazard: A Case Study in the Trail Mountain Area, Emery County, Utah, *Bulletin of the Seismological Society of America*, *95*(1), 18-30.

Bachmann, C. E., W. Foxall, and T. Daley (2014), Comparing induced seismicity on different scales, paper presented at Thirty-Ninth Workshop on Geothermal Reservoir Engineering, Stanford University, Stanford, California, February 24-26, 2014.

Bishop, I., P. Styles, and M. Allen (1993), Mining-induced seismicity in the Nottinghamshire Coalfield, *Quarterly Journal of Engineering Geology and Hydrogeology*, *26*(4), 253-279.

Boltz, M. S., K. L. Pankow, and M. K. McCarter (2014), Fine Details of Mining-Induced Seismicity at the Trail Mountain Coal Mine Using Modified Hypocentral Relocation Techniques, *Bulletin of the Seismological Society of America*, *104*(1), 193-203.

Currie, B. S. (1997), Sequence stratigraphy of nonmarine Jurassic–Cretaceous rocks, central Cordilleran foreland-basin system, *Geological Society of America Bulletin*, *109*(9), 1206-1222.

Davis, S. D., and C. Frohlich (1993), Did (or will) fluid injection cause earthquakes?-criteria for a rational assessment, *Seismological Research Letters*, *64*(3-4), 207-224.

Ellsworth, W. L. (2013), Injection-Induced Earthquakes, *Science*, *341*(6142), 1225942.

Freethey, G. W., and G. E. Cordy (1991), Geohydrology of Mesozoic Rocks in the Upper Colorado River Basin in Arizona, Colorado, New Mexico, Utah, and Wyoming, excluding the San Juan Basin, in *Regional Aquifer-System Analysis - Upper Colorado River Basin, Excluding San Juan Basin: Geological Survey Professional Paper 1411-C*, edited by USGS, U.S. Department of the Interior, Washington, DC.

Fritschen, R. (2010), Mining-Induced Seismicity in the Saarland, Germany, *Pure and Applied Geophysics*, *167*(1), 77-89.

Gibowicz, S. J. (2009), Seismicity induced by mining: Recent research, in *Advances in Geophysics*, edited by R. Dmowska, pp. 1-53, Academic Press, San Diego, CA.

Gutenberg, B., and C. F. Richter (1944), Frequency of earthquakes in California, *Bulletin of the Seismological Society of America*, *34*(4), 185-188.

Healy, J. H., W. W. Rubey, D. T. Griggs, and C. B. Raleigh (1968), The Denver Earthquakes, *Science*, *161*(3848), 1301-1310.

Hintz, L. F., and B. J. Kowallis (2009), *Geologic History of Utah*, 225 pp., Brigham Young University, Provo, Utah.

Hood, J. W., and T. W. Danielson (1979), Aquifer Tests of the Navajo Sandstone Near Caineville, Wayne County, Utah, edited by State of Utah Department of Natural Resources, U.S. Geological Survey.

Hood, J. W., and D. Patterson (1984), Bedrock aquifers in the northern San Rafael Swell area, Utah, with special emphasis on the Navajo Sandstone, in *Technical Publication No. 78*, edited by State of Utah Department of Natural Resources, U.S. Geological Survey.

Horton, S. (2012), Disposal of Hydrofracking Waste Fluid by Injection into Subsurface Aquifers Triggers Earthquake Swarm in Central Arkansas with Potential for Damaging Earthquake, *Seismological Research Letters*, *83*(2), 250-260.

Jordán, T. E., B. L. Isacks, R. W. Allmendinger, J. A. Brewer, V. A. Ramos, and C. J. Ando (1983), Andean tectonics related to geometry of subducted Nazca plate, *Geological Study of America Bulletin*, *94*, 341-361.

Keranen, K. M., M. Weingarten, G. A. Abers, B. A. Bekins, and S. Ge (2014), Sharp increase in central Oklahoma seismicity since 2008 induced by massive wastewater injection, *Science (New York, N.Y.)*, *345*(6195), 448-451.

King, V. M., L. V. Block, W. L. Yeck, C. K. Wood, and S. A. Derouin (2014), Geological structure of the Paradox Valley Region, Colorado, and relationship to seismicity induced by deep well injection, *Journal of Geophysical Research: Solid Earth*, *119*, doi: 10.1002/2013JB010651.

Kubacki, T., K. D. Koper, K. L. Pankow, and M. K. McCarter (2014), Changes in mining-induced seismicity before and after the 2007 Crandall Canyon Mine collapse, *Journal of Geophysical Research: Solid Earth*, *119*, doi: 10.1002/2014JB011037.

Li, T., M. F. Cai, and M. Cai (2007), A review of mining-induced seismicity in China, *International Journal of Rock Mechanics and Mining Sciences*, *44*(8), 1149-1171.

McGarr, A. (2014), Maximum magnitude earthquakes induced by fluid injection, *Journal of Geophysical Research: Solid Earth*, *119*, doi: 10.1002/2013JB010597.

National Research Council of the National Academies (2013), *Induced Seismicity Potential in Energy Technologies*, 300 pp., The National Academies Press, Washington, DC.

Neuhauser, K. R. (1988), Sevier-age ramp-style thrust faults at Cedar Mountain, northwestern San Rafael swell (Colorado Plateau), Emery County, Utah, *Geology*, *16*, 299-302.

Pechmann, J. C., S. J. Nava, F. M. Terra, and J. C. Bernier (2007), Local Magnitude Determinations for Intermountain Seismic Belt Earthquakes from Broadband Digital Data, *Bulletin of the Seismological Society of America*, *97*(2), 557-574.

Pechmann, J. C., W. J. Arabasz, K. L. Pankow, R. Burlacu, and M. K. McCarter (2008), Seismological report on the 6 August 2007 Crandall Canyon mine collapse in Utah, *Seismological Research Letters*, *79*(5), 620-636.

Sen, A. T., S. Cesca, M. Bischoff, T. Meier, and T. Dahm (2013), Automated full moment tensor inversion of coal mining-induced seismicity, *Geophysical Journal International*, *195*(2), 1267-1281.

Smith, R. B., P. L. Winkler, and J. G. Anderson (1974), Source mechanisms of microearthquakes associated with underground mines in eastern Utah, *Bulletin of the Seismological Society of America*, *64*(4), 1295-1317.

Stein, R. S. (1999), The role of stress transfer in earthquake occurrence, *Nature*, *402*, 605-609.

Sumy, D. F., E. S. Cochran, K. M. Keranen, M. Wei, and G. A. Abers (2014), Observations of static Coulomb stress triggering of the November 2011 M 5.7 Oklahoma earthquake sequence, *Journal of Geophysical Research: Solid Earth*, *119*, doi: 10.1002/2013JB010612.

Turcotte, D. L., and G. Schubert (2002), *Geodynamics*, Second Edition ed., 456 pp., Cambridge University Press, Cambridge.

Utah DNR, Division of Oil, Gas, and Mining (2014), Coal Mine Location Map, Utah Department of Natural Resources, Salt Lake City, Utah.

Wannamaker, P. E., et al. (2001), Great Basin-Colorado Plateau transition in central Utah: An interface between active extension and stable interior, in *The Geologic Transition, High Plateaus to Great Basin - A Symposium and Field Guide, The Mackin Volume: Utah Geological Association Publication 30 and Pacific Section American Association of Petroleum Geologists Guidebook GB 78*, edited by M. C. Erskine, J. E. Faulds, J. M. Bartley and P. D. Rowley, pp. 1-38.

Weiss, M. P., I. J. Witkind, and W. B. Cashion (1990), Geologic Map of the Price 30' x 60' Quadrangle, Carbon, Duchesne, Uintah, Utah, and Wasatch Counties, Utah, U.S. Geological Survey, Denver, CO.

Witkind, I. J. (1988), Geologic Map of the Huntington 30' x 60' Quadrangle, Carbon, Emery, Grand, and Uintah Counties, Utah, U.S. Geological Survey, Denver, CO.

Witkind, I. J., and M. P. Weiss (1991), Geologic Map of the Nephi 30' x 60' Quadrangle, Carbon, Emery, Juab, Sanpete, Utah, and Wasatch Counties, Utah, U.S. Geological Survey, Denver, CO.

Witkind, I. J., M. P. Weiss, and T. L. Brown (2006), Geologic Map of the Manti 30' x 60' Quadrangle, Carbon, Emery, Juab, Sanpete, and Sevier Counties, Utah, Utah Geological Survey.

Wong, I. G., and J. R. Humphrey (1989), Contemporary seismicity, faulting, and the state of stress in the Colorado Plateau, *Geological Society of America Bulletin*, *101*, 1127-1146.

Zuluaga, L. F., H. Fossen, and A. Rotevatn (2014), Progressive evolution of deformation band populations during Laramide fault-propagation folding: Navajo Sandstone, San Rafael monocline, Utah, U.S.A, *Journal of Structural Geology*, *68*, 66-81.